Inactivation of peptidoglycan remodeling promotes antibiotic susceptibility in vancomycin-resistant *Enterococcus faecium*

Kyong T. Fam[1#], Pavan Kumar Chodisetti[1#], Zifei Wang[2], Joshua A. Homer[2], Christopher J. Smedley[3], Seiya Kitamura[4-6], Benjamin Silva[4], Yijun Xiong[6], Althea Hansel-Harris[4], Matthew Holcomb[4], Simeon Babarinde[4], Daria Van Tyne[7], Ian A. Wilson[4], Stefano Forli[4], Benjamin F. Cravatt[6], Donghyun Park[4], Dennis W. Wolan[4,5], John E. Moses[2,3]*, Howard C. Hang[1,6]*

[1] Department of Immunology and Microbiology, Scripps Research; La Jolla, California 92037, United States.

[2] Cancer Center, Cold Spring Harbor Laboratory; Cold Spring Harbor, NY 11724, USA.

[3] La Trobe Institute for Molecular Science, La Trobe University, Science Dr., Bundoora, Melbourne, VIC, 3086 Australia.

[4] Department of Integrative Structural & Computational Biology, Scripps Research; La Jolla, California 92037, United States.

[5] Department of Molecular Medicine, Scripps Research; La Jolla, California 92037, United States.

[6] Department of Chemistry, Scripps Research; La Jolla, California 92037, United States.

[7] Division of Infectious Diseases, University of Pittsburgh School of Medicine, Pittsburgh, PA 15213.

[#] These authors contributed equally

* Corresponding authors: moses@cshl.edu, hhang@scripps.edu

Abstract

Vancomycin-resistant *Enterococcus faecium* (VREfm) is a leading cause of healthcare-associated infections globally and demands new approaches for treatment. Here we show that genetic and pharmacological inactivation of a highly conserved NlpC/P60 peptidoglycan hydrolase, secreted antigen A (SagA), enhanced antibiotic susceptibility in VREfm *ex vivo* and *in vivo*. Genetic deletion of *sagA* impaired VREfm peptidoglycan remodeling, growth and increased antibiotic susceptibility, which notably also restored vancomycin sensitivity in VREfm. We then identified first-in-class covalent NlpC/P60 peptidoglycan hydrolase inhibitors and demonstrated that pharmacological inactivation of SagA activity also impaired peptidoglycan remodeling and promoted vancomycin susceptibility across distinct VREfm clinical isolates. Our study reveals peptidoglycan hydrolases are druggable targets whose inhibition boosts the efficacy of antibiotics against VREfm.

Introduction

Increasing antimicrobial resistance (AMR) in bacterial pathogens and limited antibiotic discovery require new approaches to address this major threat to human health world-wide.[1] Amongst the ESKAPE pathogens,[2] vancomycin-resistant *E. faecium* (VREfm) infections have become more prevalent among healthcare-associated infections and can acquire resistance to last-resort antibiotics like linezolid, daptomycin, and tigecycline.[3,4] The AMR crisis demands new approaches

to prevent and treat VREfm infections, which are also correlated with poor patient outcomes leading to high mortality rates.[5,6] While the synthesis of next-generation antibiotics provides new derivatives to address AMR[7,8] and innovative approaches are being employed to discover new classes of antibiotics,[1,9,10] a better understanding of *E. faecium* biology may provide new targets for antimicrobial development.

Enterococcus is a genus of ubiquitous Gram-positive bacteria, among which *E. faecium* and *E. faecalis* are the most prominent in humans and other mammals.[11] While *E. faecium* can acquire antibiotic resistance and cause healthcare-associated infections,[2,11,12] non-pathogenic strains of *E. faecium* have been reported to have beneficial effects on host physiology and been developed into probiotics.[13] Our mechanistic dissection of commensal *E. faecium*-host interactions revealed that secreted antigen A (SagA), a highly conserved NlpC/P60 peptidoglycan hydrolase, can generate non-crosslinked muropeptides to promote host immunity.[14–19] Of note, we also demonstrated *sagA* is essential for peptidoglycan remodeling, cell separation and growth in the commensal strain of *E. faecium* (Com15).[19] Moreover, the commensal strains of *E. faecium* (Com15-D*sagA* and phage-resistant Com12 expressing catalytically inactive alleles of *sagA*) were more susceptible to cell-wall targeting antibiotics,[19–21] suggesting SagA may be a potential antimicrobial target.

As *sagA* is highly conserved amongst *E. faecium* strains, including VREfm strains containing the vancomycin resistance *vanA* and *vanB* gene clusters,[17] we investigated genetic and pharmacological inactivation of this key peptidoglycan hydrolase as a therapeutic target for treating VREfm infections. We discovered that VREfm-Δ*sagA* showed defective peptidoglycan remodeling, impaired cell separation and growth as well as increased susceptibility to front- and last-line antibiotics. Notably, even though a VREfm-Δ*sagA* strain still encodes the *vanA* operon, the minimal inhibitory concentration (MIC) of vancomycin was significantly decreased and attenuated by vancomycin treatment in a mouse model of VREfm-induced sepsis *in vivo*. In parallel, we explored pharmacological inactivation of SagA activity and identified the first-in-class covalent inhibitors of these NlpC/P60 cysteine endopeptidases from a library of Sulfur(VI) Fluoride Exchange (SuFEx)-based sulfonyl fluorides accessed through a Diversity Oriented Clicking (DOC) approach[22–24]. The most potent sulfonyl fluoride SagA inhibitor impaired peptidoglycan remodeling in VREfm, reduced the MIC of vancomycin in multiple VREfm strains, attenuated infection of macrophages *ex vivo,* and improved outcomes of VREfm-induced sepsis *in vivo*. Our studies demonstrate that peptidoglycan hydrolases are crucial for bacterial cell wall remodeling and are druggable targets to promote the efficacy of antibiotics against VREfm.

Results

SagA is critical for peptidoglycan remodeling and antibiotic susceptibility of VREfm.

SagA is a member of the highly conserved NlpC/P60-family of cysteine endopeptidases that are important for bacterial physiology.[25] We previously demonstrated SagA is crucial for commensal *E. faecium* (Com15 strain) peptidoglycan remodeling, cell separation and growth,[19] but its function in VREfm strains that express additional NlpC/P60 hydrolases (Extended Data Fig. 1a) was unknown. Using improved genetic methods for *Enterococcus*,[26,27] we generated isogenic deletion strains of all 4 NlpC/P60 hydrolases in the human clinical VREfm isolate ERV165 (sequence type 412; *vanA* genotype) (Extended Data Fig. 1b-d) and found that only the ERV165-Δ*sagA* mutant exhibited impaired growth and altered colony morphology (Fig. 1a-c and Extended Data Fig. 1e), which was rescued by *sagA* chromosomal complementation (ERV165-Δ*sagA*::*sagA*).

Transmission electron microscopy (TEM) analysis revealed that ERV165-Δ*sagA* cells failed to properly separate, resulting in the formation of aberrant cellular clusters (Fig. 1d). Further cryo-electron tomography (cryo-ET) analysis of ERV165-Δ*sagA* showed a decrease in cell wall thickness and a modest increase in septum thickness (Extended Data Fig. 2 and 3). The cell wall thickness was restored in the *sagA*-complemented strain, however no significant changes in septum thickness were observed (Extended Data Fig. 3c). Similar to Com15-Δ*sagA* mutant[19], ERV165-Δ*sagA* also exhibited lower amounts of non-crosslinked muropeptides and increased levels of crosslinked peptidoglycan fragments (Extended Data Fig. 4). These results demonstrate that in addition to its importance in commensal *E. faecium* strains, *sagA* is also essential for VREfm peptidoglycan remodeling, bacterial cell separation and growth, even though the majority of VREfm strains have acquired additional NlpC/P60 hydrolases (Extended Data Fig. 1a).

We next evaluated the contribution of SagA to VREfm antibiotic susceptibility. Similar to the commensal *E. faecium* Com15-Δ*sagA* mutant, VREfm ERV165-Δ*sagA* exhibited increased susceptibility to ampicillin, daptomycin and ceftriaxone (Extended Data Fig. 5a-c). Notably, ERV165-Δ*sagA*, but not other NlpC/P60 hydrolase deletion strains (Extended Data Fig. 5d), showed increased susceptibility to vancomycin, which was abrogated in the *sagA*-complemented strain (Fig. 2a and Extended Data Table 1). To investigate the vancomycin susceptibility of ERV165-Δ*sagA*, we performed whole-genome sequencing (WGS), evaluated antibiotic binding and analyzed peptidoglycan remodeling further. WGS of the ERV165-Δ*sagA* strain revealed 11 missense and 12 silent mutations (Extended Data Table 2 and 3), none of which were associated with peptidoglycan synthesis or vancomycin resistance (Extended Data Fig. 6). Importantly, the increased antibiotic susceptibility of ERV165-Δ*sagA* was abrogated in the *sagA*-complemented strain (Fig. 2a and Extended Data Table 4 and 5). We then employed fluorescent vancomycin (Van-BODIPY)[28] and fluorescent D-amino acid (HADA)[29] to evaluate antibiotic binding and peptidoglycan stem peptide remodeling, respectively. Fluorescence microscopy revealed increased Van-BODIPY and HADA staining in ERV165-Δ*sagA* that was abrogated by *sagA* complementation (Fig. 2b-d). These results suggest that loss of SagA expression and defective peptidoglycan remodeling lead to the restoration of vancomycin binding and increased antibiotic susceptibility.

To evaluate the impact of SagA on VREfm infection *in vivo*, we employed a mouse peritonitis infection model[30]. All three strains (ERV165, Δ*sagA* and *sagA*-complemented strain) caused similar levels of weight loss as a marker of infection and exhibited high bacterial burdens in the spleen and liver (Fig. 2e,f). However, treatment with clinical doses of vancomycin[31] significantly improved weight loss and cleared bacterial burden in mice infected with ERV165-Δ*sagA* strain, but not in those infected with the WT or *sagA*-complemented strains (Fig. 2e,f). These results demonstrate that SagA not only impacts peptidoglycan remodeling and activity of cell wall-targeting antibiotics in commensal *E. faecium* strains, but importantly also modulates vancomycin susceptibility in VREfm *ex vivo* and VREfm-induced sepsis *in vivo*.

SuFEx-based sulfonyl fluorides covalently label and inactivate SagA NlpC/P60 hydrolase activity.

To identify pharmacological inhibitors of SagA endopeptidase activity, we developed a high-throughput assay based on competitive labeling[32] of the only cysteine residue (C433) in the NlpC/P60 hydrolase domain active site[33] using a fluorescent tetramethyl rhodamine-

127 iodoacetamide (TMR-IA) probe (Fig. 3a and Extended Data Fig. 7a). TMR-IA selectively labeled
128 the recombinant SagA-NlpC/P60 hydrolase domain, but not the inactive C433A mutant or WT
129 pretreated with cysteine-reactive controls N-methylmaleimide (NMM) or iodoacetamide (IA)
130 (Extended Data Fig. 7b-d). Using this assay, we screened a focused library of Sulfur-Fluoride
131 Exchange (SuFEx)-based sulfonyl fluorides[22] for potential covalent inhibitors of SagA and
132 identified 86 sulfonyl fluorides that reduced TMR-IA labeling greater than 80% (Extended Data
133 Fig. 7e). Secondary screening of the top sulfonyl fluorides using gel-based competitive TMR-IA
134 labeling (Extended Data Fig. 7f-i) and follow-up SagA peptidoglycan hydrolase activity assays[34]
135 (Extended Data Fig. 8a), revealed a subset of β-chloro alkenyl sulfonyl fluoride compounds
136 (peptidoglycan hydrolase inhibitors, pghi-1 to 5) with low micromolar IC_{50} values *in vitro* (Fig. 3b,c
137 and Extended Data Fig. 8b). Small modifications in the phenyl ring (pghi-1 to 5) did not
138 substantially affect SagA inhibition *in vitro*, whereas substitution of the β-alkenyl position (pghi-6)
139 compromised inhibition potency (Fig. 3b,c and Extended Data Fig. 8b).

140 Computational covalent docking suggested that these peptidoglycan hydrolase inhibitors can be
141 accommodated in the active site, stabilized by interactions with nearby H494 and F522, after
142 reacting with Cys (C443) of SagA via the sulfonyl fluoride group (Fig. 3d) or β-alkenyl chloride
143 group (Extended Data Fig. 9a). Intact protein mass analysis of recombinant SagA treated with
144 pghi-4 revealed a mass shift that corresponds to the mass of the SagA-pghi-4 adduct (Fig. 3e).
145 The observed mass increase matched the calculated molecular weight loss of fluorine from pghi-
146 4, suggesting covalent modification through the sulfonyl fluoride group and formation of a
147 thiosulfonate adduct (Extended Data Fig. 9b-d). Indeed, treatment of the catalytically inactive
148 C433A SagA mutant with pghi-4 did not result in a mass shift (Fig. 3e). Incubation of SagA with
149 an inactive pghi-6 resulted in minor formation of thiosulfonate-linked SagA-pghi-6 adduct
150 (Extended Data Fig. 9e) indicating the importance of the β-vinyl chloro group for binding to SagA.
151 Our efforts to crystallize SagA-pghi-4 complex did not yield diffraction quality crystals, likely due
152 to instability of the SagA-pghi-4 adduct. Further analysis of the SagA-pghi-4 adducts (peak 1,
153 thiosulfonate, Extended Data Fig. 9b-d) identified peaks 3 and 5 with masses corresponding to
154 thiosulfonic and sulfinic acid derivatives of SagA (Extended Data Fig. 9b-d). After 16 hours of
155 treatment, the abundance of the SagA-pghi-4 adduct significantly decreased, while the levels of
156 hydrolysis products increased (Extended Data Fig. 9b-d), indicating instability of the SagA-pghi-
157 4 adduct. To explore the selectivity of identified pghi-1 to 5, we evaluated these compounds with
158 other VREfm ERV165 NlpC/P60 hydrolases *in vitro*. Pghi-1 to 5 also inhibited the endopeptidase
159 activity of peptidoglycan hydrolase 2 (PGH2), which has NlpC/P60 domain with high amino acid
160 sequence and structural homology to SagA, but not the more divergent CwlT-like peptidoglycan
161 hydrolase 3 (PGH3) (Extended Data Fig. 10a-c). Taken together, these results suggest that the
162 identified β-chloro alkenyl sulfonyl fluorides can bind and covalently react with the catalytic
163 cysteine of SagA and peptidoglycan hydrolase orthologs with structurally similar NlpC/P60
164 hydrolase domains to inactivate their enzymatic activity.

165

166 **SagA inhibitors improve antibiotic susceptibility in VREfm strains.**

167 We next evaluated the activity of pghi-1 to 6 on VREfm growth and antibiotic susceptibility. Either
168 pghi-4 or pghi-5 alone caused a mild growth delay of VREfm (ERV165), while the other
169 compounds did not significantly affect VREfm growth under laboratory conditions (Extended Data
170 Fig. 11a,b). Building upon our observations of SagA modulation of VREfm antibiotic susceptibility
171 (Figs. 1 and 2), we evaluated these compounds on VREfm growth in combination with a low dose

172 of vancomycin (Fig. 4a and Extended Data Fig. 11c). Notably, pghi-4 and pghi-5 significantly
173 enhanced the activity of vancomycin compared to the other β-chloro alkenyl sulfonyl fluorides and
174 the inactive analog pghi-6 (Fig. 4a and Extended Data Fig. 11c). The most active compound pghi-
175 4 lowered the MIC values of vancomycin in a concentration-dependent manner by checkerboard
176 assay analysis (Fig. 4b and Extended Data Table 6). Bacterial time-kill analysis showed that pghi-
177 4 in combination with vancomycin significantly limited VREfm ERV165 growth compared to either
178 agent alone (Fig. 4c and Extended Data Fig. 11d). Moreover, pghi-4 enhanced antibiotic
179 susceptibility of ampicillin and daptomycin, but not ceftriaxone in VREfm ERV165 (Extended Data
180 Fig. 11e,f).

181 To characterize the scope of pghi-4 adjuvant activity with vancomycin, we evaluated additional
182 VREfm strains including clinical isolates from patients that underwent chemotherapy or
183 hematopoietic stem cell transplantation[35]. Notably, some VREfm strains (700221, DVT1574,
184 DVT3347) showed increased susceptibility to pghi-4 and vancomycin co-treatment compared
185 ERV165 and other VREfm strains (Fig. 4d and Extended Data Fig. 12), even though they all
186 harbor *vanA*-type resistance[35], of different sequence types (Extended Data Table 7) and exhibit
187 similar vancomycin MICs (Extended Data Table 8). Interestingly, pghi-4 adjuvant activity
188 correlated with intracellular SagA protein expression levels in these VREfm strains (Extended
189 Data Fig. 12b). These results suggest β-chloro-alkenyl sulfonyl fluoride SagA inhibitors can
190 increase the antibiotic susceptibility, notably to vancomycin, of VREfm and their efficacy
191 correlates with SagA protein levels in VREfm clinical isolates.

192 To characterize the mechanism of action of SagA inhibitor pghi-4, we performed imaging,
193 peptidoglycan remodeling and chemoproteomic studies of VREfm. Differential interference
194 contrast (DIC) microscopy revealed that pghi-4 in combination with vancomycin induced aberrant
195 bacterial colony morphology and increased cell clustering compared to control or either agent
196 alone (Fig. 4e,f). Cryo-ET showed dead cells with impaired peptidoglycan cleavage in VREfm
197 treated with pghi-4 in combination with vancomycin (Extended Data Fig. 13). Both pghi-4 and
198 vancomycin alone increased cell wall thickness, but their combination resulted in reduced
199 thickness (Extended Data Fig. 14a,b). Interestingly, septum thickness was significantly increased
200 under all treatment conditions (Extended Data Fig. 14a,c). These results suggest that the
201 combination of pghi-4 and vancomycin impaired the ultrastructure of VREfm peptidoglycan.
202 Similar to VREfm ERV165-Δ*sagA*, pghi-4 also increased Van-BODIPY (Fig. 4f,g) and HADA (Fig.
203 4f,h) labeling, suggesting enhanced vancomycin binding due to inhibition of peptidoglycan
204 remodeling and the accumulation of vancomycin-target D-Ala-D-Ala-containing muropeptides [36].
205 Quantitative LC-MS analysis of pghi-4-treated ERV165 did not yield similar profiles of
206 peptidoglycan fragments compared to ERV165-Δ*sagA* (Extended Data Fig. 15e,f). However, for
207 these experiments ERV165 was only treated with sub-inhibitory and non-bactericidal dose of 50
208 mM pghi-4 to obtain sufficient material for LC-MS analysis. Moreover, the genetic inactivation of
209 *sagA* may result in accumulation or depletion of peptidoglycan fragments that are not fully
210 recapitulated with pharmacological inhibition of SagA. Nonetheless, LC-MS analysis of digested
211 peptidoglycan fragments from pghi-4 and vancomycin-treated ERV165 revealed higher levels of
212 D-Ala-D-Ala-containing GlcNAc-MurNAc-pentapeptide (Extended Data Fig. 15e,f). As pghi-4
213 targets the active site C443 of SagA *in vitro* (Fig. 3d,e), we also evaluated covalent labeling of
214 SagA and other reactive Cys-residues in ERV165 by competitive chemoproteomics using an
215 iodoacetamide-alkyne (IA-alk) probe (Extended Data Fig. 16a). Indeed, treatment of ERV165 with
216 pghi-4 reduced IA-alk labeling of the SagA by in-gel fluorescence labeling and western blot
217 analysis (Extended Data Fig. 16b). The quantitative proteomic analysis of pghi-4-competitive Cys-

218 reactive protein targets showed only a few other proteins were targeted in a dose-dependent
219 manner (Extended Data Fig. 16c). However, none of these other Cys-reactive candidate pghi-4-
220 target proteins have been implicated in VREfm peptidoglycan remodeling or antibiotic
221 susceptibility. Collectively, our data suggests that pharmacological inactivation of SagA by pghi-
222 4 increases vancomycin susceptibility of VREfm by impairing peptidoglycan remodeling and cell
223 separation, which phenocopies the effects that we observed with VREfm ERV165-Δ*sagA*.

224

225 **Pharmacological inactivation of SagA increases vancomycin susceptibility of VREfm *in***
226 ***vivo*.**

227 To investigate the therapeutic potential of SagA inhibitor pghi-4 as an antibiotic adjuvant, we
228 evaluated its ability to potentiate vancomycin activity using cellular and mouse models of VREfm
229 infection. The combination of pghi-4 and vancomycin, but not either agent alone, reduced VREfm
230 infection of murine (RAW264.7) (Fig. 4i) and human (THP-1) monocytes (Extended Data Fig. 17a)
231 in a dose-dependent manner, that was not attributed to pghi-4 cytotoxicity (Extended Data Fig.
232 17b). We next tested therapeutic efficacy of the combination therapy *in vivo*. A single dose of
233 pghi-4 in combination with vancomycin did not significantly decrease VREfm counts in mouse
234 organs 6- or 24-hours post-infection compared to PBS treatment (Extended Data Fig. 18).
235 However, a two-dose therapeutic regimen significantly reduced weight loss in VREfm-infected
236 mice co-treated with vancomycin and pghi-4 (Fig. 4j). Colony forming unit (CFU) analysis of
237 spleen and liver further demonstrated a significant reduction of VREfm burden in the vancomycin
238 and pghi-4 co-treated group compared to PBS, while monotherapies had no significant effect (Fig.
239 4k). These results demonstrate that pharmacological inactivation of SagA in combination with
240 vancomycin can attenuate VREfm infection *ex vivo* and VREfm-induced sepsis *in vivo*.

241

242 **Discussion**

243 Bacterial infections cause a significant healthcare and financial burden worldwide. While
244 antibiotics help manage bacterial infections, many bacterial pathogens have acquired antibiotic
245 resistance and now are difficult to treat, with 4.7 million deaths associated with AMR worldwide in
246 2019.[37] Progress in development of new antibiotic agents and targets have resulted in novel
247 approaches to combat antibiotic-resistant bacteria.[38–44] Recently, combination therapeutic
248 approaches using antibiotic adjuvants (non-antimicrobial agents enhancing antibiotic activity)
249 have provided new entities to extend the lifespan of clinical antibiotics.[45–50] For example,
250 combination treatment with β-lactamase inhibitors (BLIs) overcame antibiotic resistance and
251 restored β-lactam activity against bloodstream infections in hematological neutropenic patients.[51]
252 This therapeutic combination of an antibiotic adjuvant coupled with an existing antibiotic showed
253 clinical potential and is promising for further development, however, antibiotic adjuvants for other
254 classes of antibiotics are underdeveloped. The alarming increase of VREfm infections[52,53] and
255 evolution of antibiotic resistance in patients highlights the urgent need for new therapeutic
256 approaches to overcome resistance and prevent adaptation in vulnerable hosts.[35]

257 In this study, we demonstrated that SagA, an important NlpC/p60 peptidoglycan hydrolase,
258 modulates antibiotic susceptibility in VREfm and can be pharmacologically targeted for improved
259 combination therapy (Extended Data Fig. 19). Deletion of *sagA* increased VREfm susceptibility to
260 cell-wall antibiotics including vancomycin, which could be rescued by *sagA* re-expression.

Notably, the VREfm-Δ*sagA* mutant strain caused systemic infection in mice, but was effectively cleared by a clinical dose of vancomycin that failed to eliminate WT VREfm. Based on these observations, we identified the first-in-class NlpC/p60 peptidoglycan hydrolase inhibitors (pghi-1 to 5) and demonstrated these β-chloro alkenyl sulfonyl fluorides covalently label the active site of SagA and inhibit peptidoglycan hydrolase activity *in vitro*. These β-chloro alkenyl sulfonyl fluorides can also inhibit other NlpC/p60 endopeptidases *in vitro* and may covalently label other proteins in VREfm, but we showed that other peptidoglycan hydrolases and candidate protein targets are not important for VREfm growth or vancomycin susceptibility. In VREfm strains, the pharmacological inactivation of SagA by the most effective β-chloro alkenyl sulfonyl fluoride, pghi-4, inhibited peptidoglycan remodeling, increased vancomycin binding and restored its antibacterial activity *ex vivo* and *in vivo*. While new natural products and their derivatives have been reported to broadly inhibit peptidoglycan remodeling or target CHAP (cysteine, histidine-dependent amidohydrolases/peptidases) domain containing hydrolases in other Gram-positive bacterial pathogens,[54,55] our studies demonstrate NlpC/p60 peptidoglycan hydrolases and their inhibitors may serve as important antimicrobial targets and agents against VREfm. The further development of covalent NlpC/p60 hydrolase inhibitors should afford new antimicrobial adjuvants to prevent and treat VREfm infections. More broadly, our studies suggest peptidoglycan hydrolases that have also been implicated in the growth and division of bacterial pathogens[25] may be important targets for the development of new antimicrobials and adjuvants.

Methods

Chemistry

The synthesis and characterization of sulfonyl fluorides identified as SagA inhibitors in this work are reported elsewhere [22]. Characterization of resynthesized pghi-4 matched the previous report (Extended Data Fig. 20-23). ^{1}H NMR (400 MHz, $CDCl_3$) δ 7.36 (dd, *J* = 8.5, 2.4 Hz, 1H), 7.17 (d, *J* = 2.3 Hz, 1H), 6.96 (d, *J* = 2.3 Hz, 1H), 6.93 (d, *J* = 8.6 Hz, 1H), 4.88 (tt, *J* = 6.3, 3.1 Hz, 1H), 3.93 (s, 3H), 2.09 – 1.98 (m, 2H), 1.97 – 1.89 (m, 3H), 1.90 – 1.80 (m, 2H), 1.67 (tdd, *J* = 10.6, 7.5, 4.8 Hz, 2H); ^{13}C NMR (101 MHz, $CDCl_3$) δ 152.4, 152.1, 150.0, 125.7, 121.8, 115.4, 115.2, 113.6, 110.7, 80.9, 56.4, 33.0, 24.3; ^{19}F NMR (377 MHz, $CDCl_3$) δ 65.0; LCMS (ESI$^+$): calculated for $C_{14}H_{16}ClFO_4SNa$ $[M+H]^+$: m/z = 335.05, m/z found 335.09.

Bacteria

The bacterial species used in this study are listed in Extended Data Table 9. All *Enterococcus* were grown aerobically at 37 °C at 200 RPM shaking in Brain Heart Infusion (BHI) broth (Fisher Scientific, 237500) with appropriate antibiotics. Following Clinical & Laboratory Standards Institute (CLSI) guidelines, vancomycin susceptibility of *E. faecium* was evaluated in Mueller Hinton Broth (MHB, BD 275730). *E. coli* was grown in Luria-Bertani (LB, BD 244610) broth.

Plasmids construction

1. pPK99 (pJC005.gent-Δ*sagA*)

Oligo name	Oligo sequence
oPK996	GCATGAGTCAGCGATGActcgagATAATCTTTAATTTGAAAAGATTTAAGG CTTATTTAAATAAAAAATATGAGGG

oPK997	atcttgctgttgtatctgagaatATCTACAAGAGTAGAAATTATGGTGGAATGATAAGG
oPK998	ttctcagatacaacagcaagatAATTTCTACTCTTGTAGATAGCTCCATGCCTTAGTGGTGACCC
oPK999	CTCTTTTTGATTAATCATTCTCTTCATTCCTCCGACTGGCTTAATTTAATAAATATCT
oPK1000	GCCAGTCGGAGGAATGAAGAGAATGATTAATCAAAAAGAGTTAGCCCATTCTGGAC
oPK1001	CTAAGGATTCAGAACggcgcgccGGTAAAGAAAAAATGGAATGGCAAGATCAAGATG

Using oligos oPK996 and oPK997, the sRNA promoter driving the *sagA* protospacer was PCR-amplified (using pUCsRNAP plasmid as template). oPK996 contains an XhoI restriction site (indicated in lowercase), and oPK997 includes the *sagA* protospacer from *E. faecium* ERV165 (indicated in lowercase and underlined) to serve as the CRISPR-Cas12a target for counter-selection during the recombineering process. Similarly, oPK998 (which includes the identical *sagA* protospacer sequence in underlined lowercase and a repeat region in underlined uppercase) and oPK999 were used to amplify the upstream flanking region of *sagA* using *E. fm* ERV165 genomic DNA (gDNA) as template, while oPK1000 and oPK1001 (the latter containing an AscI site, shown in lowercase) amplified the downstream *sagA* flanking region using the same gDNA as template. All oligos were designed such that the three resulting PCR products contained 35–40 bp overlapping regions and were assembled using splicing by overlap extension (SOE) PCR. The resulting fragment was cloned into the pJC005.gent vector via XhoI and AscI restriction digestion followed by ligation. Positive clones were screened in *E. coli* NEB-5α, yielding the construct pPK99. This plasmid was then transformed into *E. faecium* ERV165 for generation of the clean *sagA* deletion mutant (sPK377), as described below.

2. pPK158 (pJC005.gent^{R}-*sagA* chromosomal complementation plasmid)

Oligo name	Oligo sequence
oPK996	GCATGAGTCAGCGATGActcgagATAATCTTTAATTTGAAAAGATTTAAGGCTTATTTAAATAAAAAATATGAGGG
oPK1020	tttaaggaaatttagtgctaaacATCTACAAGAGTAGAAATTATGGTGGAATGATAAGGGTTTG
oPK1021	gtttagcactaaatttccttaaaAATTTCTACTCTTGTAGATGGGCTTTGGAAGAAAAAGGCTACAATCC
oPK1022	CAACGATTCTTTTTCGCTTTCGACCAAAAACCGGGCTCTACTTTTCAGAGAGTC
oPK1023	TAGAGCCCGGTTTTTGGTCGAAAGCGAAAAAGAATCGTTGTTATC
oPK1024	TTTAAGGAAATTTAGTGCTAAACGACTGATTTCTATTTTATCACAATAAAAAAAGAGTTAGTCCAG

oPK1025	TTATTGTGATAAAATAGAAATCAGTCGTTTAGCACTAAATTTCCTTAAAAA GTAGAAAAG
oPK1026	GCTAAGGATTCAGAACggcgcgccTTAAATGAATTTTTTTATCACAGTATAC TCCTTTTTTCAC

For *sagA* chromosomal complementation in the VREfm ERV165 Δ*sagA* clean deletion mutant (sPK377), a neutral chromosomal locus was selected downstream of the Holliday junction resolvase gene *ruvX*, where no signatures of nearby gene promoters or terminators were detected (Extended Data Fig. 1b). This site contained a protospacer adjacent motif (PAM), making it suitable for CRISPR-Cas12a-based counter-selection. The *sagA* complementation plasmid (pPK158) was constructed by integrating the *sagA* gene into the selected PAM site, thereby disrupting it for CRISPR-Cas12a-based counter-selection. The construct included all essential regulatory elements of ERV165 *sagA*: the native *sagA* promoter, ribosome binding site (RBS), open reading frame (ORF), and transcriptional terminator.

Briefly, the small RNA (sRNA) promoter, derived from the pUCsRNAP template and driving the neutral locus protospacer, was PCR-amplified using oligos oPK996 and oPK1020. oPK996 includes an XhoI restriction site (in lowercase), while oPK1020 contains the neutral locus protospacer from *E. faecium* ERV165 (in lowercase and underlined), which served as the CRISPR-Cas12a target during recombineering. The upstream region of the neutral locus was amplified using *sagA* clean deletion (sPK377) gDNA as template with oligos oPK1021 and oPK1022. oPK1021 has the protospacer (underlined lower case) and a repeat region (underlined uppercase). The ERV165 *sagA* promoter, RBS, ORF, and both translational and transcriptional terminators were amplified using oPK1023 and oPK1034 using *E. fm* ERV165 gDNA as template. Finally, the downstream region of the neutral locus was amplified using sPK377 gDNA as template with oPK1025 and oPK1026, which include AscI restriction sites (in lowercase). All oligos were designed such that the three resulting PCR products contained 35–40 bp overlapping regions and were assembled using splicing by overlap extension (SOE) PCR. The resulting fragment was cloned into the pJC005.gent vector *via* XhoI and AscI restriction digestion followed by ligation. Positive clones were screened in *E. coli* NEB-5α, yielding the construct pPK158. This plasmid was then transformed into *E. faecium* ERV165 for generation of *sagA* chromosomal complementation strain in Δ*sagA* clean deletion mutant (sPK394), as described below.

3. pPK156 (pJC005.gent- Δ*pgh2*)

Oligo name	Oligo sequence
oPK996	GCATGAGTCAGCGATGActcgagATAATCTTTAATTTGAAAAGATTTAAGGC TTATTTAAATAAAAAATATGAGGG
oPK1002	gcagtcagttggatcttaccaatATCTACAAGAGTAGAAATTATGGTGGAATGATAAG G
oPK1003	attggtaagatccaactgactgcAATTTCTACTCTTGTAGATTGCAATTAGTATTTGTA CCTTTACTTTCATTAGTTATCACGGTTCC
oPK1004	AGTGTCACATCCCCTTTTTAATTTATTAATAAACTAGTCCTTTTCCTTTCAT TGATTTTCTGTCTTATTCAGCA

oPK1005	CAATGAAAGGAAAAGGACTAGTTTATTAATAAATTAAAAAGGGGATGTGA CACTGTCACACTCCC
oPK1006	AGGATTCAGAACggcgcgccGGCACGGGTTGTTCATTTTCAAACAATAATCG ATAATGA
oPK1002	GCAGTCAGTTGGATCTTACCAATATCTACAAGAGTAGAAATTATGGTGGA ATGATAAGG

Using oligos oPK996 and oPK1002, the sRNA promoter driving the *pgh2* protospacer was PCR-amplified (using pUCsRNAP plasmid as template). oPK996 contains an XhoI restriction site (indicated in lowercase), and oPK1002 includes the *pgh2* protospacer from *E. faecium* ERV165 (indicated in lowercase and underlined) to serve as the CRISPR-Cas12a target for counter-selection during the recombineering process. Similarly, oPK1003 (which includes the identical *pgh2* protospacer sequence in underlined lowercase and a repeat region in underlined uppercase) and oPK1004 were used to amplify the upstream flanking region of *pgh2* using *E. fm* ERV165 genomic DNA (gDNA) as template, while oPK1005 and oPK1006 (the latter containing an AscI site, shown in lowercase) amplified the downstream *pgh2* flanking region using the same gDNA as template. All oligos were designed such that the three resulting PCR products contained 35–40 bp overlapping regions and were assembled using splicing by overlap extension (SOE) PCR. The resulting fragment was cloned into the pJC005.gent vector via XhoI and AscI restriction digestion followed by ligation. Positive clones were screened in *E. coli* NEB-5α, yielding the construct pPK156. This plasmid was then transformed into *E. faecium* ERV165 for generation of the clean *pgh2* deletion mutant, as described below.

4. pPK107 (pJC005.gent- Δ*pgh3*)

Oligo name	Oligo sequence
oPK656	CTAAATAAAAAGATGCCAGTGTGCTGGAATTCGTCATAATCTTTAATTTGAAA AGATTTAAG
oPK639	ATAATCTTTAATTTGAAAAGATTTAAGGCTTATTTAAATAAAAAATATGAGGG AAG
opK844	actacttccttcactgtcttcacATCTACAAGAGTAGAAATTATGGTGGAATGATAAGG
opK845	gtgaagacagtgaaggaagtagtAATTTCTACTCTTGTAGATTTATGATGCGAGCAGG AGTTACTTT
opK846	TTTTATCTTCATTCTTTTTCCTCTTTTCTCTTTTTCTCACCTGACCTTGGTTTG GG
opK847	CCCAAACCAAGGTCAGGTGAGAAAAAGAGAAAAGAGGAAAAAGAATGAAGA TAAAAATTGAACGGAATC
opK848	CTTGCATGTCTGCAGGCCTCGAGGGATGGGCGACTTCTGCCTGAAATAAG
oPK659	CACGACGTTGTAAAACGACGGCCAGTGCCAAGCTTGCATGTCTGCAGGCC

Using oligos oPK639, the sRNA promoter driving the *pgh3* protospacer was PCR-amplified (using pUCsRNAP plasmid as template). oPK844 contains *pgh3* protospacer from *E. faecium* ERV165

359 (indicated in lowercase and underlined) to serve as the CRISPR-Cas12a target for counter-
360 selection during the recombineering process. Similarly, oPK845 (which includes the identical *pgh3*
361 protospacer sequence in underlined lowercase and a repeat region in underlined uppercase) and
362 oPK846 were used to amplify the upstream flanking region of *pgh3* using *E. fm* ERV165 genomic
363 DNA (gDNA) as template, while oPK847 and oPK848 amplified the downstream *pgh3* flanking
364 region using the same gDNA as template. All oligos were designed such that the three resulting
365 PCR products contained 35–40 bp overlapping regions and were assembled using splicing by
366 overlap extension (SOE) PCR using oPK656 and oPK659. The resulting fragment was cloned
367 into the pJC005.gent vector via XhoI and AscI restriction digestion followed by ligation. Positive
368 clones were screened in *E. coli* NEB-5α, yielding the construct pPK107. This plasmid was then
369 transformed into *E. faecium* ERV165 for generation of the clean *pgh3* deletion mutant, as
370 described below.

371 5. pPK154 (pJC005.gent- Δ*pgh4*)

Oligo name	Oligo sequence
oPK996	GCATGAGTCAGCGATGActcgagATAATCTTTAATTTGAAAAGATTTAAGGCTTATTT AAATAAAAAATATGAGGG
oPK1007	ttttgaaaaagattcggctaaagATCTACAAGAGTAGAAATTATGGTGGAATGATAAGG
oPK1008	ctttagccgaatctttttcaaaaAATTTCTACTCTTGTAGATtagtcattacgactgcattcagtatctccacgat
oPK1009	CATTTTCCATTCCTCTTTTCATCTTTTCTCACCTGGCTTTGGTTTTGGG
oPK1010	GCCAGGTGAGAAAAGATGAAAAGAGGAATGGAAAATGAAGATAAAAATTGAGCGA AGTAACAAGG
oPK1011	GCTAAGGATTCAGAACggcgcgccAAGCTATTGCACAACACAAACATTTGAACGACG

372 Using oligos oPK996 and oPK1007, the sRNA promoter driving the *pgh4* protospacer was PCR-
373 amplified (using pUCsRNAP plasmid as template). oPK996 contains an XhoI restriction site
374 (indicated in lowercase), and oPK1007 includes the *pgh4* protospacer from *E. faecium* ERV165
375 (indicated in lowercase and underlined) to serve as the CRISPR-Cas12a target for counter-
376 selection during the recombineering process. Similarly, oPK1008 (which includes the identical
377 *pgh4* protospacer sequence in underlined lowercase and a repeat region in underlined
378 uppercase) and oPK1009 were used to amplify the upstream flanking region of *pgh4* using *E. fm*
379 ERV165 genomic DNA (gDNA) as template, while oPK1010 and oPK1011 (the latter containing
380 an AscI site, shown in lowercase) amplified the downstream *pgh4* flanking region using the same
381 gDNA as template. All oligos were designed such that the three resulting PCR products contained
382 35–40 bp overlapping regions and were assembled using splicing by overlap extension (SOE)
383 PCR. The resulting fragment was cloned into the pJC005.gent vector via XhoI and AscI restriction
384 digestion followed by ligation. Positive clones were screened in *E. coli* NEB-5α, yielding the
385 construct pPK154. This plasmid was then transformed into *E. faecium* ERV165 for generation of
386 the clean *pgh4* deletion mutant, as described below.

387 **Preparation of electrocompetent *E. faecium* ERV165 cells and electroporation**

388 The protocol described below is a standardized procedure used in our lab. A single colony of *E.*
389 *faecium* ERV165 and their mutant derivatives were inoculated into 4 mL of plain BHI and grown
390 overnight. The culture was then diluted 1:50 into 200 mL GS-BHI (BHI + 4% glycine + 0.5 M

391 sucrose) and incubated overnight (14–16 hours). From this point onward, cells were handled
392 gently to preserve viability. Cells were harvested by centrifugation at 1,000 × *g* for 15 min at room
393 temperature (RT), gently resuspended in 100 mL GS-BHI (as described below), and incubated
394 without shaking at 37°C for 1.5 hours. Cells were re-pelleted (1,000 × *g*, 15 min, 4°C), gently
395 washed with 35–40 mL ice-cold electroporation solution, and kept on ice. The harvested cells
396 were then resuspended in 1–2 mL electroporation solution and homogenized using a sterile
397 serological pipette. Aliquots (100 µL) were prepared in pre-chilled Eppendorf tubes and stored at
398 –80°C. For electroporation, thawed 100 µL aliquots were mixed with 2-4 µg DNA and transferred
399 to 0.2 cm gap cuvettes. Electroporation was carried out at 25 µF, 400 Ω, and 2.5 kV. Immediately
400 after, 0.9 mL of 1X SBHI was added, and cells were recovered for 3 h at 37°C without shaking
401 before plating on selective BHI agar. For recombineering, the entire transformation mixture was
402 pelleted (7,000 × *g*, 2 min) and plated to maximize recovery.

403 **Generation of the ERV165 Δ*sagA* clean deletion mutant (Δ*sagA*)**

404 The gene-editing CRISPR-cas12a protocol from Chua et al.[27] was modified to account for the
405 robustness of the Δ*sagA* mutant, which made deletion challenging.

406 *a.* *Generation of the ΔsagA mutant:* Briefly, pPK99 plasmid was electroporated into VREfm
407 ERV165 electrocompetent cells. A few transformants were inoculated into 5 mL of BHI broth
408 supplemented with 250 µg/mL gentamycin and grown at 37°C with shaking for two days. Sub-
409 culture (1:1,000 dilution) into fresh BHI broth supplemented with 250 µg/mL gentamycin and
410 incubated under the same conditions for an additional two days. Subsequently, 1 µL of the
411 culture was streaked onto BHI agar plates supplemented with 250 µg/mL gentamycin and 250
412 ng/mL anhydrotetracycline (ahTC) and incubated at 37°C for 3 to 5 days. Smaller single
413 colonies were picked and grown in BHI broth supplemented with 250 µg/mL gentamycin and
414 250 ng/mL ahTC. Since D*sagA* mutant exhibits a sedimentation phenotype, the sedimented
415 cells were selectively taken and re-inoculated into fresh BHI broth with the same supplements.
416 This enrichment step was repeated twice to enhance the recovery of Δ*sagA* mutants.

417 *b.* *Morphology-based screening and validation of ΔsagA mutants:* Based on our previous studies
418 [19], the *E. faecium* Com15 Δ*sagA* mutant is known to exhibit growth defects. Therefore,
419 numerous sick colonies were screened but were ultimately found to be false positives. During
420 this study, we identified an alternative screening method for Δ*sagA* mutants, as they exhibit a
421 distinct colony morphology that can be visualized using light microscopy (Fig. 1d). To identify
422 such mutants, BHI plates were continuously monitored for the appearance of smaller and sick
423 colonies. Numerous BHI plates were examined under a light microscope using differential
424 interference contrast (DIC) imaging with a 10× objective lens, and colonies were extensively
425 analyzed for the characteristic Δ*sagA* mutant morphology. Colonies with a smaller size and a
426 rough halo texture were selected for further screening by colony PCR. However, DNA
427 sequencing analysis revealed a high frequency of false positives. In these cases, the *sagA*
428 open reading frame (ORF) remained intact, but the protospacer was disrupted,likely due to
429 CRISPR-Cas12a-mediated double-stranded break and repair events, leading to a phenotype
430 that mimicked the *sagA* mutant. Despite these challenges, we successfully isolated a single,
431 confirmed colony that carried a clean deletion of *sagA*. The whole genome sequence analysis
432 was done to check for background mutations (Extended Data Tables 3 and 4).

433 **Generation of ERV165 Δ*sagA* chromosomal complementation strain (Δ*sagA*::*sagA*)**

434 The complementation strain was constructed using the pPK158 plasmid, following a method
435 similar to that described above for generating the Δ*sagA* mutant. Whole-genome sequencing
436 analysis confirmed that the observed growth defect of Δ*sagA* mutant was not due to background
437 mutations (Extended Data Tables 5 and 6).

438 **Generation of the ERV165 *pgh2, pgh3 and pgh4* clean deletion mutants (Δ*pgh2*, Δ*pgh3***
439 **Δ*pgh4*)**

440 Strains were constructed using the pPK156, pPK107 or pPK154 plasmids respectively, following
441 a method similar to that described above for generating the Δ*sagA* mutant.

442 **Recombinant protein expression and purification**

443 Truncated SagA_NlpC/P60 proteins were expressed and purified from *E. coli* BL21-RIL (DE3) as
444 previously described.[16,34] pET-21a(+) plasmids containing the truncated SagA_NlpC/P60 genes
445 with a C-terminal His_6 tag were transformed into BL21-CodonPlus (DE3)-RIL *E. coli* (Agilent
446 230245) according to the manufacturer's protocol and maintained in LB broth supplemented with
447 100 µg mL^{-1} ampicillin and 25 µg mL^{-1} chloramphenicol. Overnight bacterial culture was
448 subcultured in 1 L fresh BHI supplemented with appropriate antibiotics, grown until OD_{600}~0.5,
449 induced with 1 mM isopropyl-*D*-thiogalactopyranoside, and additionally grown for 2 hours at 37
450 °C and 200 RPM shaking. Bacterial cells were collected by centrifugation at 4 °C, resuspended
451 in 20 mL lysis buffer (20 mM Tris-HCl, pH 8.0, 150 mM NaCl, 0.1% SDS, 0.025 U/mL benzonase,
452 and 1× protease inhibitor cocktail). After 15 min of sonication followed by centrifugation at 18,000
453 × *g* for 30 min at 4°C, the supernatant containing the soluble target protein was collected and
454 loaded on 2 mL of Ni-NTA agarose (Invitrogen) equilibrated with the binding buffer (PBS). The
455 protein-bound resin was washed with 20 mM and 40 mM imidazole sequentially, then
456 SagA_NlpC/P60 protein was eluted with 300 mM imidazole. Semi-purified protein was dialyzed
457 into PBS buffer at 4°C overnight using 10K MWCO Slide-A-Lyzer MINI dialysis devices (Thermo
458 Fisher Scientific). Protein was further purified on a ENrich™ SEC 650 column (Bio-Rad) pre-
459 equilibrated with PBS using NGC chromatography system (Bio-Rad). Fractions containing the
460 target protein were combined and concentrated. Protein concentration was estimated by Pierce™
461 BCA Protein Assay (ThermoFisher) and protein was stored at −80°C.

462 **Fluorescence polarization (FP) cysteine activity assay**

463 The assay is based on competitive reaction of a tested compound with broad-spectrum cysteine-
464 reactive probe tetramethylrhodamine-5-iodoacetamide (Anaspec) and was adapted from [56]. 16
465 µL of recombinant SagA_NlpC/P60 (0.5 µM) in PBS was added to black 384-well plate. Tested
466 compound (50 µM) were then added to corresponding wells using Bravo instrument (Agilent). The
467 plate was covered with aluminum seal and incubated for 1 hour at room temperature with
468 agitation, followed by treatment with tetramethylrhodamine-5-iodoacetamide (20 nM) for 30 min
469 at 37˚C shielded from light with agitation. Fluorescence polarization was measured using
470 EnVision plate reader 2105 (Perkin Elmer) with BODIPY TMR FP filter set and calculated as
471 follows:

472 Polarization (mP) = 1000 * (S – G*P)/(S + G*P), where S and P are the measured results with the
473 S and P emission filters respectively. G is a correction factor (effect of emission filter transmission
474 variations, differences in the emission light paths and sample viscosity).

475 Inhibition (%) = 100-(mP_{sample}-$mP_{negative}$)/($mP_{Positive}$-$mP_{negative}$), where mP_{sample} is FP value of
476 SagA_NlpC/P60 treated with a corresponding testing compound, $mP_{positive}$ is FP value of
477 SagA_NlpC/P60 treated with DMSO, $mP_{negative}$ is FP value of SagA_NlpC/P60 (C433A, inactive
478 mutant) treated with DMSO. Calculated inhibition > 100% was assigned as 100%.

479 **Gel-based cysteine activity assay**

480 The assay was adapted from [56]. For gel-based SagA activity assay, the conditions were similar
481 to FP assay, except for treatment with tetramethylrhodamine-5-iodoacetamide (50 nM). The
482 reaction was quenched with 4 × Laemmli buffer, heat-inactivated for 5 min at 90 °C, separated by
483 SDS-PAGE. The gel was visualized using ChemiDoc MP imaging system (Bio-Rad). Relative
484 labeling was determined by extracting fluorescence intensity of the band and compared to DMSO
485 control. For analysis of bacterial proteome, after treatment with pghi-4, 100 µg of precipitated
486 secreted proteins from supernatants or bacterial proteome from cell pellets lysed in PBS were
487 treated with *N*-5-hexyn-1-yl-2-iodoacetamide (IA-alk, 100 µM) for 1 hour at room temperature with
488 agitation, followed by 1 hour treatment with click mixture: 1 mM tris(2-carboxyethyl)phosphine
489 hydrochloride (TCEP), 1 mM $CuSO_4$, 0.1 mM tris[(1-benzyl-1H-1,2,3-triazol-4-yl)methyl]amine
490 (TBTA), and 100 µM rhodamine-azide. The reactions were quenched by addition 4 × Laemmli
491 buffer and proteins were separated by SDS-PAGE. In-gel fluorescence was detected by
492 ChemiDoc MP imaging system (Bio-Rad). Relative labeling was determined by extracting
493 fluorescence intensity of the SagA band and compared to DMSO control using Image Lab
494 software (Bio-Rad). Protein loading was analyzed by Coomassie blue staining for recombinant
495 SagA and by α-SagA Western Blot for bacterial proteome.

496 Biotin pull-down protocol was adapted from [57]. For biotin pull-down experiments from bacterial
497 lysates, 250 µg of each total cell lysates in PBS were treated IA-alk (100 µM) for 1 hour at room
498 temperature with agitation, followed by 1 hour treatment with click mixture: 1 mM tris(2-
499 carboxyethyl)phosphine hydrochloride (TCEP), 1 mM $CuSO_4$, 0.1 mM tris[(1-benzyl-1*H*-1,2,3-
500 triazol-4-yl)methyl]amine (TBTA), and 100 µM biotin-azide. Proteins were precipitated with 4 ×
501 volume cold methanol. Precipitated proteins were pelleted by centrifugation (18,000 × *g*, 4°C, 10
502 min), sequentially washed with cold methanol and centrifuged 3 times, followed by drying in
503 SpeedVac. Resulted pellets were resuspended in 100 µL 4% SDS in PBS with bath sonication.
504 2.5% of solution was used as input (protein loading control). Total volume of incubated with 20
505 µL PBS-T-washed High Capacity NeutrAvidin agarose (Pierce) (500 µL PBS-T-washed twice,
506 2,500 × *g* for 60 s) at room temperature for 1 hour with end-to-end rotation. The agarose was then
507 washed with 500 µL PBS (1% SDS) 3 times, 500 µL 1 M Urea in PBS three times, and 500 µL
508 PBS three times. Samples were boiled with 2 × Laemmli buffer 95°C for 5 min and analyzed by
509 western blot.

510 For biotin pull-down experiments from bacterial supernatants, proteins were precipitated from
511 supernatants with 4 × volume cold methanol. Precipitated proteins were pelleted by centrifugation
512 (18,000 × *g*, 4°C, 10 min). Resulted pellets were resuspended in PBS and protein concentration
513 was estimated by BCA assay with BCA Protein Assay Kit (Thermo). 250 µg of each total proteins
514 were processed further as described above.

515 **Competitive cysteine-directed chemoproteomic analysis**

516 The protocol was adapted from [58]. VREfm ERV165 were grown from overnight culture in 15 mL
517 of fresh BHI till OD_{600}~0.6. Bacteria were then centrifuged and resuspended in 1 mL of BHI
518 (OD_{600}~9), followed by incubation with pghi-4 (10, 25 or 50 µM) for 1 hour at 37°C and 200 RPM

519 shaking. Bacterial pellets were collected by centrifugation (4,800 × *g* for 10 min), washed twice
520 with PBS and immediately processed or stored at −80 °C. Bacterial pellets were resuspended in
521 360 µL PBS and lysed with 0.1 mm glass beads (BioSpec) using FastPrep system (MP
522 Biomedicals, settings: 6 m/s, 2 cycles, 45 s for each cycle). Proteins were quantified by Pierce™
523 BCA Protein Assay (ThermoFisher) and normalized to 2 mg/mL. 1 mg/0.5 mL of bacterial
524 proteome was incubated with iodoacetamide-desthiobiotin (IA-DTB, 100 µM) for 1 hour at room
525 temperature agitating. Bacterial proteins were precipitated by cold methanol (600 µL), chloroform
526 (200 µL), and water (100 µL), followed by vortexing and centrifugation at 16,000 × *g* for 10 min at
527 4°C. Liquids were carefully aspirated, proteins were washed with cold methanol, pelleted by
528 centrifugation (16,000 × *g* for 10 min at 4°C) and air-dried for 5 min. Protein pellets were
529 resuspended in 90 µL of buffer (9 M urea, 10 mM DTT, 50 mM triethylammonium bicarbonate
530 (TEAB) pH 8.5), heated at 65°C for 20 min, followed by treatment with iodoacetamide (50 mM)
531 for 30 min at 37°C. The insoluble residues were pelleted by centrifugation and clear solutions
532 were sonicated. Samples were diluted with 300 µL TEAB buffer and trypsinized (5 µL of 0.4 µg/µL
533 trypsin in trypsin buffer supplemented with 25 mM $CaCl_2$) overnight at 37°C. Samples were treated
534 with 400 µL of wash buffer (50 mM TEAB, 150 mM NaCl, 0.2% NP-40) containing 50 µL of
535 streptavidin agarose to the peptide samples, followed by rotation at room temp for 2 hours.
536 Suspensions were briefly centrifuged, and beads-containing suspensions were loaded on BioSpin
537 columns. The beads were sequentially washed with 3 × 1 mL wash buffer, 3 × 1 mL PBS, 3 × 1 mL
538 MiliQ water. Beads-bound peptides were eluted by addition of 2 × 200 µL of 80% acetonitrile
539 (0.1% formic acid) and the eluate was concentrated by SpeedVac. Peptides were resuspended
540 in 70 µL EPPS buffer (200 mM, pH 8.0), supplemented with 30% acetonitrile, vortexed and
541 sonicated for 5 min. Peptides were tandem mass tag (TMT)-labeled by adding 3 µL of 10 mg/mL
542 TMT^{10plex} tag and incubating for 1 hour at room temperature. The reaction was quenched by
543 sequential addition of hydroxylamine (3 µL of a 5% aqueous solution, 15 min at room temperature)
544 and formic acid (5 µL), followed by concentration using SpeedVac. Samples were resuspended
545 in 500 µL Velos buffer A (95% water, 5% acetonitrile, 0.1% formic acid), acidified with 20 µL of
546 formic acid, desalted (Sep-Pak C18 Cartridge) and concentrated by SpeedVac. Desalted and
547 concentrated samples were redissolved in 500 µL Velos buffer A and HPLC-fractionated.
548 Fractionation and TMT LC-MS analysis was followed as previously described [58]. Pghi-4 cysteine-
549 directed activity was calculated as competition (%) of a cysteine site relative to DMSO treatment
550 when IA-DTB fully occupies accessible cysteines (100%).

551 **Peptidoglycan isolation**

552 The peptidoglycan isolation was followed as previously described.[34] Overnight VREfm cultures
553 were subcultured in fresh BHI supplemented with or without vancomycin, pghi-4 or in combination
554 and were grown till OD_{600}~0.8-1. Bacterial cell pellets were collected by centrifugation and lysed
555 in 0.25% SDS solution in 0.1 M Tris-HCl, pH 6.8 and boiling the suspension for 20 min at 100°C.
556 The insoluble bacterial cell wall was collected by centrifugation, washed with distilled water to
557 remove SDS. The cell wall was next sonicated for 30 min in distilled water and treated with
558 benzonase followed by trypsin digestion. Then, insoluble cell wall was recovered by centrifugation
559 (16,000 × *g*, 10 min, 4°C), and washed with distilled water. Next, the cell wall was treated with 1
560 M HCl for 4 hours at 37°C and 200 RPM shaking. The insoluble material was collected by
561 centrifugation (16,000 × *g*, 10 min) and washed with distilled water until the pH was 5-6. Purified
562 insoluble peptidoglycan was digested with mutanolysin from *Streptomyces globisporus* (Sigma,
563 10 KU/mL of mutanolysin in MiliQ H_2O) in 10 mM sodium phosphate buffer, pH 4.9 for 16 hours

564 at 37°C shaking. The mutanolysin was heat-inactivated and resulting soluble peptidoglycan was
565 used in gel-based peptidoglycan hydrolase activity assay or LC-MS analysis.

566 **Gel-based peptidoglycan hydrolase activity assay**

567 The peptidoglycan hydrolase activity assay is based on in-gel analysis of peptidoglycan fragments
568 labeled with 8-aminonaphthalene-1,3,6-trisulfonic acid (ANTS). The assay was followed as
569 previously described[34] with some modifications. 10 µM recombinant SagA_NlpC/P60 (or other
570 NlpC/P60 peptidoglycan hydrolase) was incubated with 250 µg of the mutanolysin-digested
571 peptidoglycan in 50 mM Bis-Tris, pH 5.5 overnight at 37 °C and 220 RPM shaking. The enzymatic
572 activity was heat-inactivated at 100°C for 5 min. The samples were centrifuged at 16,000 x *g* for
573 5 min and supernatants were transferred and concentrated. The concentrated samples were
574 resuspended and incubated with 5 µL of each reagent (0.2M ANTS in water supplemented with
575 15% acetic acid and 1M $NaBH_3CN$ in DMSO) overnight at 37 °C, 220 RPM shaking and protected
576 from light. The reaction mixtures were diluted with 10 µL 50% glycerol (*v/v*) and ANTS-labeled
577 peptidoglycan fragments were separated by Native PAGE on 4-20% Criterion TGX precast gels
578 (Bio-Rad) ran at 100 V for 30 min, and visualized by ChemiDoc MP imaging system (Bio-Rad)
579 and SYBR-Safe settings. Inhibition was determined by extracting fluorescence intensity of the
580 ANTS-labelled enzymatic product (GlcNAc-MurNAc dipeptide) and compared to DMSO control.

581 **Computational covalent docking**

582 The docking receptor file was prepared from PDB: 6B8C.[16] All crystallographic waters and
583 alternative residue positions were removed with PyMOL (https://pymol.org/). The receptor was
584 then protonated using Reduce[59] and prepared for docking using Meeko
585 (https://github.com/forlilab/Meeko) to assign atomtypes and Gasteiger partial charges and convert
586 to a PDBQT file[60]. Gridmaps were calculated with AutoGrid4 with a box size of 16 Å, 18 Å, 27 Å
587 (0.375 Å grid spacing) and with the box center at 101 Å, 80 Å, 140.5 Å. His 506 was also
588 designated to be in the HID (neutral, δ-nitrogen protonated) form. The Cys 443 Cα and sidechain
589 were also removed.

590 Covalent docking as performed using the "flexible side chain" model described by Bianco et al.[61].
591 2D line drawings of pghi-4 adducts as either the (a) thioenol sulfonyl fluoride (Michael addition
592 product) and (b) vinylchloride thiosulfonate (sulfonyl fluoride exchange product) were prepared in
593 ChemDraw. The 3D conformation of the vinylchloride thiosulfonate was then prepared with
594 MolScrubber (https://github.com/forlilab/molscrub) and checked to ensure the optimal
595 cyclopentane conformation was generated with the ether in equatorial position. For the thioenol
596 sulfonyl fluoride, a torsional energy scan of the phenyl-thioenol torsion was performed using
597 Gaussian16 with 10-degree incremental steps between energy calculations. Minima were found
598 for torsions of approximately 45° and -143° between the thioenol sulfur and the phenyl carbon
599 adjacent to that bearing the methyl ether. Both thioenol sulfonyl fluoride geometries (with the
600 phenyl-thioenol torsion held as non-rotatable) and the single vinylchloride thiosulfonate were
601 prepared for docking using Meeko to add Gasteiger partial charges and convert to PDBQTs[60]. All
602 three models were then docked as flexible side chains with AutoDock-GPU [62], keeping the top
603 scoring pose for further analysis. The two docked thioenol sulfonyl fluoride models were evaluated
604 visually, with the -143° model selected as the most reasonable docked conformation. Models
605 were additionally corroborated using reactive docking[63] to confirm the state prior to reaction could
606 be accommodated.

607 **Intact protein analysis by mass spectrometry**

608 10 μM recombinant SagA_NlpC/P60 (or C433A inactive control) was incubated with 50 μM pghi-
609 4 (or inactive pghi-6) in 50 mM Tris-Cl, pH 7.6, 150 mM NaCl buffer for 1 hour (or 16 hours) at
610 room temperature and shaking at 600 RPM. The mixtures were analyzed by ESI-TOF mass
611 spectrometry.

612 **Bacterial growth defect and antibiotic susceptibility assay**

613 Starting cultures were grown from single bacterial colonies overnight at 37°C at 200 RPM shaking
614 in Brain Heart Infusion (BHI) broth. Next, the starting culture were diluted to OD_{600} ~0.1 in fresh
615 BHI in a sterile 96-well plate and supplemented with vancomycin alone, SagA inhibitor alone or
616 combination of vancomycin and SagA inhibitor at indicated concentrations. The OD_{600} values were
617 measured at 37°C with continuous orbital shaking using BioTek Cytation 5 plate reader (Agilent).
618 For inhibition heat-maps, inhibition was calculated as percentage of OD_{600} values of treatment
619 groups over vehicle control at the single time point. Following Clinical & Laboratory Standards
620 Institute (CLSI) guidelines, vancomycin susceptibilities of ERV165 WT and generated mitants
621 were also tested in Mueller Hinton Broth (MHB). Minimal inhibitory concentrations (MICs) were
622 determined as the lowest concentration that inhibited the visible growth.

623 **LC-MS-based peptidoglycan analysis**

624 The analysis was followed as we previously described.[19,34] The mutanolysin-digested
625 peptidoglycan was treated with sodium borohydride in 0.25 M boric acid (pH 9) for 1 hour at room
626 temperature, quenched with orthophosphoric acid, and pH adjusted to 2-3. The samples were
627 centrifuged at 20,000 × *g* for 10 minutes. Then, the reduced peptidoglycan was analyzed by 1290
628 Infinity II LC/MSD system (Agilent technologies) using Poroshell 120 EC-C18 column (3 × 150
629 mm, 2.7 μm). Samples were run at flow rate 0.5 mL/min in mobile phase (A: water, 0.1% formic
630 acid) and an eluent (B: acetonitrile, 0.1% formic acid) using following gradient: 0-5 min: 2% B, 5-
631 65 min: 2-10% B. All solvents were HPLC grade. The absorbance of the eluting peaks was
632 detected at 205 nm. Masses of peaks were detected with MSD API-ES Scan mode (m/z = 200-
633 2,500) (Extended Data Table 11). For quantification of relative abundance of muropeptides, the
634 area under the curve of assigned individual peak from chromatograms was integrated and
635 percentage of individual peak was calculated relative to all assigned peaks.

636 **Western blot analysis.**

637 Western blot analysis was performed as described previously.[16,19] Overnight VREfm cultures were
638 sub-cultured in fresh BHI to OD_{600}~0.1 and were grown overnight at 37°C and shaking at 200
639 RPM. The cultures were centrifuged at 4,800 x *g* for 10 min, cell pellets and supernatants were
640 separated. Cell pellets were washed with PBS and lysed in PBS with 0.1 mm glass beads
641 (BioSpec) using FastPrep system (MP Biomedicals, settings: 6 m/s, 2 cycles, 45 s for each cycle).
642 Proteins were quantified by Pierce™ BCA Protein Assay (ThermoFisher) and separated by SDS-
643 PAGE on 4-20% Criterion TGX precast gels (Bio-Rad), then transferred to nitrocellulose
644 membrane. The membrane was blocked in 0.1% TBST supplemented with 5% milk for 1 hour at
645 room temperature with agitation, incubated with primary antibody (rabbit anti-SagA polyclonal
646 sera, diluted 1:50000 in 0.1% TBST supplemented with 5% milk) overnight at 4°C with agitation.
647 After 2 washes (2 min each) the membrane was incubated with secondary antibody (goat anti-
648 rabbit antibody, HRP-conjugate, diluted 1:20,000 in 0.1% TBST supplemented with 5% milk) for
649 1 h at room temperature with agitation. Membranes were washed with 0.1% TBST three times

650 (10 min each) at room temperature with agitation. Blots were developed using Clarity Western
651 ECL substrate (Bio-Rad) and imaged using a ChemiDoc MP imaging system (Bio-Rad).

652 **Fluorescence microscopy**

653 VREfm were grown to OD_{600} ~ 0.4 with or without pghi-4 (50 μM) in BHI and sequentially labeled
654 with 5 mM HADA (Tocris Bioscience) for 30 min and 1 μg/mL Vancomycin-BODIPY (Invitrogen)
655 for 15 min at 220 RPM shaking, 37°C and protected from light. The cultures were centrifuged at
656 4,800 × *g* for 10 min. The cells were washed with PBS twice and fixed with 1% formaldehyde in
657 PBS for 10 min, followed by washing and resuspending in PBS. To image cells, an aliquot of cell
658 suspensions was transferred to the surface of a 2% (*w/v*) agarose pad prepared in PBS, covered
659 with a glass coverslip, and imaged with fluorescence microscope (Nikon Ti2-E Inverted) using
660 DAPI and GFP filters. For single-cell fluorescence analysis, fluorescence intensities from single
661 cells normalized to similar region of interest were extracted from images. The images were
662 processed using Icy open source imaging software[64].

663 **Cryo-electron tomography**

664 The protocol was adapted from [19] with some modifications. VREfm ERV165 strains or ERV165
665 strain treated with vancomycin (5 μg/mL), pghi-4 (50 μM) or in combination used in the cryo-ET
666 experiments were grown overnight at 37 °C in BHI broth. Fresh cultures were prepared from a
667 1:50 dilution of the overnight culture and then grown at 37 °C to early log phase. The culture was
668 centrifuged at 4,800 × *g* for 10 min. The pellet was resuspended with growth media supplemented
669 with 5% glycerol to OD600 ~ 3. Next, 5 μL of bacterial samples were deposited onto freshly glow-
670 discharged (Pelco easiGlow; 25 s glow at 15mA) Quantifoil R2/1 copper 200 mesh grids for 1 min,
671 back-side blotted with filter paper (Whatman Grade 1 filter paper), and frozen in liquid ethane
672 using a gravity-driven homemade plunger apparatus (inside a 4°C cold room with a ≥95% relative
673 humidity). The samples were frozen using a Vitrobot Mark IV (Thermo Fisher Scientific) in liquid
674 ethane/propane mixture. The Vitrobot was set to 22°C at 90% humidity, and manually back-side
675 blotted. The vitrified grids were later clipped with Cryo-FIB autogrids (Thermo Fisher Scientific)
676 prior to milling.

677 Cryo-FIB milling was performed using an Aquilos2 dual-beam cryo-FIB/SEM instrument (Thermo
678 Fisher Scientific). Vitrified samples were sputter-coated with metallic platinum for 15 s, followed
679 by a 30 s coating with organometallic platinum, and then sputter-coated again with metallic
680 platinum for 15 s to prevent drift during milling. Targets were selected and milled at an 8° angle
681 using MAPS and AutoTEM software, respectively (Thermo Fisher Scientific). The milling template
682 performed rough milling with a current of 0.30 nA, followed by medium milling at 0.1 nA. Thinning
683 was conducted with a current of 50 pA. Automated milling produced lamellae with a thickness of
684 ~300 nm, which were then manually polished to <200 nm using a 30 pA current. A final 20 s
685 metallic platinum coating was applied to facilitate bead-like fiducial inclusions for tilt series
686 alignment.

687 Cryo-lamellae were imaged using a 300 keV Titan Krios microscope (Thermo Fisher Scientific)
688 equipped with a field emission gun, an energy filter, and a direct electron detector (Gatan K3). An
689 energy filter with a slit width of 20 eV was used during data acquisition. The SerialEM[65] package
690 with PACEtomo[66] scripts was used to collect 35 image stacks at tilt angles ranging from +51° to
691 −51° in 3° increments using a dose-symmetric scheme with a cumulative dose of ~105 $e^{-}/Å^2$.

692 Data were collected at a magnification corresponding to 2.64 Å/pixel and a nominal defocus of ~
693 −5 µm.

694 Image stacks containing 10 frames were motion-corrected using MotionCor2[67], then assembled
695 into drift-corrected stacks using IMOD[68]. These were aligned and reconstructed into tomograms
696 using IMOD marker-based alignment. Tomograms were binned 4×, resulting in a final pixel size
697 of 10.55 Å/pixel. Missing wedge artifacts were corrected using IsoNet[69], a deep learning-based
698 software. Segmentation of cell membranes was performed using MemBrain[70]. ColabSeg[71] was
699 used to isolate segmented membranes of interest. A MATLAB script[72] was used to pick
700 subtomograms with defined Euler angles perpendicular to the membrane, spaced ~30 nm apart.
701 Segmented membranes and subtomogram picks were validated in UCSF Chimera [73].
702 Subtomogram averaging was performed using the Dynamo [74] software package. Subtomograms
703 were extracted with a box size of 120 pixels. Five iterations of averaging with minimal translational
704 and angular searches were conducted to generate averages. To generate density profiles, IMOD
705 drawing tools were used to draw a line through the subtomogram average. Density values along
706 the line were extracted, plotted and used for cell wall components assignment. Manual
707 measurements of the cell envelope (CE) were performed on the apical and septal regions of cells
708 using IMOD's measurement tool. Workflow of subtomogram averaging and analysis is
709 summarized in Extended Data Fig. 2.

710 **Macrophage infection**

711 The protocol was adapted from [50]. Macrophages (RAW264.7, ATCC TIB-71, or THP-1, ATCC
712 TIB-202, differentiated with phorbol 12-myristate 13-acetate) were plated in 96-well plate in the
713 growth media (DMEM supplemented with 4.5 g/L glucose, 2 mM L-glutamine, 10% FBS) at the
714 cell density 3×10^4 cells/ well. Cells were left to adhere and grow overnight at 37°C in humidified
715 atmosphere with 5% CO_2. VREfm (ERV165 strain) were grown to OD~0.6 in BHI by sub-culturing
716 starting cultures grown overnight from a single colony. Bacterial cultures were centrifuged, and
717 pellets were washed with sterile PBS twice, followed by resuspension in DMEM with or without
718 pghi-4 (25, 50 or 100 µM), vancomycin (100 µg/mL) or in combination. Macrophages were
719 incubated with bacterial suspensions for 3 hours at 37°C, 5% CO_2. Next, bacterial suspensions
720 were removed, and macrophages were washed with PBS three times. Macrophages were
721 incubated with 1% Triton X-100 (Sigma-Aldrich) in PBS for 5 mins at room temperature to lyse
722 cells for colony-forming units (CFU) analysis. Lysates of macrophages were immediately plated
723 on BHI agar, incubated overnight at 37°C and intracellular VREfm were enumerated.

724 **Mouse peritonitis infection**

725 The protocol was adapted from [30]. Specific pathogen-free C57BL/6 (B6,000664) mice were
726 obtained from Scripps Rodent Breeding. Mice were fed with gamma-irradiated chow (LabDiet,
727 5053) and sterile drinking water ad libitum. Animal care and experiments were conducted in
728 accordance with NIH guidelines and approved by the Institutional Animal Care and Use
729 Committee at Scripps Research. For evaluating vancomycin susceptibility of Δ*sagA in vivo,*
730 bacterial cultures of VREfm strains (WT, Δ*sagA* or Δ*sagA*::*sagA*) grown in BHI (OD_{600} ~ 0.6) were
731 washed with PBS and resuspended in PBS at 5×10^8 CFU/mL. Next, 6-8 weeks female mice were
732 infected with 10^9 VREfm CFU intraperitoneally. After 30 minutes, PBS or vancomycin (Van, 100
733 mg/kg) was administered subcutaneously. The second dose of treatment was administered 24-
734 hour post-infection. VREfm infection was monitored by mice weight loss compared to initial weight
735 (before infection) over 48 hours post-infection. Mice were euthanized once the weight reached

736 80% of the initial weight. Spleen and liver were collected, homogenized in sterile PBS for colony-
737 forming units (CFU) analysis. Homogenates were plated on HiCrome™ selective *Enterococcus*
738 *faecium* agar plates (HIMEDIA 1580) with *Enterococcus faecium* selective supplement (FD226,
739 HIMEDIA), incubated at 37°C overnight and viable colonies were enumerated.

740 For evaluating combination therapy, bacterial cultures of VREfm (ERV165 strain) grown in BHI
741 (OD_{600} ~ 0.6) were washed with PBS and resuspended in PBS (0.25% carboxymethyl cellulose,
742 CMC) at 5×10^8 CFU/mL. Next, 6-8 weeks female mice were co-injected intraperitoneally with 0.2
743 mL of bacterial suspension (10^9 CFU) and treatment: PBS (0.25% CMC) alone or supplemented
744 with vancomycin (100 mg/kg), pghi-4 (25 mg/kg) or in combination. The second dose of treatment
745 (PBS 0.25% CMC alone or supplemented with vancomycin (100 mg/kg), pghi-4 (25 mg/kg) or in
746 combination was administered 24-hour post-infection. VREfm infection was monitored by mice
747 weight loss compared to initial weight (before infection) over 48 hours post-infection. Mice were
748 euthanized once the weight reached 80% of the initial weight. Spleen and liver were collected and
749 processed as described above.

750

751 **Acknowledgements**

752 This project was funded by the National Institutes of Health R21AT012958 grant and Scripps
753 Research start-up funds to H.C.H. J.E.M. thanks Cold Spring Harbor Laboratory for
754 developmental funds from the NCI Cancer Center Support Grant (5P30CA045508), the Australian
755 Research Council (ARC) for a Future Fellowship (FT170100156), and the F.M. Kirby Foundation.
756 We thank Juliel Espinosa for providing constructs for recombinant expression of PGH2 and
757 PGH3. We thank Francisco Martínez-Peña, Luke Lairson, Kayla Nutsch, Caroline Stanton and
758 Michael Bollong for assisting with automated liquid handlers and EnVision plate readers. We
759 thank Kathryn Spenser and Scott Henderson for assistance at the Scripps Microscopy Core, K.
760 Barry Sharpless and the Hang laboratory members for their feedback.

761

762 **Author information**

763 These authors contributed equally: Kyong T. Fam, Pavan Kumar Chodisetti

764

765 **Authors and Affiliations**

766 **Department of Immunology and Microbiology, Scripps Research; La Jolla, California**
767 **92037, United States**
768 Kyong T. Fam, Pavan Kumar Chodisetti, Howard C. Hang
769
770 **Cancer Center, Cold Spring Harbor Laboratory; Cold Spring Harbor, NY 11724, USA**
771 Zifei Wang, Joshua A. Homer, John E. Moses
772
773 **La Trobe Institute for Molecular Science, La Trobe University, Science Dr., Bundoora,**
774 **Melbourne, VIC, 3086 Australia**
775 Christopher J. Smedley, John E. Moses
776

Department of Integrative Structural & Computational Biology, Scripps Research; La Jolla, California 92037, United States
Seiya Kitamura, Benjamin Silva, Althea Hansel-Harris, Matthew Holcomb, Simeon Babarinde, Ian A. Wilson, Stefano Forli, Donghyun Park, Dennis W. Wolan

Department of Molecular Medicine, Scripps Research; La Jolla, California 92037, United States
Seiya Kitamura, Dennis W. Wolan

Department of Chemistry, Scripps Research; La Jolla, California 92037, United States
Seiya Kitamura, Yijun Xiong, Benjamin F. Cravatt, Howard C. Hang

Division of Infectious Diseases, University of Pittsburgh School of Medicine, Pittsburgh, PA 15213
Daria Van Tyne

Contributions

K.T.F. and H.C.H. conceived the project and planned initial experiments. P.K.C. generated ERV165 isogenic deletion and their derivative strains. K.T.F. and P.K.C. characterized all generated strains. C.J.S, S.K. generated screening library of sulfonyl fluorides. J.E.M and C.J.S. both designed, and C.J.S. generated the lead sulfonyl fluorides. Z.W., J.H. resynthesized pghi-4. K.T.F. developed assays, conducted screening and identified hits. K.T.F. performed all biochemical and microbiological characterizations of identified hits. K.T.F. and Y.X. conducted competitive cysteine-directed chemoproteomics. A.H.-H., M.H. performed computational docking. B.S. and D.P. performed cryoET experiments. K.T.F. and S.B. attempted X-ray crystallography studies. D.V.T. provided VREfm clinical isolates. H.C.H, J.E.M., D.W.W, D.P., I.A.W., S.F., B.F.C. supervised experiments. K.T.F. conducted all animal studies. K.T.F., H.C.H wrote the manuscript, which was edited by all the other authors. All authors approved the manuscript before submission.

Corresponding authors

John E. Moses, Howard C. Hang

Ethics declarations

Authors declare no competing interests.

References

1. Lewis, K. The Science of Antibiotic Discovery. *Cell* **181**, 29–45 (2020).
2. Miller, W. R. & Arias, C. A. ESKAPE pathogens: antimicrobial resistance, epidemiology, clinical impact and therapeutics. *Nat. Rev. Microbiol.* **22**, 598–616 (2024).

3. Arias, C. A. & Murray, B. E. The rise of the Enterococcus: beyond vancomycin resistance. *Nat. Rev. Microbiol.* **10**, 266–278 (2012).
4. Wei, Y., Palacios Araya, D. & Palmer, K. L. Enterococcus faecium: evolution, adaptation, pathogenesis and emerging therapeutics. *Nat. Rev. Microbiol.* **22**, 705–721 (2024).
5. Shono, Y. & van den Brink, M. R. M. Gut microbiota injury in allogeneic haematopoietic stem cell transplantation. *Nat. Rev. Cancer* **18**, 283–295 (2018).
6. Contreras, G. A. *et al.* Contemporary Clinical and Molecular Epidemiology of Vancomycin-Resistant Enterococcal Bacteremia: A Prospective Multicenter Cohort Study (VENOUS I). *Open Forum Infect. Dis.* **9**, ofab616 (2021).
7. Wu, Z.-C. & Boger, D. L. Maxamycins: Durable Antibiotics Derived by Rational Redesign of Vancomycin. *Acc. Chem. Res.* **53**, 2587–2599 (2020).
8. Wright, P. M., Seiple, I. B. & Myers, A. G. The Evolving Role of Chemical Synthesis in Antibacterial Drug Discovery. *Angew. Chem. Int. Ed.* **53**, 8840–8869 (2014).
9. Cook, M. A., Michael A. Cook, Wright, G. D., & Gerard D. Wright. The past, present, and future of antibiotics. *Sci. Transl. Med.* **14**, (2022).
10. Homer, J. A., Johnson, R. M., Koelln, R. A., Moorhouse, A. D. & Moses, J. E. Strategic re-engineering of antibiotics. *Nat. Rev. Bioeng.* **3**, 213–229 (2025).
11. Van Tyne, D. & Gilmore, M. S. Friend Turned Foe: Evolution of Enterococcal Virulence and Antibiotic Resistance. *Annual Review of Microbiology* vol. 68 337–356 (2014).
12. Stein-Thoeringer, C. K. *et al.* Lactose drives *Enterococcus* expansion to promote graft-versus-host disease. *Science* **366**, 1143–1149 (2019).
13. Hanchi, H., Mottawea, W., Sebei, K. & Hammami, R. The Genus Enterococcus: Between Probiotic Potential and Safety Concerns—An Update. *Front. Microbiol.* **9**, 1791 (2018).
14. Rangan, K. J. *et al.* A secreted bacterial peptidoglycan hydrolase enhances tolerance to enteric pathogens. *Science* **353**, 1434–1437 (2016).
15. Pedicord, V. A. *et al.* Exploiting a host-commensal interaction to promote intestinal barrier function and enteric pathogen tolerance. *Sci. Immunol.* **1**, eaai7732 (2016).
16. Kim, B. *et al. Enterococcus faecium* secreted antigen A generates muropeptides to enhance host immunity and limit bacterial pathogenesis. *eLife* **8**, e45343 (2019).
17. Griffin, M. E. *et al. Enterococcus* peptidoglycan remodeling promotes checkpoint inhibitor cancer immunotherapy. *Science* **373**, 1040 (2021).
18. Jang, K. K. *et al.* Antimicrobial overproduction sustains intestinal inflammation by inhibiting Enterococcus colonization. *Cell Host Microbe* **31**, 1450-1468.e8 (2023).
19. Klupt, S. *et al.* Secreted antigen A peptidoglycan hydrolase is essential for *Enterococcus faecium* cell separation and priming of immune checkpoint inhibitor therapy. *eLife* **13**, RP95297 (2024).
20. Canfield Gregory S. *et al.* Lytic Bacteriophages Facilitate Antibiotic Sensitization of Enterococcus faecium. *Antimicrob. Agents Chemother.* **65**, 10.1128/aac.00143-21 (2021).
21. Arya, G. *et al. Enterococcus faecium* sagA mutants have cell envelope defects influencing antibiotic resistance and bacteriophage susceptibility. *bioRxiv* (2025) doi:10.1101/2025.07.21.665895.
22. Cheng, Y. *et al.* Diversity oriented clicking delivers β-substituted alkenyl sulfonyl fluorides as covalent human neutrophil elastase inhibitors. *Proc. Natl. Acad. Sci.* **119**, e2208540119 (2022).

23. Smedley, C. J. *et al.* Diversity Oriented Clicking (DOC): Divergent Synthesis of SuFExable Pharmacophores from 2-Substituted-Alkynyl-1-Sulfonyl Fluoride (SASF) Hubs. *Angew. Chem. Int. Ed.* **59**, 12460–12469 (2020).
24. Wang, Z. *et al.* Diversity oriented clicking for modular synthesis. *Nat. Rev. Methods Primer* **5**, 52 (2025).
25. Griffin, M. E., Klupt, S., Espinosa, J. & Hang, H. C. Peptidoglycan NlpC/P60 peptidases in bacterial physiology and host interactions. *Cell Chem. Biol.* **30**, 436–456 (2023).
26. Chen, V., Griffin, M.E., Maguin, P., Varble, A., & Hang, H. C. RecT Recombinase Expression Enables Efficient Gene Editing in *Enterococcus* spp. *Appl. Environ. Microbiol.* **87**, e00844-21 (2021).
27. Chua, M. J. & Collins, J. Rapid, Efficient, and Cost-Effective Gene Editing of *Enterococcus faecium* with CRISPR-Cas12a. *Microbiol. Spectr.* **10**, e02427-21 (2022).
28. Daniel, R. A. & Errington, J. Control of Cell Morphogenesis in Bacteria: Two Distinct Ways to Make a Rod-Shaped Cell. *Cell* **113**, 767–776 (2003).
29. Kuru, E. *et al.* In Situ Probing of Newly Synthesized Peptidoglycan in Live Bacteria with Fluorescent D-Amino Acids. *Angew. Chem. Int. Ed.* **51**, 12519–12523 (2012).
30. Singh, K. V., Arias, C. A. & Murray, B. E. Efficacy of Omadacycline against Multidrug-Resistant Enterococcus faecium Strains in a Mouse Peritonitis Model. *Antimicrob. Agents Chemother.* **65**, 10.1128/aac.00709-21 (2021).
31. Rybak, M. J. *et al.* Vancomycin Therapeutic Guidelines: A Summary of Consensus Recommendations from the Infectious Diseases Society of America, the American Society of Health-System Pharmacists, and the Society of Infectious Diseases Pharmacists. *Clin. Infect. Dis.* **49**, 325–327 (2009).
32. Niphakis, M. J. & Cravatt, B. F. Enzyme Inhibitor Discovery by Activity-Based Protein Profiling. *Annu. Rev. Biochem.* **83**, 341–377 (2014).
33. Espinosa, J. *et al. Enterococcus* NlpC/p60 Peptidoglycan Hydrolase SagA Localizes to Sites of Cell Division and Requires Only a Catalytic Dyad for Protease Activity. *Biochemistry* **59**, 4470–4480 (2020).
34. Kim, B., Espinosa, J. & Hang, H. C. Chapter Six - Biochemical analysis of NlpC/p60 peptidoglycan hydrolase activity. in *Methods in Enzymology* (ed. Chenoweth, D. M.) vol. 638 109–127 (Academic Press, 2020).
35. Chilambi, G. S. *et al.* Evolution of vancomycin-resistant *Enterococcus faecium* during colonization and infection in immunocompromised pediatric patients. *Proc. Natl. Acad. Sci.* **117**, 11703–11714 (2020).
36. Hubbard, B. K. & Walsh, C. T. Vancomycin assembly: nature's way. *Angew. Chem.* **42**, 730–765 (2003).
37. Naghavi, M. *et al.* Global burden of bacterial antimicrobial resistance 1990–2021: a systematic analysis with forecasts to 2050. *The Lancet* **404**, 1199–1226 (2024).
38. Hutchings, M. I., Truman, A. W. & Wilkinson, B. Antibiotics: past, present and future. *Antimicrobials* **51**, 72–80 (2019).
39. Wong, F. *et al.* Discovery of a structural class of antibiotics with explainable deep learning. *Nature* **626**, 177–185 (2024).
40. Noto Guillen, M., Li, C., Rosener, B. & Mitchell, A. Antibacterial activity of nonantibiotics is orthogonal to standard antibiotics. *Science* **384**, 93–100 (2024).

41. Muñoz, K. A. *et al.* A Gram-negative-selective antibiotic that spares the gut microbiome. *Nature* **630**, 429–436 (2024).
42. Jangra, M. *et al.* A broad-spectrum lasso peptide antibiotic targeting the bacterial ribosome. *Nature* **640**, 1022–1030 (2025).
43. Wu, K. J. Y. *et al.* An antibiotic preorganized for ribosomal binding overcomes antimicrobial resistance. *Science* **383**, 721–726 (2024).
44. Krieger, I. V. *et al.* SuFEx-based antitubercular compound irreversibly inhibits Pks13. *Nature* (2025) doi:10.1038/s41586-025-09286-3.
45. Tyers, M. & Wright, G. D. Drug combinations: a strategy to extend the life of antibiotics in the 21st century. *Nat. Rev. Microbiol.* **17**, 141–155 (2019).
46. Blondiaux, N. *et al.* Reversion of antibiotic resistance in *Mycobacterium tuberculosis* by spiroisoxazoline SMARt-420. *Science* **355**, 1206–1211 (2017).
47. Flipo, M. *et al.* The small-molecule SMARt751 reverses Mycobacterium tuberculosis resistance to ethionamide in acute and chronic mouse models of tuberculosis. *Sci. Transl. Med.* **14**, eaaz6280 (2022).
48. Shatalin, K. *et al.* Inhibitors of bacterial H2S biogenesis targeting antibiotic resistance and tolerance. *Science* **372**, 1169–1175 (2021).
49. Stokes, J. M. *et al.* Pentamidine sensitizes Gram-negative pathogens to antibiotics and overcomes acquired colistin resistance. *Nat. Microbiol.* **2**, 1–8 (2017).
50. Silva, R. A. G. da *et al.* Mitoxantrone targets both host and bacteria to overcome vancomycin resistance in *Enterococcus faecalis*. *Sci. Adv.* **9**, eadd9280 (2023).
51. Gudiol Carlota *et al.* Efficacy of β-Lactam/β-Lactamase Inhibitor Combinations for the Treatment of Bloodstream Infection Due to Extended-Spectrum-β-Lactamase-Producing Enterobacteriaceae in Hematological Patients with Neutropenia. *Antimicrob. Agents Chemother.* **61**, e00164-17 (2017).
52. Tacconelli, E. *et al.* Discovery, research, and development of new antibiotics: the WHO priority list of antibiotic-resistant bacteria and tuberculosis. *Lancet Infect. Dis.* **18**, 318–327 (2018).
53. O'Driscoll, T. & Crank, C. W. Vancomycin-resistant enterococcal infections: epidemiology, clinical manifestations, and optimal management. *Infect. Drug Resist.* **8**, 217–230 (2015).
54. Culp, E. J. *et al.* Evolution-guided discovery of antibiotics that inhibit peptidoglycan remodelling. *Nature* **578**, 582–587 (2020).
55. Scharnow, A. M. *et al.* In Situ Biofilm Affinity-Based Protein Profiling Identifies the Streptococcal Hydrolase GbpB as the Target of a Carolacton-Inspired Chemical Probe. *J. Am. Chem. Soc.* **146**, 23449–23456 (2024).
56. Bachovchin, D. A., Brown, S. J., Rosen, H. & Cravatt, B. F. Identification of selective inhibitors of uncharacterized enzymes by high-throughput screening with fluorescent activity-based probes. *Nat. Biotechnol.* **27**, 387–394 (2009).
57. Yang, X., Zhao, X., Chen, V. & Hang, H. C. Chemical proteomic analysis of bile acid-protein targets in Enterococcus faecium. *RSC Chem Biol* **3**, 1397–1402 (2022).
58. Njomen, E. *et al.* Multi-tiered chemical proteomic maps of tryptoline acrylamide–protein interactions in cancer cells. *Nat. Chem.* **16**, 1592–1604 (2024).

59. Word, J. M., Lovell, S. C., Richardson, J. S. & Richardson, D. C. Asparagine and glutamine: using hydrogen atom contacts in the choice of side-chain amide orientation. *J. Mol. Biol.* **285**, 1735–1747 (1999).
60. Forli, S. *et al.* Computational protein–ligand docking and virtual drug screening with the AutoDock suite. *Nat. Protoc.* **11**, 905–919 (2016).
61. Bianco, G., Forli, S., Goodsell, D. S. & Olson, A. J. Covalent docking using autodock: Two-point attractor and flexible side chain methods. *Protein Sci.* **25**, 295–301 (2016).
62. Santos-Martins, D. *et al.* Accelerating AutoDock4 with GPUs and Gradient-Based Local Search. *J. Chem. Theory Comput.* **17**, 1060–1073 (2021).
63. Bianco, G. *et al.* Reactive Docking: A Computational Method for High-Throughput Virtual Screenings of Reactive Species. *J. Chem. Inf. Model.* **63**, 5631–5640 (2023).
64. de Chaumont, F. *et al.* Icy: an open bioimage informatics platform for extended reproducible research. *Nat. Methods* **9**, 690–696 (2012).
65. Mastronarde, D. N. Automated electron microscope tomography using robust prediction of specimen movements. *J. Struct. Biol.* **152**, 36–51 (2005).
66. Eisenstein, F. *et al.* Parallel cryo electron tomography on in situ lamellae. *Nat. Methods* **20**, 131–138 (2023).
67. Zheng, S. Q. *et al.* MotionCor2: anisotropic correction of beam-induced motion for improved cryo-electron microscopy. *Nat. Methods* **14**, 331–332 (2017).
68. Mastronarde, D. N. & Held, S. R. Automated tilt series alignment and tomographic reconstruction in IMOD. *J. Struct. Biol.* **197**, 102–113 (2017).
69. Liu, Y.-T. *et al.* Isotropic reconstruction for electron tomography with deep learning. *Nat. Commun.* **13**, 6482 (2022).
70. Lamm, L. *et al.* MemBrain v2: an end-to-end tool for the analysis of membranes in cryo-electron tomography. *bioRxiv* (2024) doi:10.1101/2024.01.05.574336.
71. Siggel, M., Jensen, R. K., Maurer, V. J., Mahamid, J. & Kosinski, J. ColabSeg: An interactive tool for editing, processing, and visualizing membrane segmentations from cryo-ET data. *J. Struct. Biol.* **216**, 108067 (2024).
72. Pyle, E., Hutchings, J. & Zanetti, G. Strategies for picking membrane-associated particles within subtomogram averaging workflows. *Faraday Discuss* **240**, 101–113 (2022).
73. Pettersen, E. F. *et al.* UCSF Chimera—A visualization system for exploratory research and analysis. *J. Comput. Chem.* **25**, 1605–1612 (2004).
74. Castaño-Díez, D., Kudryashev, M., Arheit, M. & Stahlberg, H. Dynamo: A flexible, user-friendly development tool for subtomogram averaging of cryo-EM data in high-performance computing environments. *J. Struct. Biol.* **178**, 139–151 (2012).

982 **Figures and Captions**

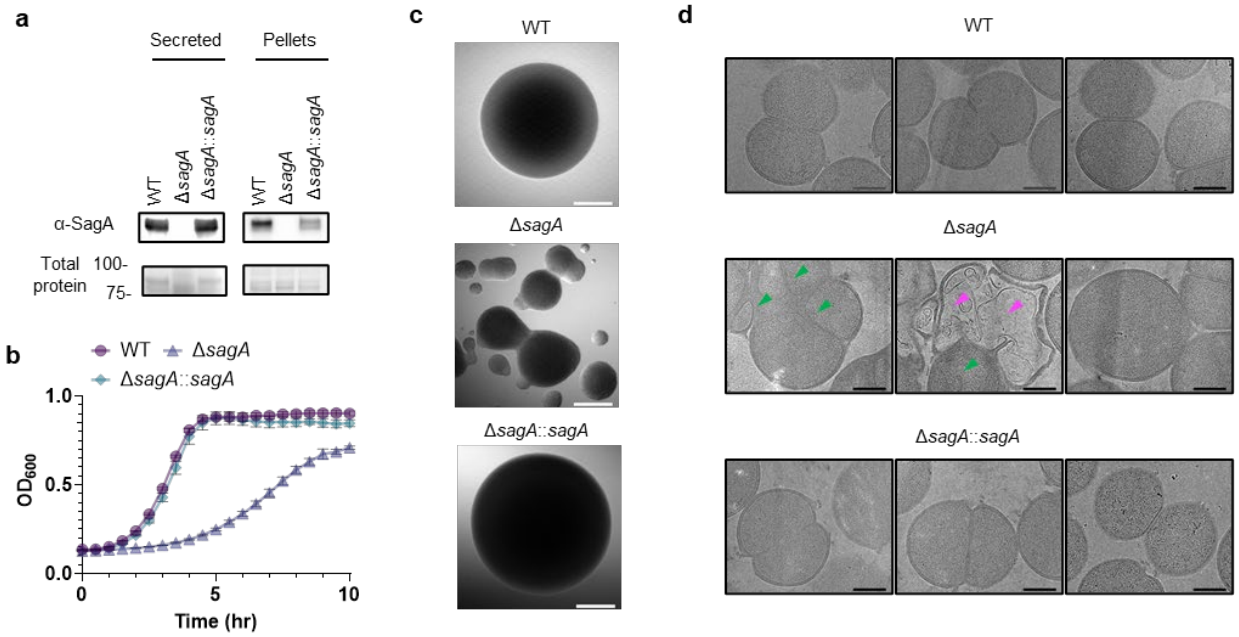

983

984 **Fig. 1 | SagA is important for peptidoglycan remodeling, cell separation and growth in**
985 **VREfm.**

986 **a**, α-SagA western blot analysis of bacterial proteins (secreted and in cell pellets) of VREfm
987 ERV165 strains (WT, Δ*sagA* or Δ*sagA*::*sagA*). Stain-free imaging serves as total protein loading
988 control. **b**, Growth curves of VREfm ERV165 strains in BHI. **c**, Representative DIC images of
989 single colonies of VREfm strains. Scale bar, 200 μm. **d**, Representative low-magnification (3600×)
990 electron microscopy images from lamellae of VREfm ERV165 strains. Dead cells are indicated
991 with magenta arrows; defective cell divisions are marked with green arrows. Scale bars, 500 nm.

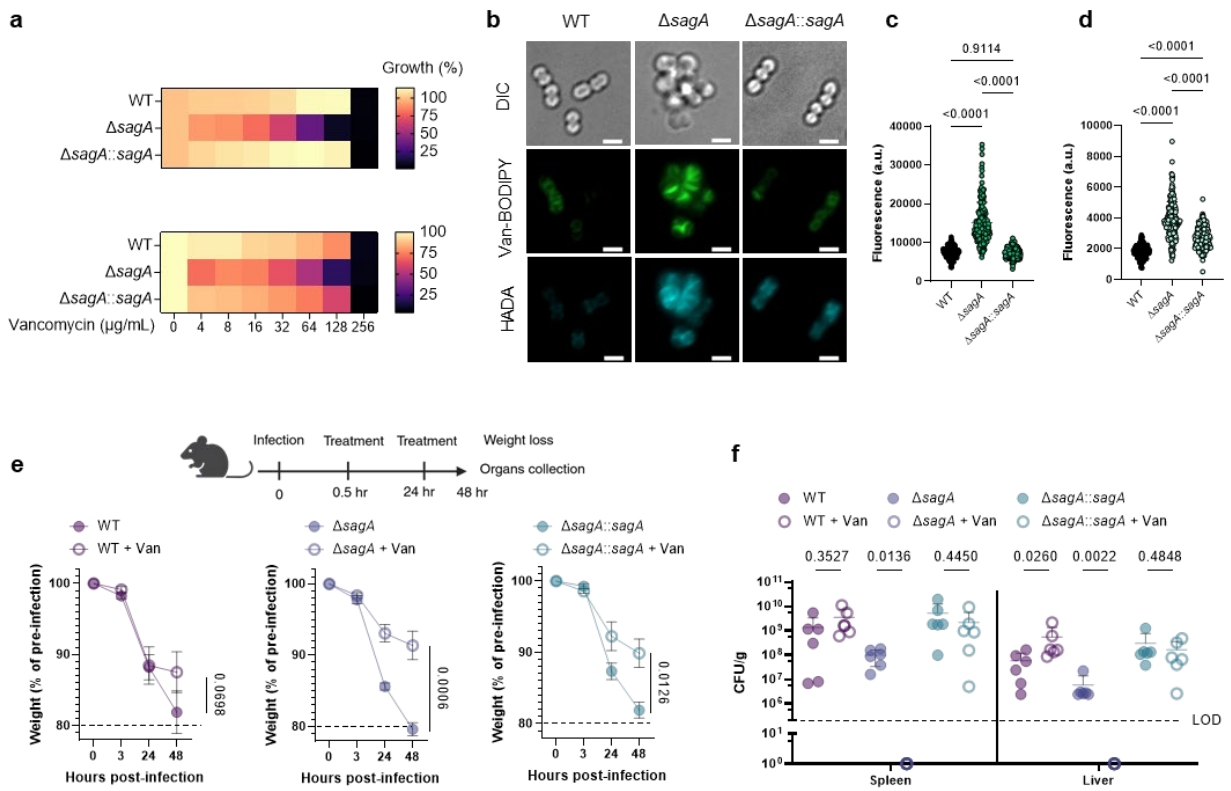

Fig. 2 | SagA is important for VREfm antibiotic susceptibility *ex vivo* and *in vivo*.

a, Vancomycin susceptibility of ERV165 strains after 10 hours of growth. Top: susceptibility in BHI. Bottom: susceptibility in MHB. Data is a heat map of mean values, n=3 biological replicates. **b**, Fluorescence microscopy imaging of VREfm strains stained with Van-BODIPY (50 μg/mL) and fluorescent D-amino acids (HADA, 0.5 mM). Differential Interference Contrast (DIC) images show cell wall morphology, with cell clustering apparent in Δ*sagA*. Scale bar, 2 μm. **c**, Fluorescence of Van-BODIPY-stained VREfm strains. **d**, Fluorescence of HADA-stained VREfm strains. For (**c**), (**d**) each dot is an individual cell, n=200. **e**, Scheme of systemic infection *in vivo* with VREfm strains (ERV165 WT, Δ*sagA* or Δ*sagA*::*sagA*): mice were infected with 10^9 VREfm CFU intraperitoneally. PBS or vancomycin (Van, 100 mg/kg) was administered subcutaneously. Weight was monitored at 3, 24, and 48 hours post-infection. Mice were sacrificed, organs were collected and VREfm burdens were analyzed by CFU counting. Weight (% of pre-infection) of mice infected with VREfm ERV165 strains (WT, Δ*sagA* or Δ*sagA*::*sagA*) ± vancomycin (Van, 100 mg/kg). Data is mean ± S.E.M. and analyzed by one-way ANOVA with uncorrected Fisher's LSD post-test, n=6 mice. **f**, CFU analysis of organs from mice infected with VREfm strains (ERV165 WT, Δ*sagA* or Δ*sagA*::*sagA*) ± vancomycin (Van, 100 mg/kg). Horizontal line is mean ± S.E.M. Data is analyzed by unpaired Mann-Whitney test. Each dot is an individual mouse, n=6.

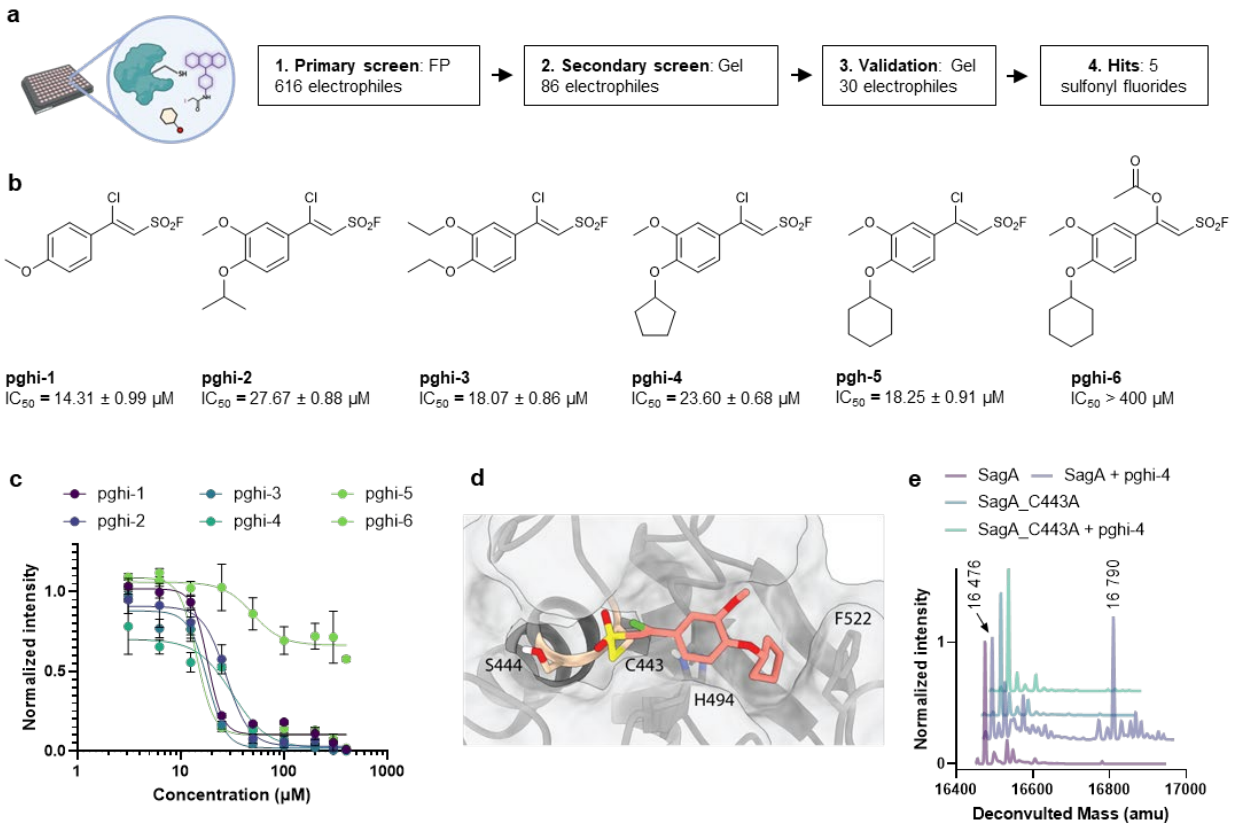

Fig. 3 | Activity-guided screening identifies sulfonyl fluorides as SagA inhibitors.

a, Scheme and workflow of activity-guided screening. An agnostic screen of 616 electrophiles in competitive fluorescence polarization (FP) assay led to selection of 86 electrophiles that were screened in a competitive gel-based cysteine activity assay. Activities of 30 molecules were further validated in a gel-based peptidoglycan hydrolase activity assay (Extended Data Fig. 7). **b**, Structures of identified 5 most active (pghi-1 to 5) and inactive (pghi-6) sulfonyl fluorides as SagA inhibitors with biochemical IC_{50} for SagA activity (Extended Data Fig. 8a,b). **c**, IC_{50} curves of sulfonyl fluorides determined by gel-based peptidoglycan hydrolase activity assay. Data is mean ± S.E.M., n=3 biological replicates. **d**, Covalent docking model of pghi-4 bound to C433 of SagA active site as the product of reaction *via* sulfonyl fluoride. **e**, Intact protein mass analysis of SagA (10 μM) ± pghi-4 (200 μM) and inactive mutant SagA_C433A (10 μM) ± pghi-4 (200 μM). Numbers indicate detected masses of SagA and SagA-pghi-4 adduct.

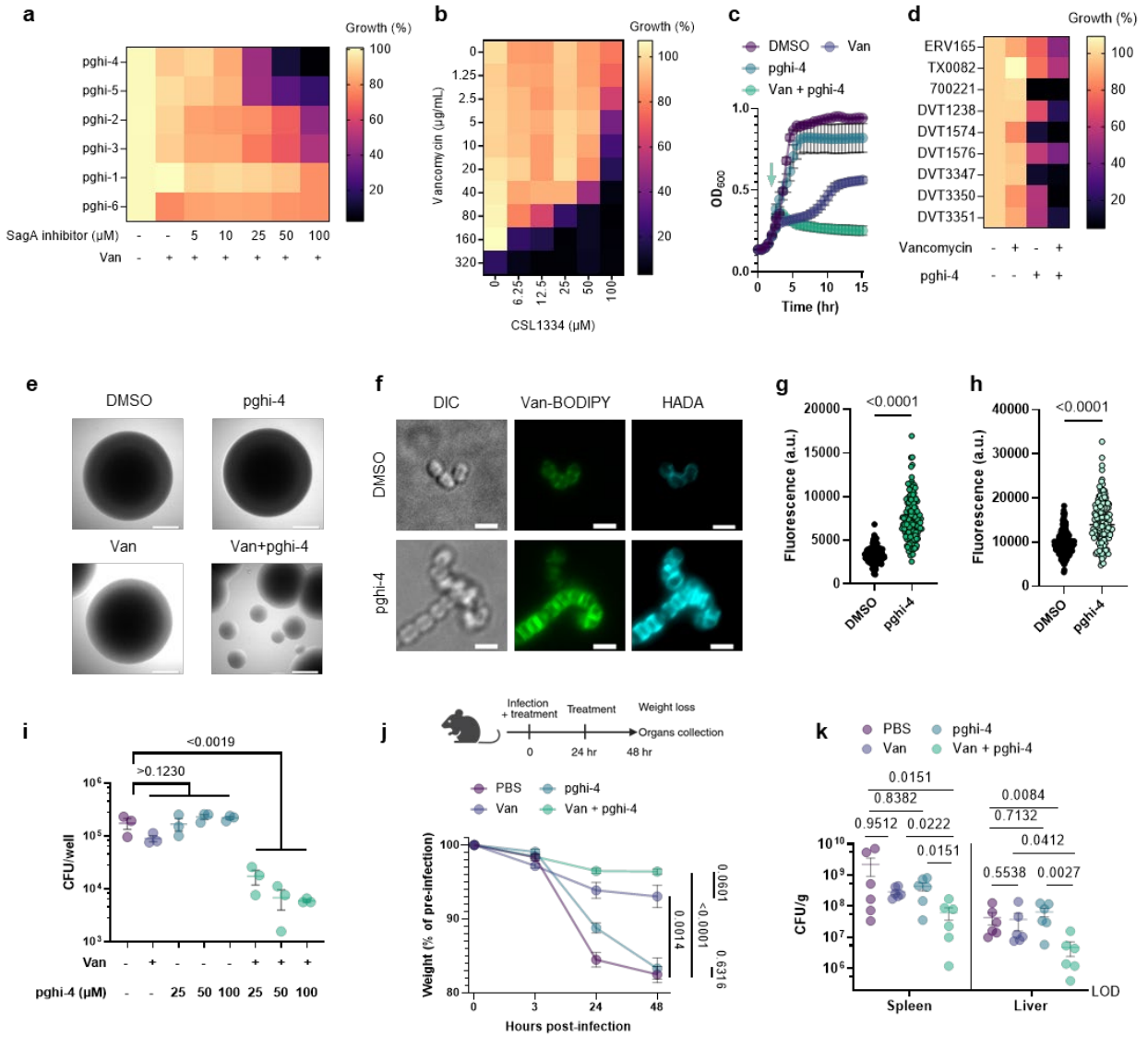

Fig. 4 | Pghi-4 is an antibiotic adjuvant against VREfm.

a, Effect of sulfonyl fluorides + vancomycin (Van, 5 μg/mL) on VREfm (ERV165) growth. **b**, Pghi-4 synergism with vancomycin against ERV165 evaluated by checkerboard assay. Data in **a** and **b** is heatmap of median values relative to DMSO control, n=3. **c**, Bacteria-kill growth curves. Exponentially grown ERV165 were treated with pghi-4 (100 μM), vancomycin (Van, 100 μg/mL) or in combination for 18 hours, followed by OD600 measurement and CFU analysis (Extended Data Fig. 11d). The green arrow indicates the time point when the treatment was added. **d**, Effect of pghi-4 (50 μM) ± vancomycin (Van, 5 μg/mL) on growth of VREfm clinical isolates. Data is heatmap of median values relative to DMSO control, n=3 biological replicates. **e**, DIC images of single colonies of VREfm ± vancomycin (Van, 100 μg/mL) ± pghi-4 (100 μM). Scale bar, 200 μm. **f**, Fluorescence microscopy imaging of VREfm ± pghi-4 (50 μM) stained with Van-BODIPY (50 μg/mL) and HADA (0.5 mM). Scale bar, 2 μm. **g**, Fluorescence of Van-BODIPY-stained VREfm ± pghi-4 (50 μM). **h**, Fluorescence of HADA-stained VREfm ± pghi-4 (50 μM). For **g-h** each dot is individual cell, n=143. **i**, CFU analysis of VREfm-infected RAW264.7 cells treated with

1038 vancomycin (100 μg/mL), pghi-4 alone or in combination. Data is mean and analyzed by one-way
1039 ANOVA with uncorrected Fisher's LSD post-test ± S.E.M., n=3 biological replicates. **j**, Top:
1040 scheme of systemic infection *in vivo* with VREfm (ERV165): mice were infected with 10^9 VREfm
1041 CFU with PBS (0.25% CMC), pghi-4 (25 mg/kg 0.25% CMC) ± vancomycin (Van, 100 mg/kg
1042 0.25% CMC) intraperitoneally. 24 hours post-infection mice were given the second dose. Weight
1043 was monitored at 3, 24, 48 hours post-infection. Mice were sacrificed, organs were collected and
1044 VREfm burden was analyzed by CFU. Bottom: weight (% of pre-infection) of mice VREfm-infected
1045 ± 2 doses of pghi-4 (25 mg/kg 0.25% CMC) ± vancomycin (Van, 100 mg/kg 0.25% CMC). Data
1046 is mean ± S.E.M. and analyzed by one-way ANOVA with uncorrected Fisher's LSD post-test, n=6
1047 mice. **k**, CFU analysis of organs from VREfm-infected mice ± 2 doses of pghi-4 (25 mg/kg 0.25%
1048 CMC) ± vancomycin (Van, 100 mg/kg 0.25% CMC). Y axis starts from the limit of detection (LOD),
1049 horizontal line is mean ± S.E.M. Data is analyzed by Kruskal-Wallis test with Dunn's uncorrected
1050 post-test. Each dot is individual mouse, n=6.

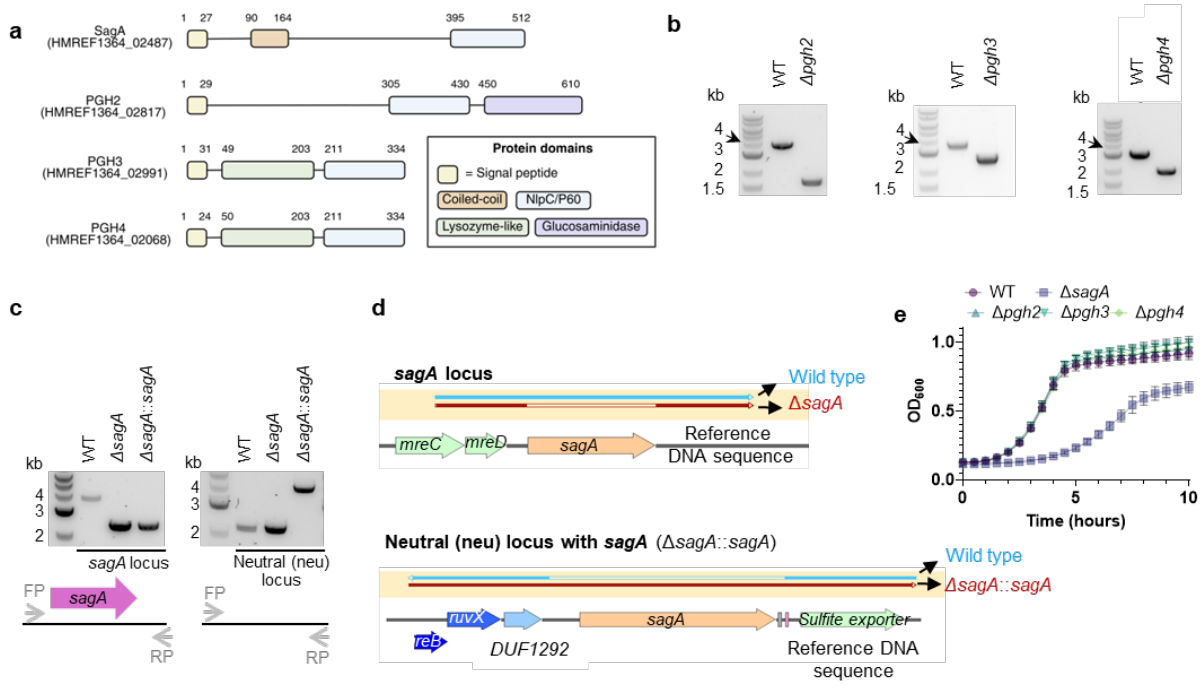

Extended Data Fig. 1 | Characterization of *E. faecium* ERV165 NlpC/P60 hydrolases mutants.

a, Identification of SagA orthologs in vancomycin-resistant *E. faecium* and comparison of their primary sequence homology and domain architecture. Numbers above each bar are amino acid coordinates of the indicated domains. **b,** Colony PCR analysis of successful deletion of *phg2*, *pgh3*, *pgh4*. **c**, Colony PCR analysis using primers flanking the *sagA* and neutral loci to verify the *sagA* deletion mutant and chromosomal complementation strain, respectively. The left agarose gel shows successful deletion of *sagA* in both the mutant and the complementation strain. The right gel confirms *sagA* gene insertion at the neutral locus in the chromosomal complementation strain, but not in the wild-type (WT) or *sagA* mutant. **d**, Top: DNA sequencing reads from WT (blue) and *sagA* mutant (red) aligned to the ERV165 WT reference, confirming deletion. Bottom: DNA sequencing reads from WT (blue) and the chromosomal complementation strain (red) aligned to the complementation strain reference, confirming integration of *sagA* at a neutral locus. **e,** Growth curves of ERV165 strains in BHI. is mean ± S.D., n=3 biological replicates.

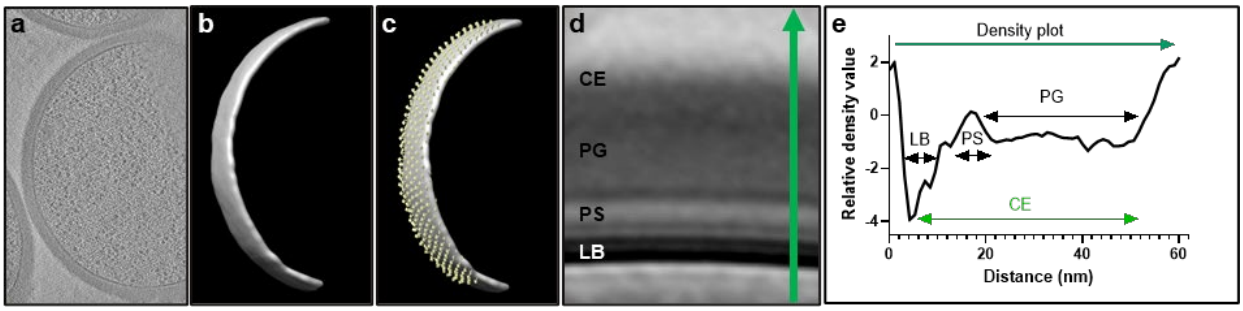

Extended Data Fig. 2 | Subtomogram averaging and analysis workflow.

a, Representative tomographic slice after reconstruction. **b**, 3D rendering of the segmented lipid bilayer. **c**, Subtomogram picks visualized on the segmentation (yellow); arrows indicate subtomogram positions and orientations. **d**, Averaged subtomogram map. Annotated layers include: CE, total cell envelope; PG, peptidoglycan (cell wall); PS, periplasmic space; LB, lipid bilayer. A green arrow is drawn across the cell envelope in the average map to collect relative density values. **e,** Plot of relative density values across the average map. Lower density values correspond to darker regions. Measurements were taken based on peak distances in the density profiles.

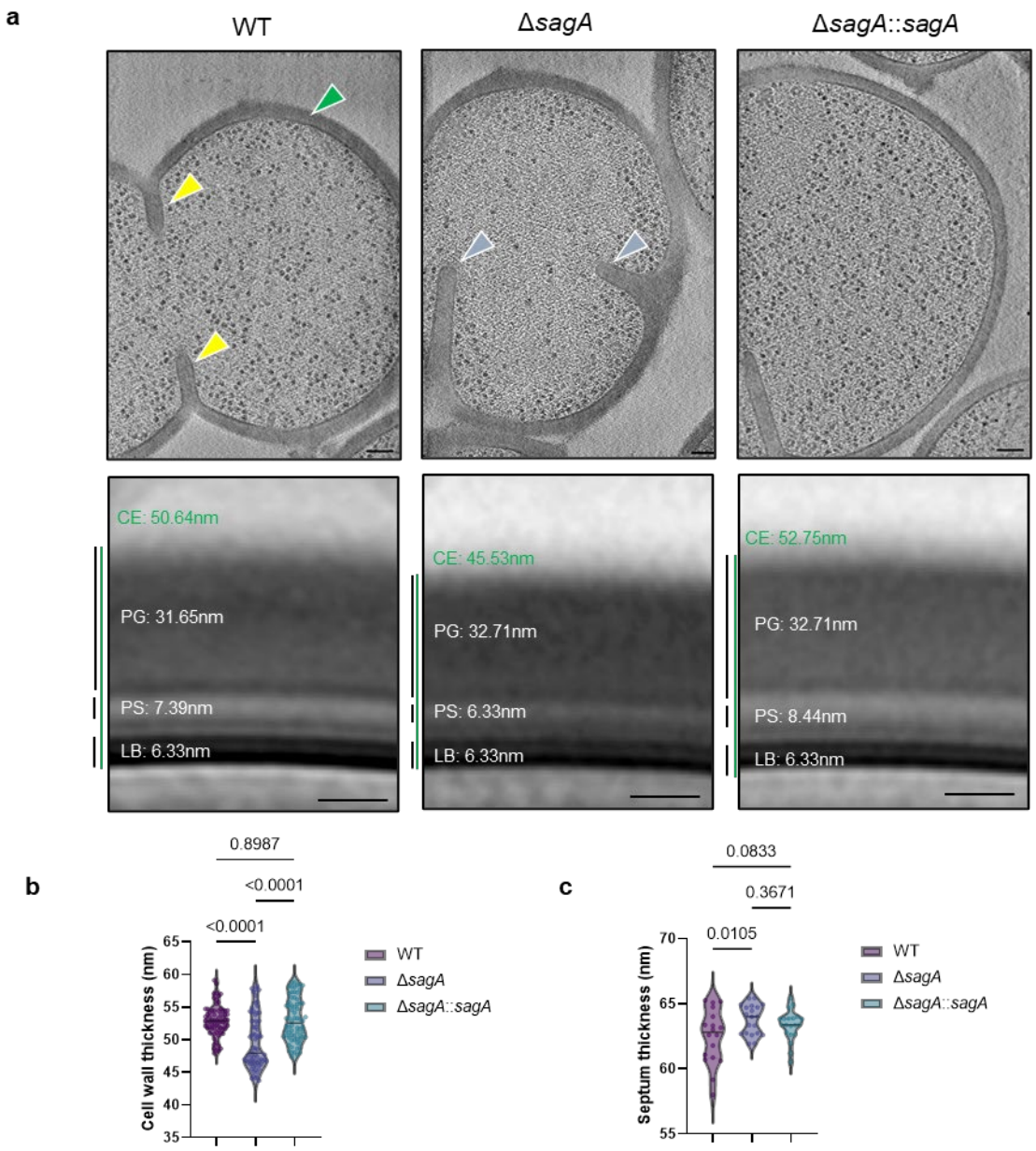

Extended Data Fig. 3 | Ultrastructure of VREfm ERV165 strains. a, Top panel: representative cryo-electron tomographic (cryo-ET) slices of VREfm ERV165 strains. The cell wall is annotated with green arrows; normal septa are indicated with yellow arrows; and defective division septa are also marked with blue arrows. Images were acquired at a magnification corresponding to a pixel size of 2.638 Å (38,000×). Tomograms were 4× binned, resulting in a final pixel size of 10.55 Å. Scale bar, 100 nm. Bottom panel: subtomogram averages of the cell envelope of VREfm ERV165 strains were generated using Dynamo. Measured thicknesses of various envelope layers are indicated. Thickness measurements were derived from density plots of the subtomogram averages. Abbreviations: CE, total cell envelope; PG, cell wall; PS, periplasmic space; LB, lipid bilayer. Thickness measurements were obtained from density plots of the subtomogram averages (see Methods, Extended Data Fig. 2). Scale bar, 100 nm. **b**, Comparison of cell wall thickness.

1088 Data are shown as violin plots with dots representing individual data points and analyzed by one-
1089 way ANOVA with uncorrected Fisher's LSD post-test, n=70. Grey horizontal lines represent
1090 median (WT: 52.93 nm, Δ*sagA*: 49.63 nm, Δ*sagA*::*sagA*: 53.01 nm). Grey dotted lines represent
1091 quartiles. **c**, Comparison of septum thickness. Data are shown as violin plots with dots
1092 representing individual data points and analyzed by one-way ANOVA with uncorrected Fisher's
1093 LSD post-test, n=70. Grey horizontal lines represent median (WT: 62.48 nm, Δ*sagA*: 63.73 nm,
1094 Δ*sagA*::*sagA*: 63.40 nm).

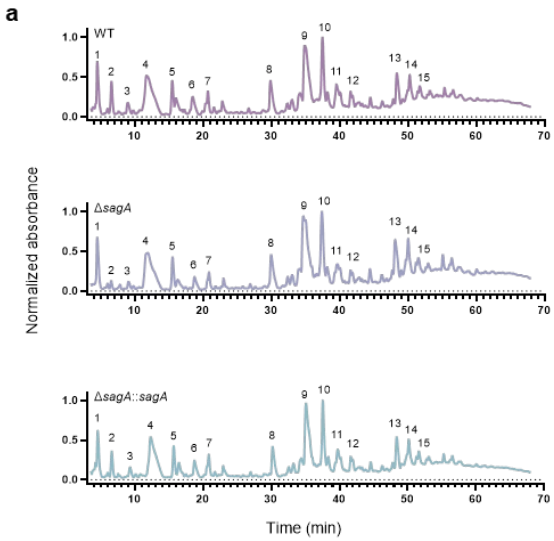

b

Peak #[a]	Proposed structure[b]
1	GM-tri
2	GMDP
3	GM-tetra
4	GM-tri (Asn)[c]
5	GM-tri (Asp)[c]
6	GM-tetra (Asn)
7	GM-penta (Asx)
8	2GM-tri (Asx) - tetra
9	2GM-tri (Asn) - tetra (Asn)[c]
10	2GM-tri (Asx) - tetra (Asx)[c]
11	2GM-tetra (Asn) - tetra (Asn)[c]
12	2GM-tetra (Asp) - tetra (Asp)[c]
13	3GM-tetra (Asx) - tetra (Asx) - tri (Asx)[c]
14	3GM-tetra (Asx) - tetra (Asx) - tri (Asx)[c]
15	3GM-tetra (Asx) - tetra (Asx) - tetra (Asx)

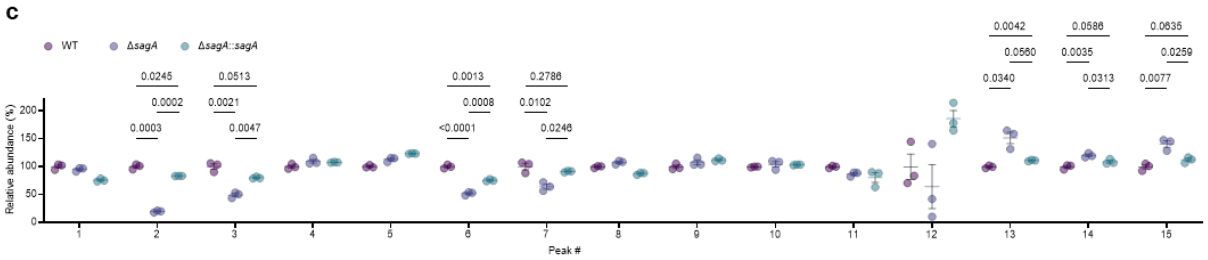

Extended Data Fig. 4 | Inactivation of peptidoglycan remodeling in VREfm.

a, Representative LC-MS chromatograms of mutanolysin-digested peptidoglycan isolated from sacculi of VREfm ERV165 strains. **b**, Composition of peptidoglycan isolated from VREfm sacculi. [a] Peak numbers refer to **a**. [b] GM, disaccharide (GlcNAc-MurNAc); 2 GM, disaccharide-disaccharide (GlcNAc-MurNAc-GlcNAc-MurNAc); 3 GM, disaccharide-disaccharide-disaccharide (GlcNAc-MurNAc-GlcNAc-MurNAc-GlcNAc-MurNAc); GM-Tri, disaccharide tripeptide (L-Ala-D-iGln-L-Lys); GM-Tetra, disaccharide tetrapeptide (L-Ala-D-iGln-L-Lys-D-Ala); GM-Penta, disaccharide pentapeptide (L-Ala-D-iGln-L-Lys-D-Ala -D-Ala). [c] The assignment of the amide and the hydroxyl functions to either peptide stem is arbitrary. Masses and retention time of peptidoglycan fragments are in Extended Data Table 11. **c**, Normalized abundance (relative to WT) of peptidoglycan fragments isolated from mutanolysin-digested sacculi of VREfm and analyzed by LC-MS. For **c** peak numbers indicate corresponding peptidoglycan fragment from LC-MS analysis listed in (**a**), data are mean ± S.D., n=3 biological replicates, analyzed with uncorrected Fisher's LSD post-test, and p values of significant differences are indicated.

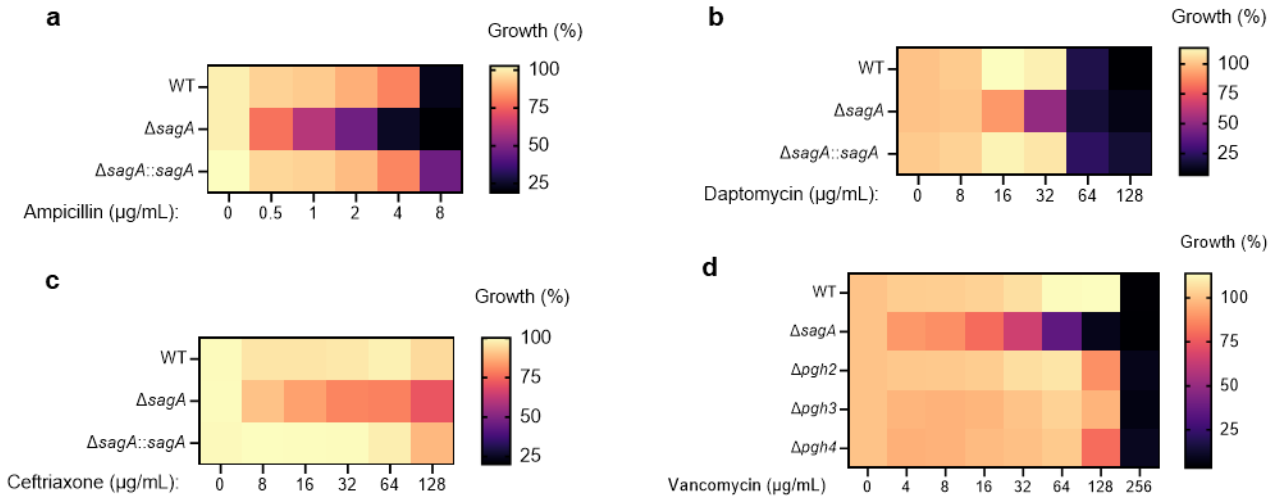

Extended Data Fig. 5 | Antibiotic susceptibility of VREfm strains.

a, Ampicillin susceptibility of ERV165 strains after 10 hours. **b**, Daptomycin susceptibility of ERV165 strains after 10 hours. **c**, Ceftriaxone susceptibility of ERV165 strains after 10 hours. **d**, Vancomycin susceptibility of ERV165 strains after 10 hours. For **a-d,** data are shown as a heat map of mean values, n=3 biological replicates.

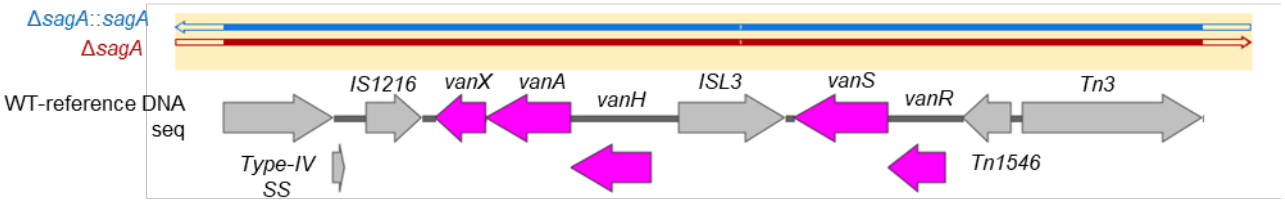

Extended Data Fig. 6 | DNA sequencing reads from Δ*sagA*::*sagA* (blue) and *sagA* mutant (red) aligned to the ERV165 WT reference confirming intact *van* genes.

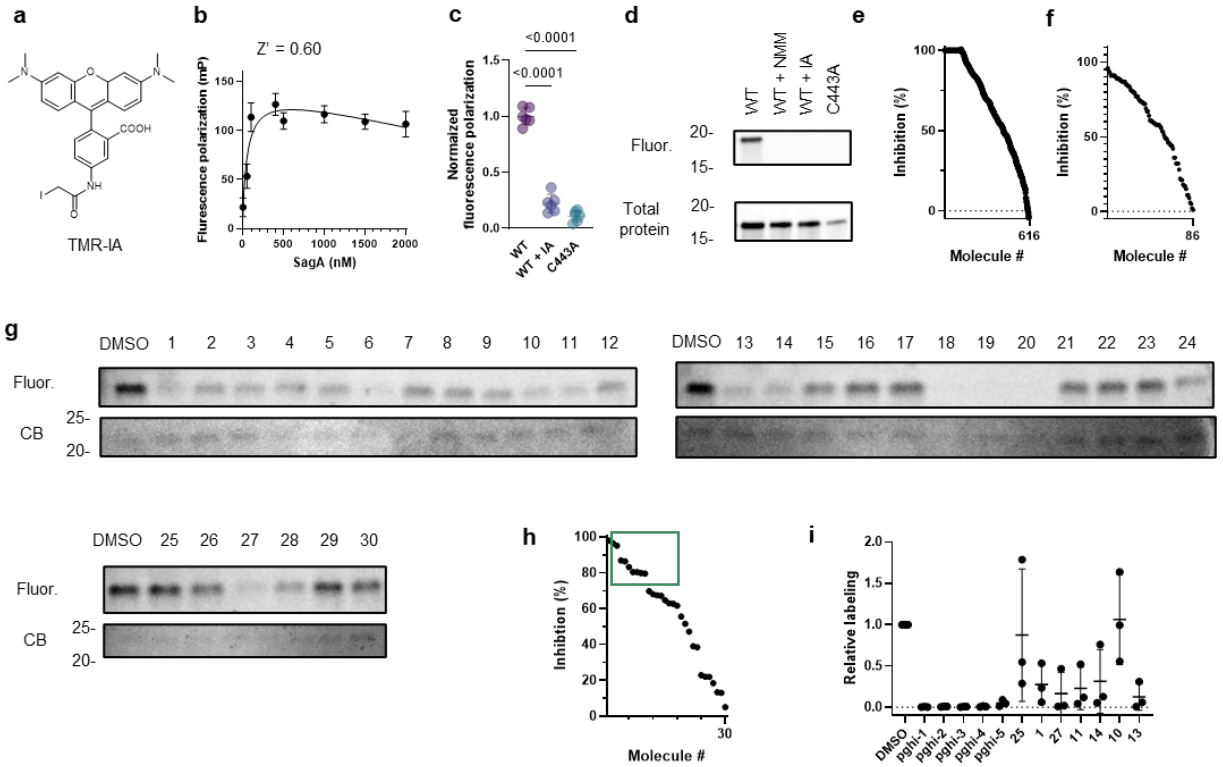

Extended Data Fig. 7 | Validation of sulfonyl fluorides as SagA inhibitors.

a, Structure of TMR-IA probe. **b**, Fluorescence polarization of TMR-IA (20 nM) with increasing concentration of recombinant SagA after 30 min incubation at room temperature in 384-well format. Z' factor > 0.5 indicates the assay is suited for high-throughput screening. **c**, Fluorescence polarization (FP) assay for evaluating SagA (500 nM) cysteine reactivity with TMR-IA probe (20 nM) in 384-well format. FP signal was depleted when SagA was co-treated with non-specific cysteine-active iodoacetamide (IA, 1 mM) and TMR-IA (20 nM); or inactive SagA_C433A was treated with TMR-IA (20 nM). Data is mean ± S.D. and analyzed by one-way ANOVA, n=6 biological replicates. **d**, Gel of recombinant SagA (500 nM) treated with TMR-IA (50 nM) separated by SDS-PAGE and visualized by fluorescence. Fluorescent bands were absent when SagA was co-treated with non-specific cysteine-active *N*-methylmaleimide (NMM, 1mM), iodoacetamide (IA, 1 mM). TMR-IA treatment failed to produce fluorescent band of recombinant inactive mutant SagA_C443A (C433A). Stain-free imaging serves as total protein loading control. **e,** Plot of primary screen using competitive FP assay and TMR-IA probe. TMR-IA-treated inactive mutant SagA_C433A treated was used as lower limit of FP signal. Note: some molecules produce FP signal lower than SagA_C433A resulting in inhibition >100% that were assigned as 100% inhibition **f**, Plot of secondary screen of 86 molecules using competitive gel-based assay and TMR-IA probe. Inhibition (%) was calculated as TMR-IA competition relative to DMSO control, n=1. **g**, Gels of validation of 30 sulfonyl fluorides. Recombinant SagA (0.5 μM) treated with sulfonyl fluorides (50 μM), followed by TMR-IA (50 nM), separated by SDS-PAGE and visualized by fluorescence. Coomassie blue (CB) staining served as total protein control. **h**, Plot of validation of 30 molecules using competitive gel-based assay and TMR-IA probe. For **f**, **h** inhibition (%) was calculated as competition with TMR-IA relative to DMSO control, n=1. **i**, Plot of revalidation of 12

1143 most active sulfonyl fluorides (green box in **e**) using competitive gel-based assay. Data are mean
1144 labeling values relative to DMSO ± S.D, n=3 biological replicates.

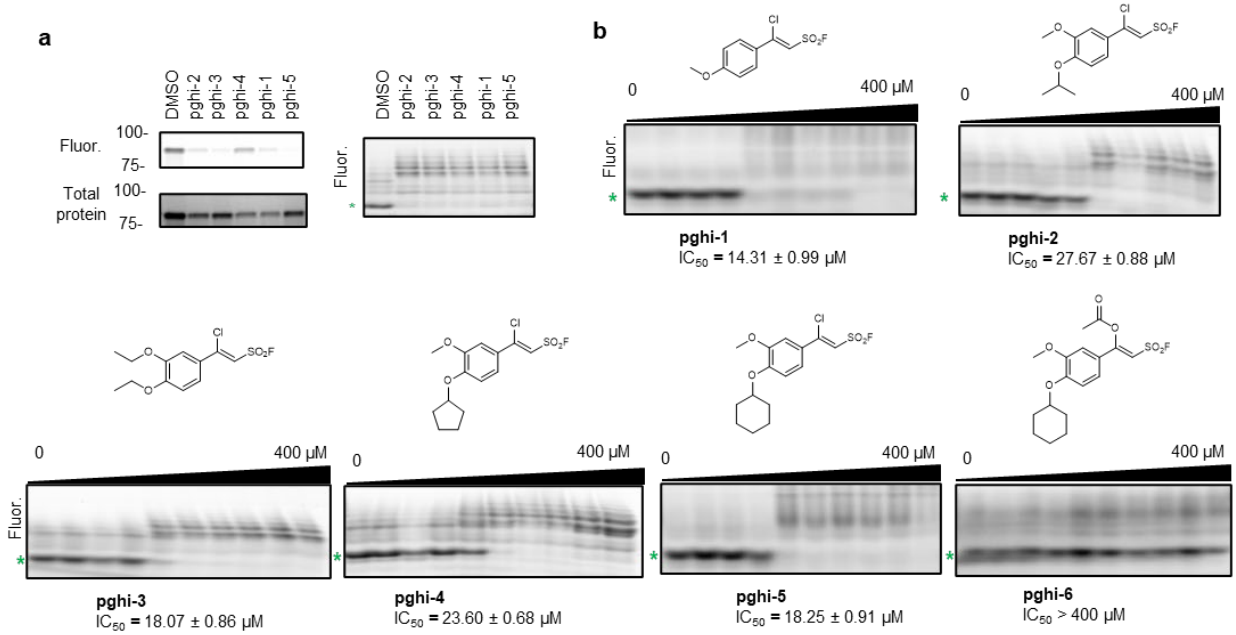

Extended Data Fig. 8 | Structure-activity relationship of SagA inhibitors.

a, Activity of top 5 sulfonyl fluorides (50 μM) against of recombinant SagA (10 μM) profiled in competitive gel-based (on the left) and peptidoglycan hydrolase activity (on the right) assays. **b**, Native gel profiling assay of hydrolase activity of recombinant SagA (10 μM) treated with sulfonyl fluorides (0 - 400 μM) and mutanolysin-digested peptidoglycan from Efm (100 μg) followed by peptidoglycan labeling with ANTS (0.2 M), separated by gel electrophoresis. For **a** and **b,** green asterisk indicates the main enzymatic product GlcNAc-MurNAc-L-Ala-D-isoGln (GlcNAc-MDP)

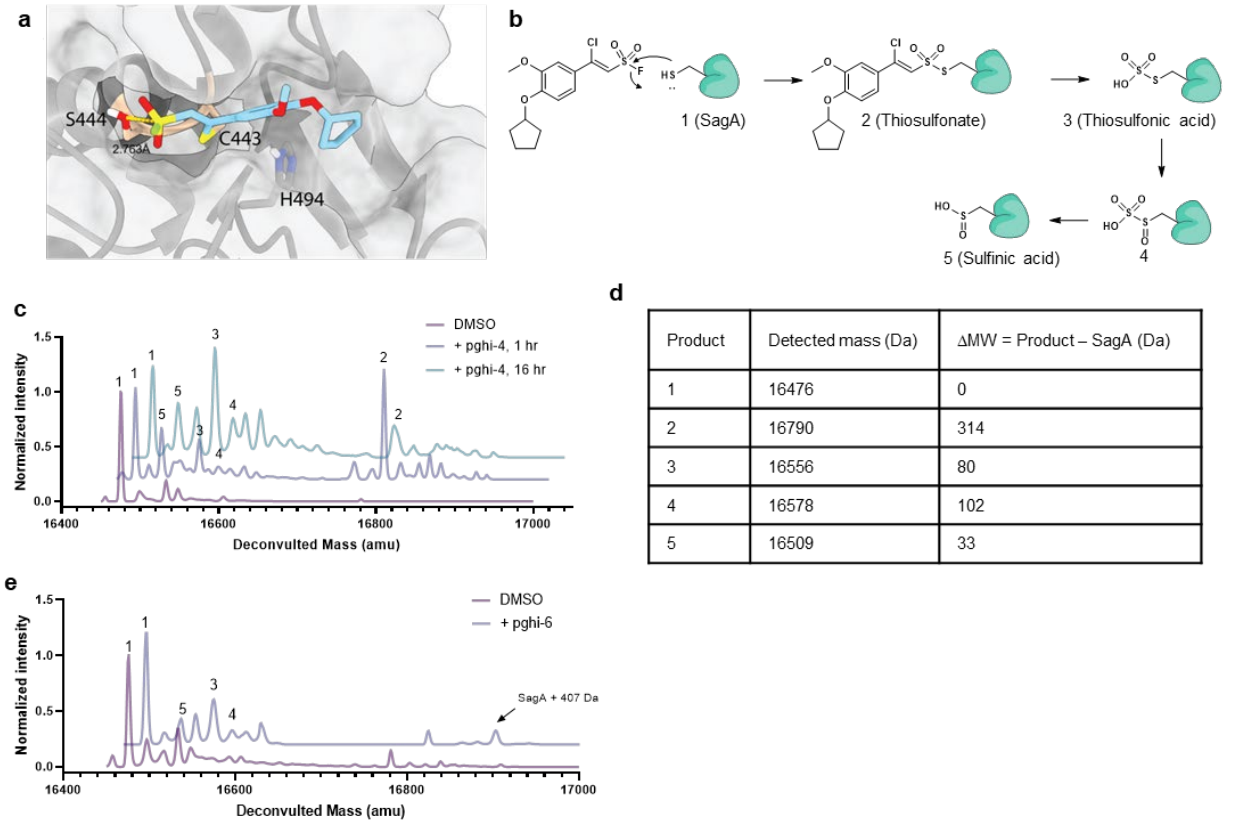

Product	Detected mass (Da)	ΔMW = Product – SagA (Da)
1	16476	0
2	16790	314
3	16556	80
4	16578	102
5	16509	33

Extended Data Fig. 9. Sulfonyl fluorides are covalent inhibitors of SagA.

a, Covalent docking model of pghi-4 to cysteine (C433) of SagA as adduct of vinyl chloride activity. **b,** Proposed structures of pghi-4-SagA adduct and products of hydrolysis detected by intact protein analysis (ESI). **c,** Intact protein analysis (ESI) of SagA (10 μM) treated with pghi-4 (50 μM) for 1 or 16 hours at room temperature. Numbers indicate products from scheme (**b**). **d,** Table of detected masses of SagA (10 μM) treated with pghi-4 (50 μM) and calculated differences in masses compared to unmodified SagA (ΔMW). **e,** Intact protein analysis (ESI) of SagA (10 μM) treated with inactive pghi-6 (50 μM) for 1 hr. A minor formation of pghi-6-SagA adduct (SagA+407 Da) and products of hydrolysis were detected: 3, 4 and 5. Numbers indicate products from scheme (**b**).

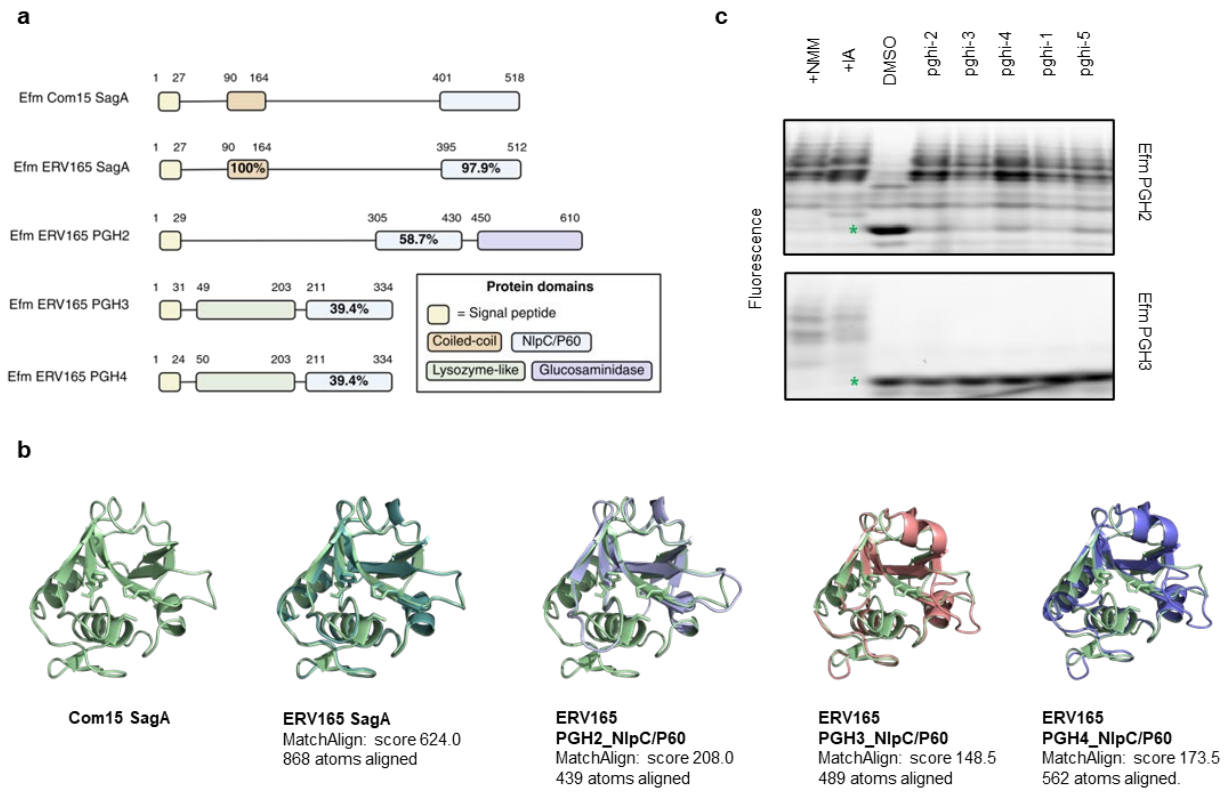

Extended Data Fig. 10. *Enterococcus* NlpC/P60 hydrolases.

a, Comparison of primary sequence homology and domain architecture of SagA orthologs and SagA-like proteins from commensal and vancomycin-resistant *E.* faecium. Numbers above each bar are amino acid coordinates of the indicated domains, and percentages are amino acid sequence identity relative to Efm Com15 SagA. **b**, 3D homology modeling of SagA orthologs from commensal and vancomycin-resistant *E. faecium*. Predicted structure models for catalytic domains were generated in AlphaFold3. Predicted structures were aligned with published structure of SagA (PDB: 6B8C) in PyMOL. The amino acid residues of the SagA catalytic triad are shown using stick models in light green. MatchAligh score and number of atoms aligned are analyzed in PyMol and indicated. **c**, Native gel profiling assay of hydrolase activity of representative recombinant SagA orthologs containing NlpC/P60 domain from *E. faecium* and *E. faecalis* treated with sulfonyl fluorides. Green star indicates a major enzymatic product GlcNAc-MDP.

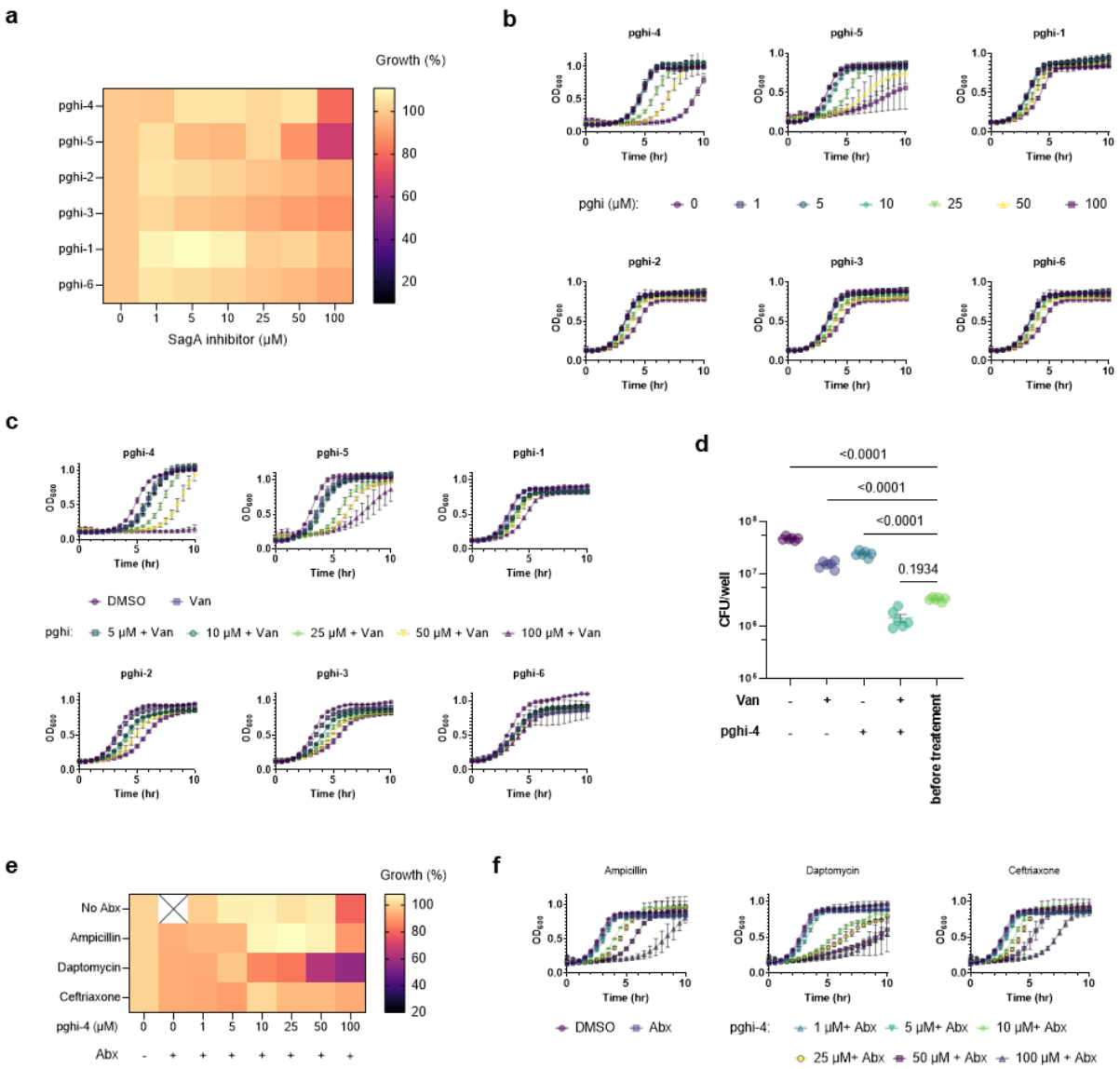

Extended Data Fig. 11. Antibacterial activity of SagA inhibitors.

a, Heat map of VREfm ERV165 growth (%) in the presence of sulfonyl fluorides after 10 hours. **b,** Growth curves VREfm ERV165 in the presence of sulfonyl fluorides in BHI. **c,** Growth curves of VREfm ERV165 in the presence of pghi-4 and subinhibitory dose of vancomycin (Van, 5 μg/mL) in BHI. **d,** Colony-forming unit (CFU) analysis of ERV165 after treatment with pghi-4 (100 μM), vancomycin (Van, 100 μg/mL) or in combination for 18 hours. VREfm before treatment were used for comparison. Data is mean ± S.E.M. and analyzed by one-way ANOVA with uncorrected Fisher's LSD post-test, n=3 biological replicates. **e,** Heat map of VREfm (ERV165) growth (%) in the presence of pghi-4 ± subinhibitory dose of ampicillin (1 μg/mL), daptomycin (4 μg/mL) or ceftriaxone (1 μg/mL) in BHI after 10 hours. Data is mean value, n=3 biological replicates. Cross indicates no data. **f,** Growth curves VREfm ERV165 in the presence of pghi-4 ± subinhibitory dose of ampicillin (1 μg/mL), daptomycin (4 μg/mL) or ceftriaxone (1 μg/mL) in BHI. For **a**, **e,** data are a heat map of mean values, n=3 biological replicates. For **b, c** and **f,** data are mean ± S.D., n=3 biological replicates.

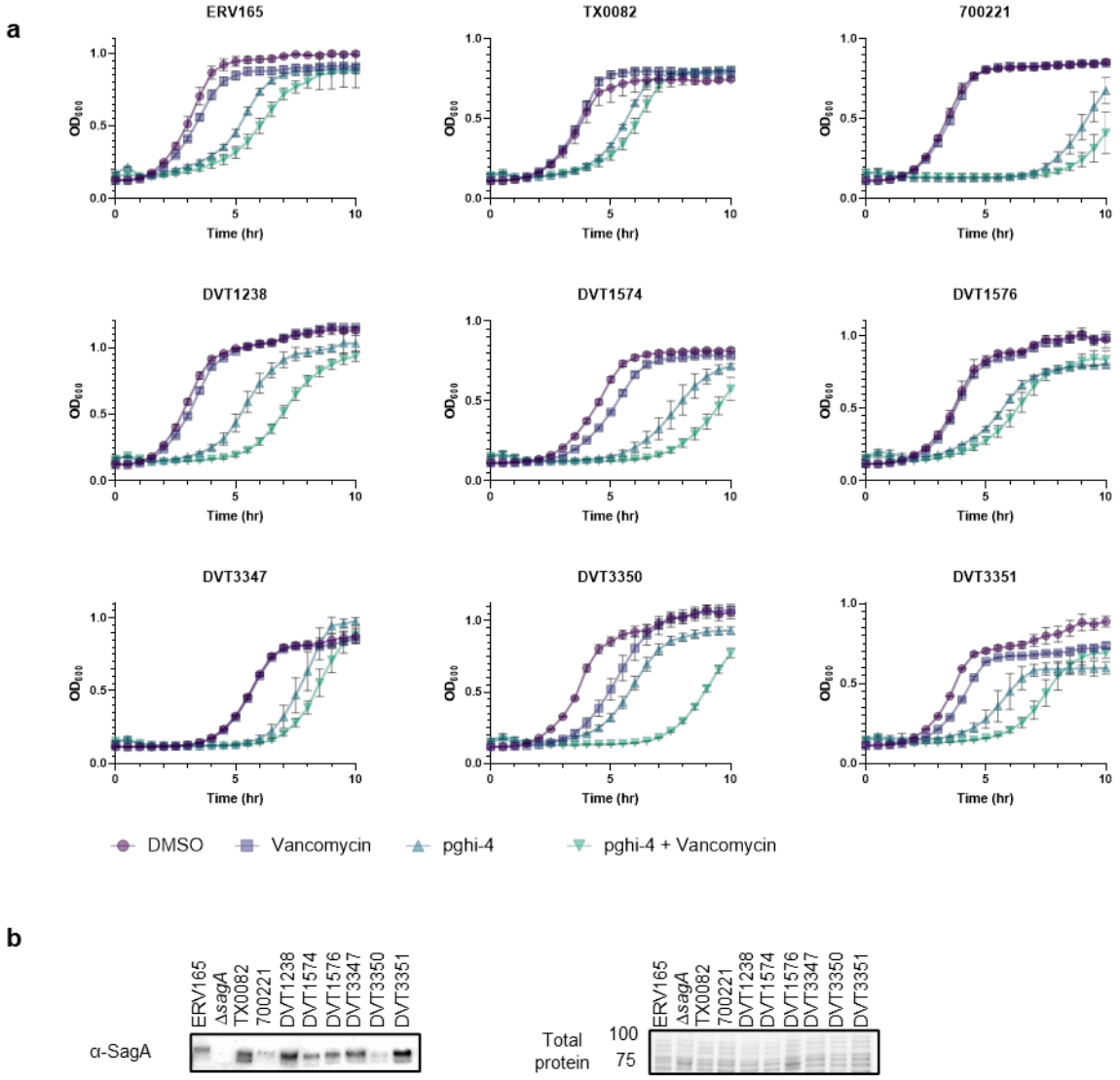

Extended Data Fig. 12. Therapeutic efficacy of pghi-4 as vancomycin adjuvant *in vitro*.

a, Growth curves of VREfm clinical isolates ± vancomycin (Van, 5 µg/mL) ± pghi-4 (50 µM) in BHI. Data is mean ± S.D., n=3 biological replicates. **b,** Left: α-SagA western blot of VREfm clinical isolates cell lysate. Right: Stain-free imaging served as protein loading control, numbers indicate molecular weight (kDa).

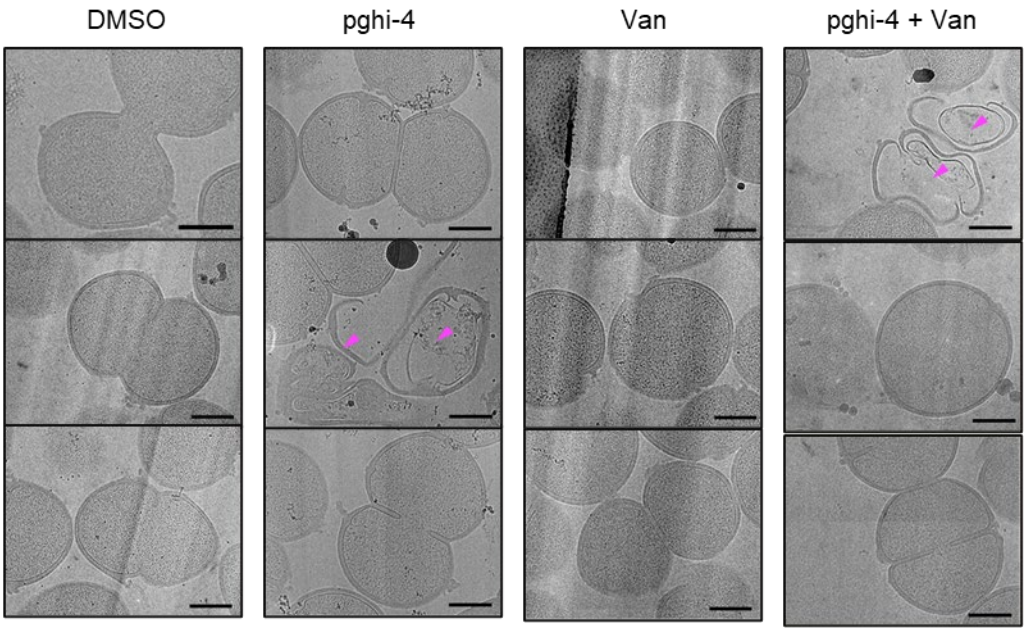

Extended Data Fig. 13. SagA inhibitor in combination with vancomycin alters VREfm cell morphology. Representative low-magnification (3600×) electron microscopy images from cryo-lamellae of VREfm in the presence of vancomycin (Van, 5 μg/mL) ± pghi-4 (50 μM). Each column contains three images of the same condition. Dead cells with undegraded peptidoglycan are indicated with magenta arrows. Scale bars, 500 nm.

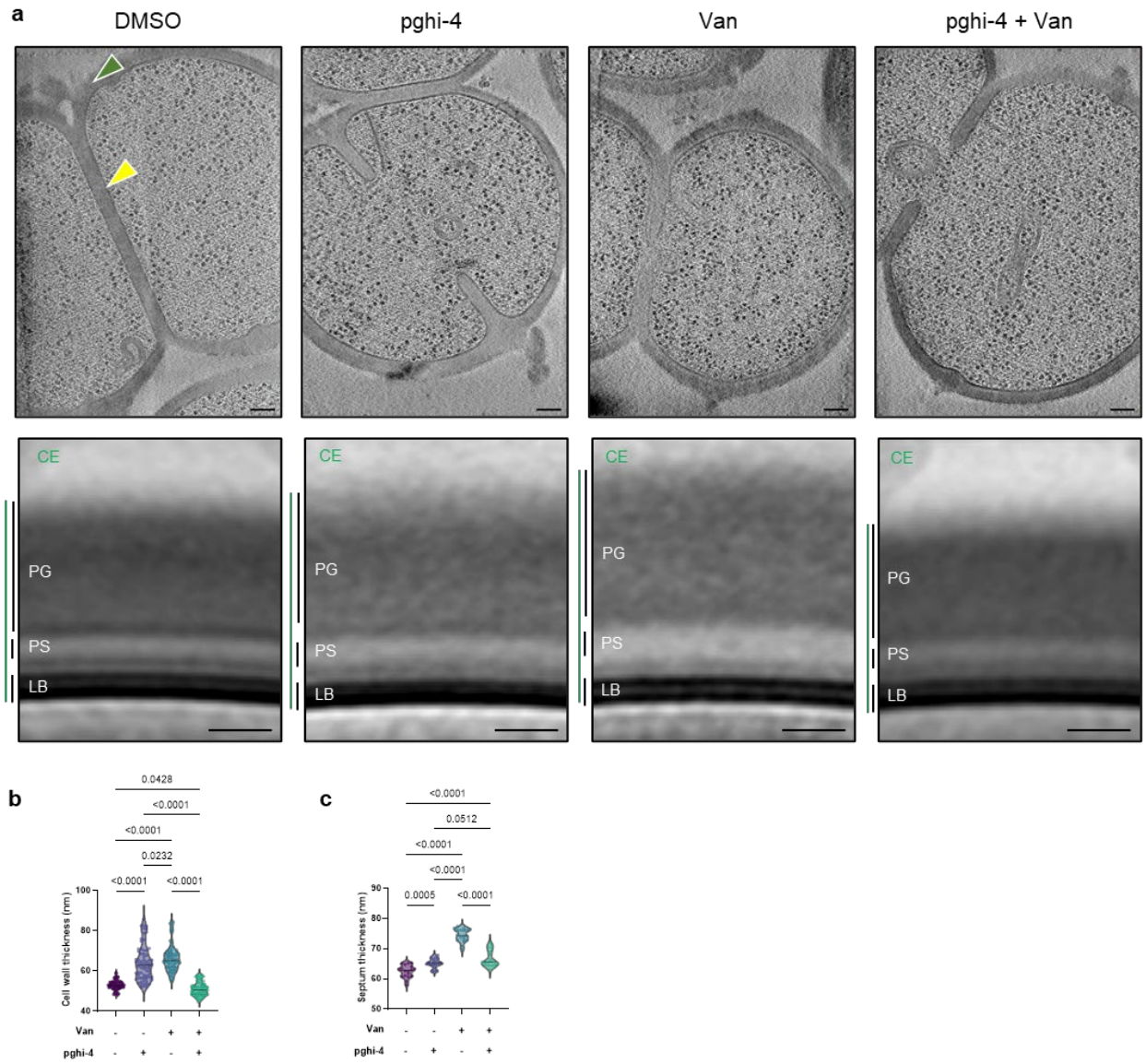

Extended Data Fig. 14. Ultrastructure of VREfm treated with SagA inhibitor pghi-4 ± vancomycin.

a, Top: representative cryo-electron tomography (cryo-ET) images of VREfm ± vancomycin (Van, 5 µg/mL) ± pghi-4 (50 µM) in BHI are shown in the top row. The cell wall is annotated with green arrows; normal septa are indicated with yellow arrows. Bottom: subtomogram averages of the cell envelope were generated using Dynamo. Measured thicknesses of various envelope layers are indicated. Thickness measurements were derived from density plots of the subtomogram averages. Abbreviations: CE, total cell envelope; PG, cell wall; PS, periplasmic space; LB, lipid bilayer. Thickness measurements were obtained from density plots of the subtomogram averages (see Methods). Scale bar, 100 nm. Note: images and analysis of “DMSO” are the same as “WT” in Extended Data Fig. 3a. **b,** Comparison of cell wall thickness. Data is violin plot with dots representing individual data points and analyzed by one-way ANOVA with uncorrected Fisher’s LSD post-test, n=70. Grey horizontal lines represent median (DMSO: 52.93 nm, pghi-4: 63.96 nm, Van: 66.20 nm, Van+pghi-4: 50.93 nm). **c,** Comparison of septum thickness. Data are shown

1220 as violin plots with dots representing individual data points and analyzed by one-way ANOVA with
1221 uncorrected Fisher's LSD post-test, n=70. Grey horizontal lines represent median (DMSO: 62.48
1222 nm, pghi-4: 65.24 nm, Van: 74.45 nm, Van+pghi-4: 66.56 nm). Note: images and data for DMSO
1223 are same as WT in Extended Data Fig. 3; workflow of the analysis is in Extended Data Fig. 2.

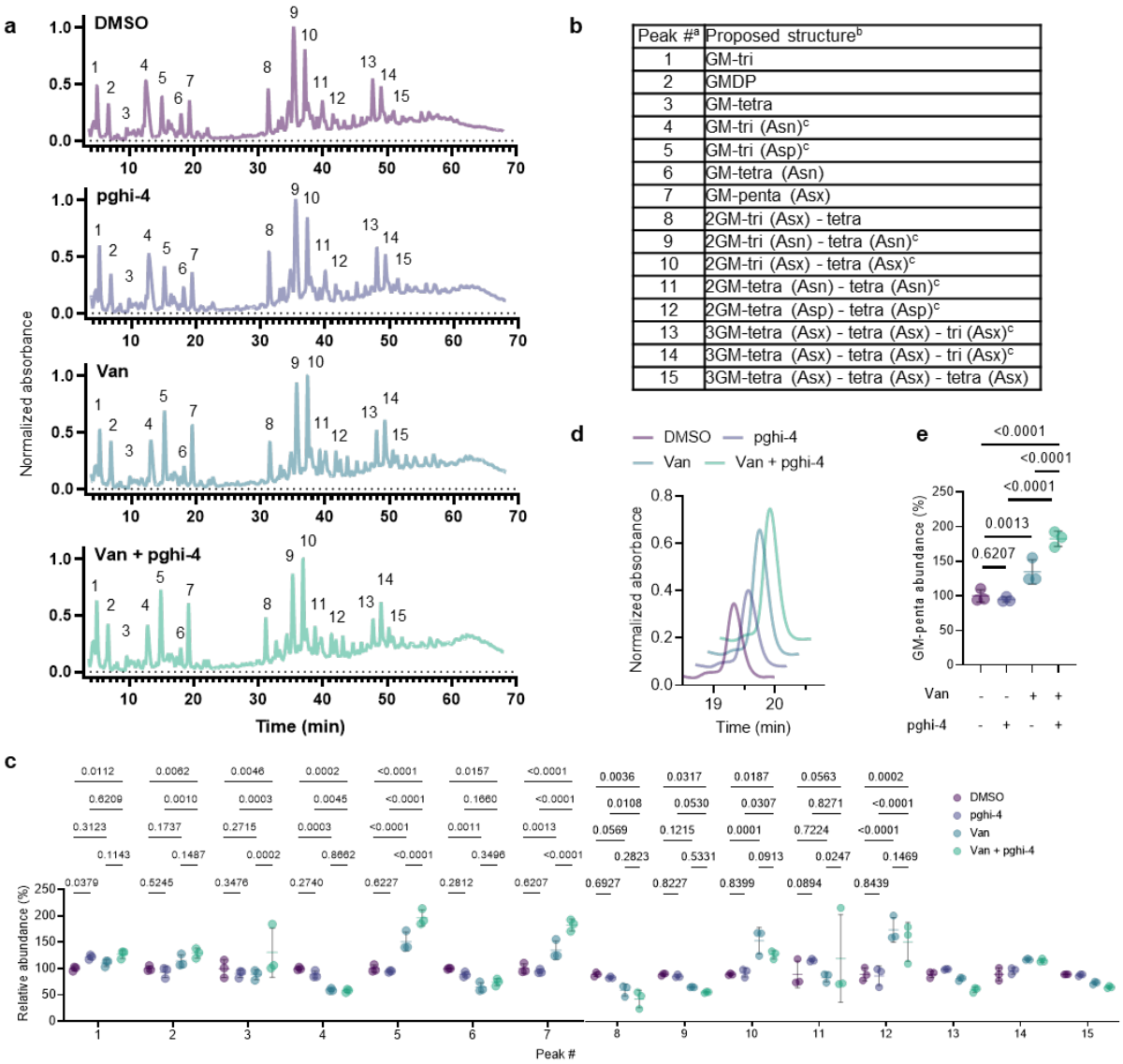

Peak #[a]	Proposed structure[b]
1	GM-tri
2	GMDP
3	GM-tetra
4	GM-tri (Asn)[c]
5	GM-tri (Asp)[c]
6	GM-tetra (Asn)
7	GM-penta (Asx)
8	2GM-tri (Asx) - tetra
9	2GM-tri (Asn) - tetra (Asn)[c]
10	2GM-tri (Asx) - tetra (Asx)[c]
11	2GM-tetra (Asn) - tetra (Asn)[c]
12	2GM-tetra (Asp) - tetra (Asp)[c]
13	3GM-tetra (Asx) - tetra (Asx) - tri (Asx)[c]
14	3GM-tetra (Asx) - tetra (Asx) - tri (Asx)[c]
15	3GM-tetra (Asx) - tetra (Asx) - tetra (Asx)

Extended Data Fig. 15. Inactivation of peptidoglycan remodeling in VREfm.

a, Representative LC-MS chromatograms of mutanolysin-digested peptidoglycan isolated from sacculi of VREfm after treatment with pghi-4 (50 μM), vancomycin (5 μg/mL) alone, or in combination. **b,** Composition of peptidoglycan isolated from VREfm sacculi. [a] Peak numbers refer to (**a**). [b] GM, disaccharide (GlcNAc-MurNAc); 2 GM, disaccharide-disaccharide (GlcNAc-MurNAc-GlcNAc-MurNAc); 3 GM, disaccharide-disaccharide-disaccharide (GlcNAc-MurNAc-GlcNAc-MurNAc-GlcNAc-MurNAc); GM-Tri, disaccharide tripeptide (L-Ala-D-iGln-L-Lys); GM-Tetra, disaccharide tetrapeptide (L-Ala-D-iGln-L-Lys-D-Ala); GM-Penta, disaccharide pentapeptide (L-Ala-D-iGln-L-Lys-D-Ala -D-Ala). [c] The assignment of the amide and the hydroxyl functions to either peptide stem is arbitrary. Masses and retention time of peptidoglycan fragments are in Extended Data Table 11. **c,** Normalized abundance (relative to DMSO) of peptidoglycan fragments isolated from mutanolysin-digested sacculi of VREfm after treatment with pghi-4 (50 μM), vancomycin (5 μg/mL) alone, or in combination and analyzed by LC-MS. For **c** peak numbers indicate corresponding peptidoglycan fragment from LC-MS analysis listed in (**a**), data is heat-

1239 map of mean values, n=3 biological replicates. **d,** Abundance of GM-penta muropeptide (peak 7
1240 in LC-MS chromatogram (**a**) shown as representative extracted LC-MS chromatogram of
1241 mutanolysin-digested peptidoglycan isolated from sacculi of VREfm after treatment with pghi-4
1242 (50 μM), vancomycin (5 μg/mL) alone, or in combination. **e,** Normalized abundance of GM-penta
1243 muropeptide (relative to DMSO) within peptidoglycan composition of VREfm ± pghi-4 (50 μM) ±
1244 vancomycin (5 μg/mL) from LC-MS chromatograms (**a**) and (**c**). For **c**, **e**, data are mean ± S.D.,
1245 n=3 biological replicates, analyzed with one-way ANOVA and uncorrected Fisher's LSD post-test,
1246 p values of significant differences are indicated.

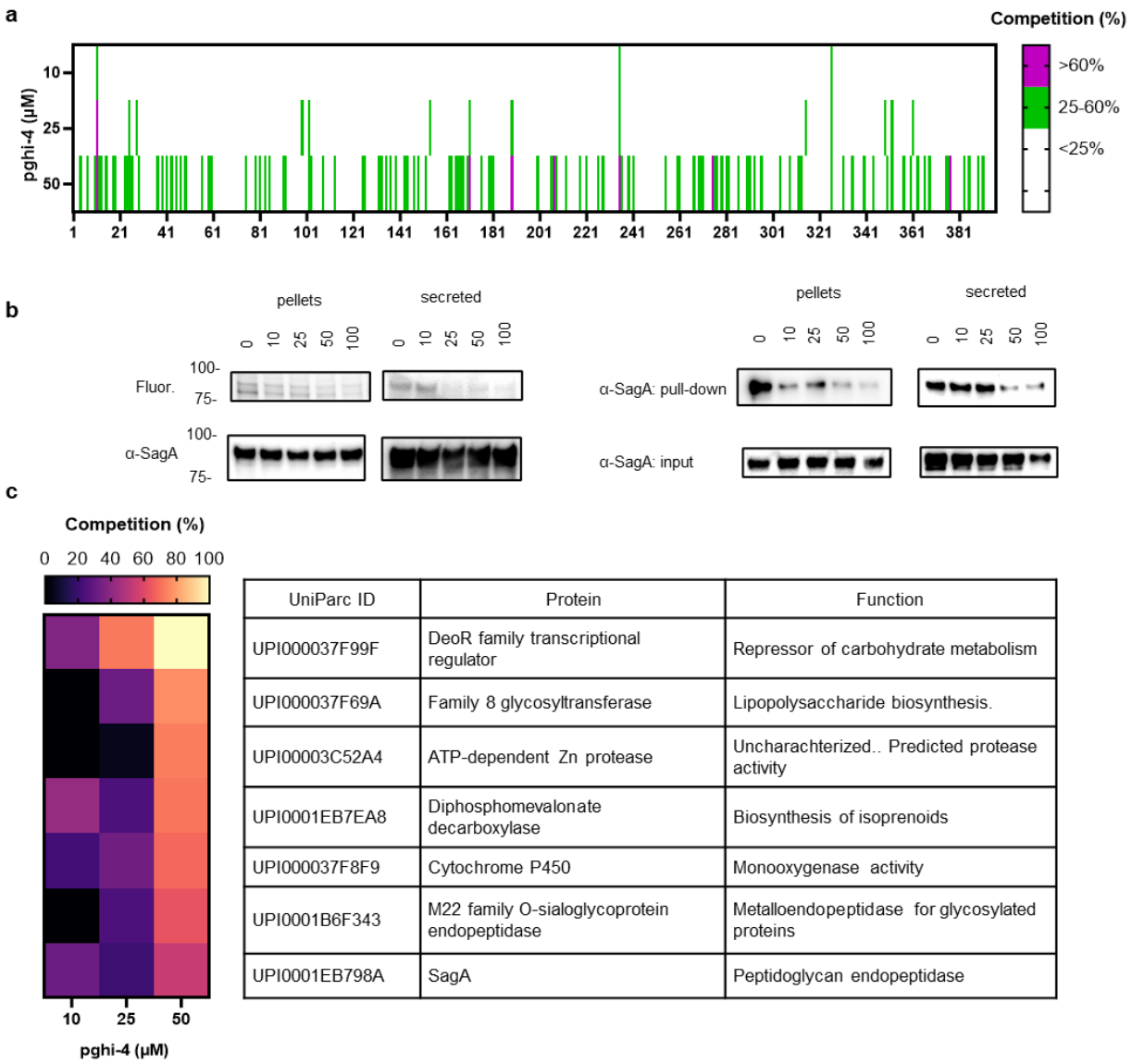

UniParc ID	Protein	Function
UPI000037F99F	DeoR family transcriptional regulator	Repressor of carbohydrate metabolism
UPI000037F69A	Family 8 glycosyltransferase	Lipopolysaccharide biosynthesis.
UPI00003C52A4	ATP-dependent Zn protease	Uncharachterized.. Predicted protease activity
UPI0001EB7EA8	Diphosphomevalonate decarboxylase	Biosynthesis of isoprenoids
UPI000037F8F9	Cytochrome P450	Monooxygenase activity
UPI0001B6F343	M22 family O-sialoglycoprotein endopeptidase	Metalloendopeptidase for glycosylated proteins
UPI0001EB798A	SagA	Peptidoglycan endopeptidase

Extended Data Fig. 16. Cysteine-directed chemoproteomic analysis.

a, Competitive cysteine-directed chemoproteomic analysis of VREfm (ERV165) proteome after treatment with pghi-4. Data are clustering as percentage of competition for cysteine occupancy relative to desthiobiotin-iocoacetamide activity. **b,** Pghi-4-treated ERV165 cell lysates and secreted proteins were reacted with iodoacetamide-alkyne probe. Left: clicked to rhodamine-azide, followed by SDS-PAGE separation and visualized by fluorescence. α-SagA western blot analysis served as protein loading control. Right: clicked to biotin-azide, followed by enrichment, SDS-PAGE separation and analyzed by α-SagA western blot. α-SagA western blot analysis of input (2.5%) served as protein loading control. **c,** Heat-map of activity of top 7 cysteine-directed protein targets of pghi-4 with their functions in ERV165. Data are representative biological replicates of two independent datasets.

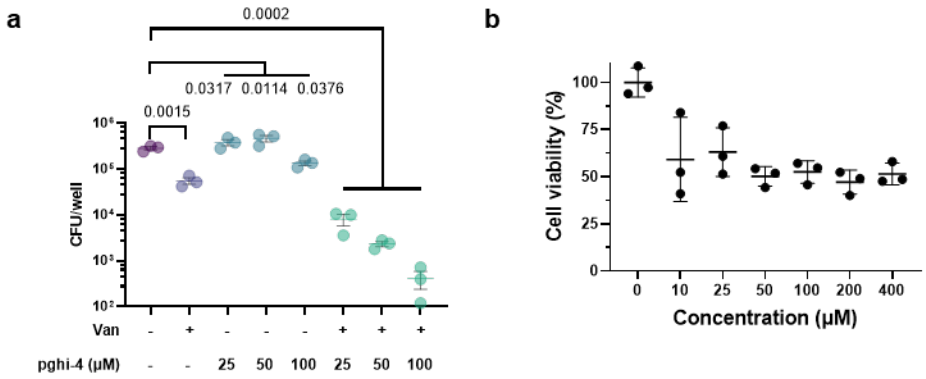

Extended Data Fig. 17.

a, CFU analysis of VREfm-infected THP-1 cells treated with vancomycin (100 μg/mL), pghi-4 alone or in combination. Data are mean ± S.E.M. and analyzed by analyzed with one-way ANOVA and Tukey's multiple comparison post-test, p values are indicated, n=3 biological replicates. **b,** Cytotoxicity of pghi-4 on RAW264.7 cells assessed by WST-8 assay. Data are mean ± S.D., n=3 biological replicates.

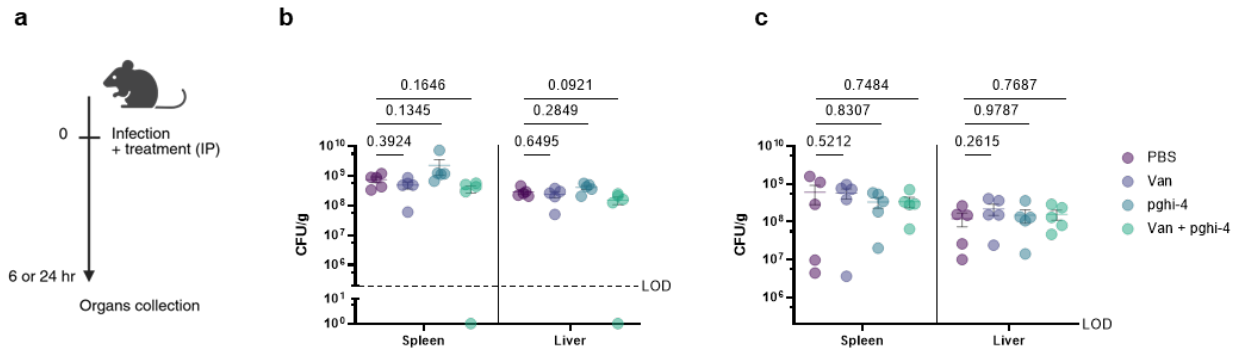

Extended Data Fig. 18. Single-dose therapeutic efficacy of pghi-4 as vancomycin adjuvant *in vivo*.

a, Scheme of systemic infection *in vivo* with VREfm (ERV165): mice were infected with 10^9 VREfm CFU with PBS (0.25% CMC), pghi-4 (25 mg/kg 0.25% CMC) ± vancomycin (Van, 100 mg/kg 0.25% CMC) intraperitoneally. 6- or 24 hours post-infection mice were sacrificed, organs were collected and VREfm burden was analyzed by CFU. **b,** CFU analysis of organs from VREfm-infected mice pghi-4 (25 mg/kg 0.25% CMC) ± vancomycin (Van, 100 mg/kg 0.25% CMC). collected after 6 hours post-infection. Dotted horizontal line is limit of detection (LOD). **c,** CFU analysis of organs from VREfm-infected mice ± pghi-4 (25 mg/kg 0.25% CMC) ± vancomycin (Van, 100 mg/kg 0.25% CMC) collected after 24 hours post-infection. Y axis starts with the limit of detection (LOD). For **b, c,** horizontal line is mean ± S.E.M. and analyzed by Kruskal-Wallis test with Dunn's uncorrected post-test. Each dot is an individual mouse, n=5.

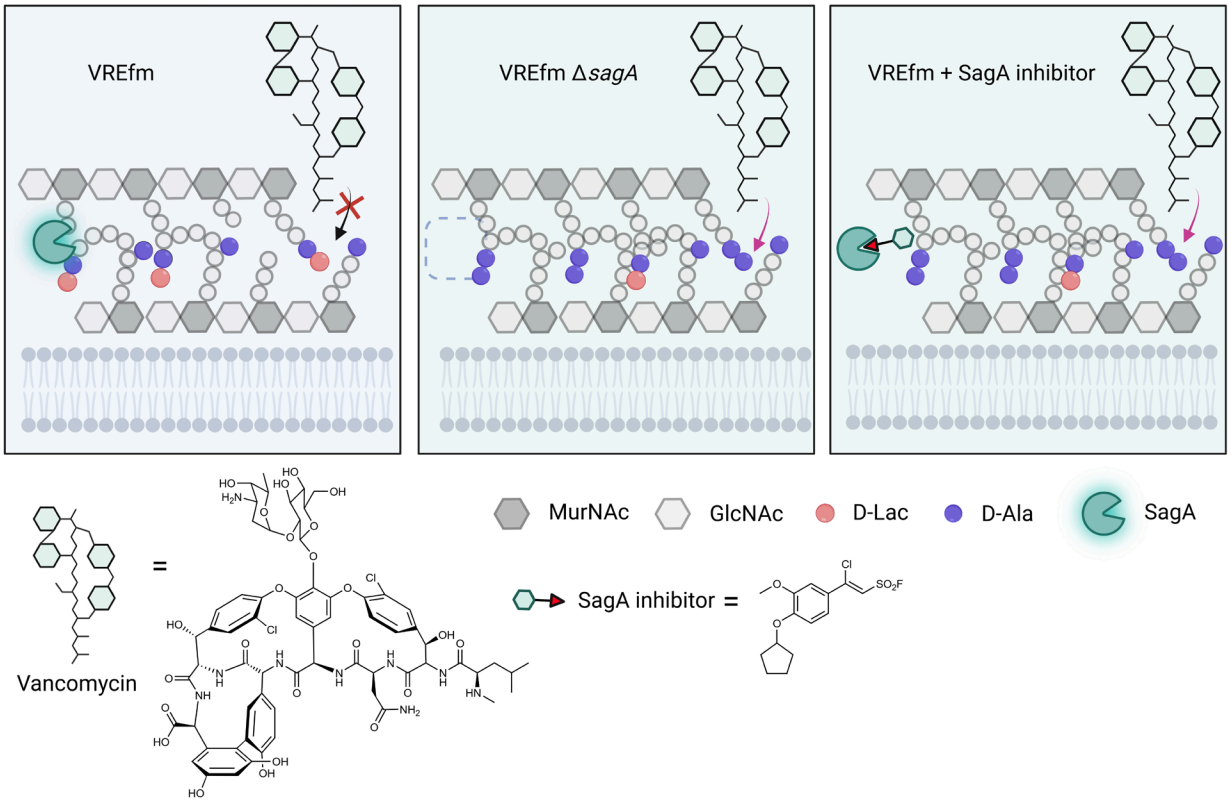

1279

1280 **Extended Data Fig. 19. Summary of SagA inactivation and impact on vancomycin**
1281 **susceptibility in VREfm.**

1282 VREfm with functional SagA peptidoglycan remodeling display D-Lac-ending peptidoglycan
1283 fragments unabling vancomycin binding. Genetic and pharmacological inactivation of SagA
1284 impairs peptidoglycan remodeling in VREfm leading to accumulation of D-Ala-D-Ala-containing
1285 unprocessed peptidoglycan and restoration antibiotic activity of vancomycin. Created with
1286 BioRender.

1287

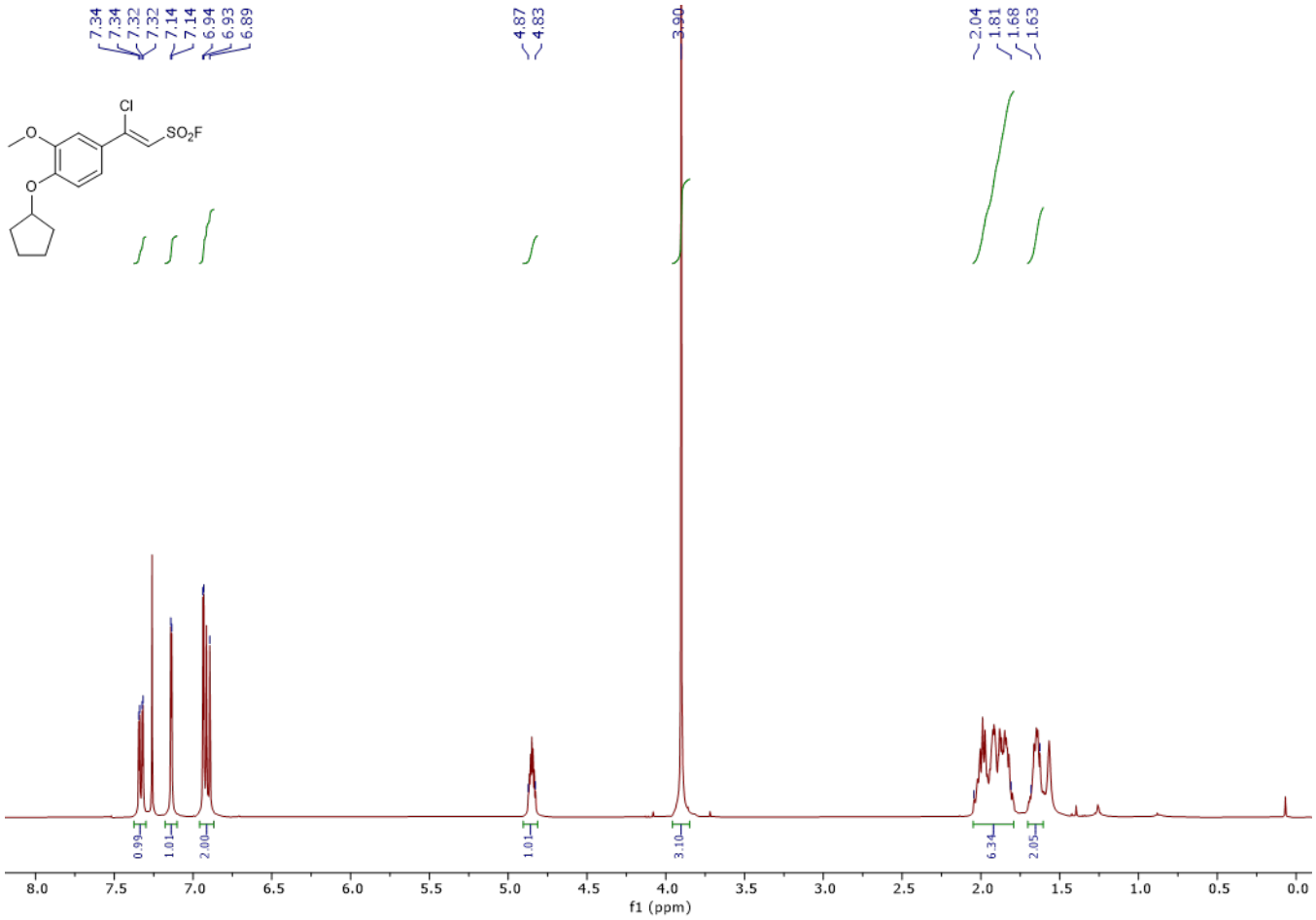

1288

1289 **Extended Data Fig. 20.** ^{1}H NMR Spectrum for pghi-4 (400 MHz, $CDCl_3$)

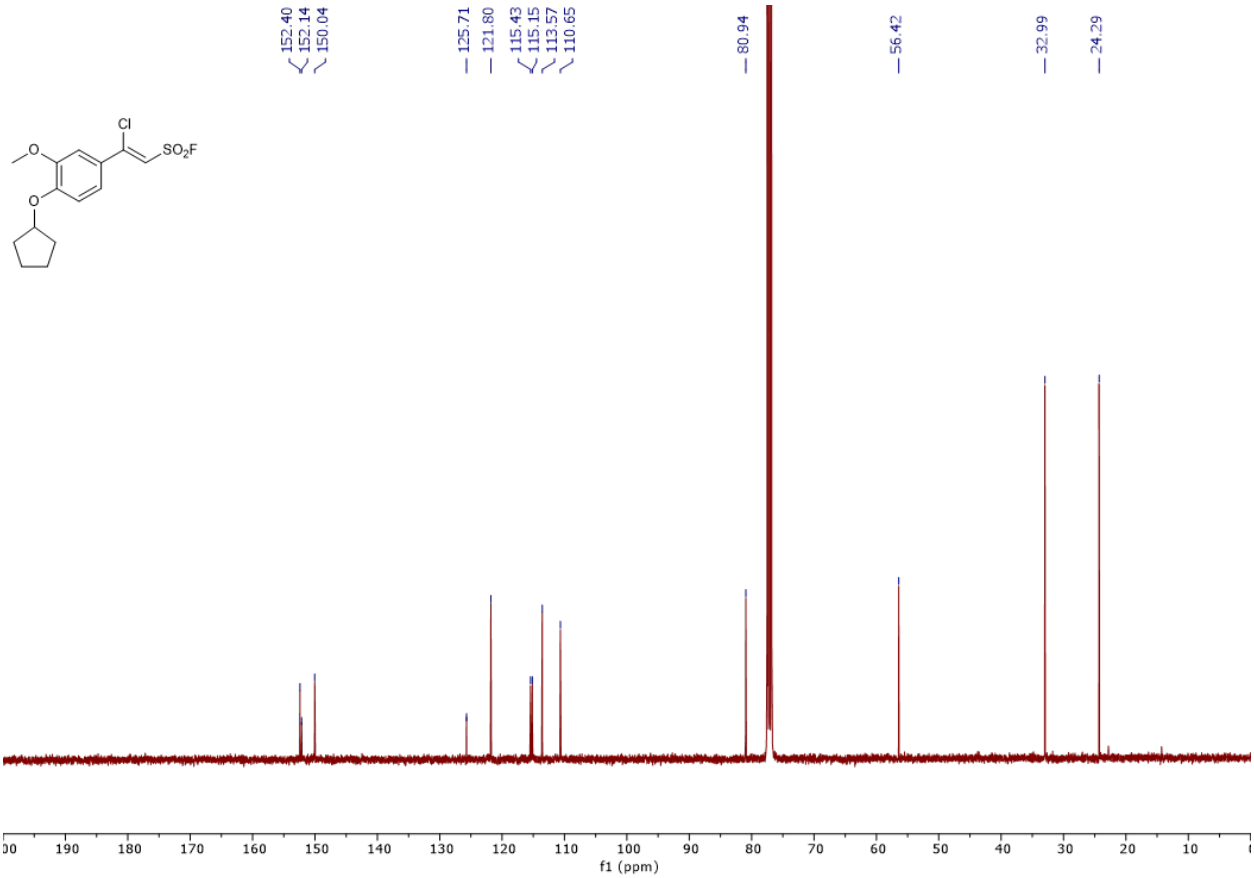

Extended Data Fig. 21. ^{13}C NMR Spectrum for pghi-4 (101 MHz, $CDCl_3$)

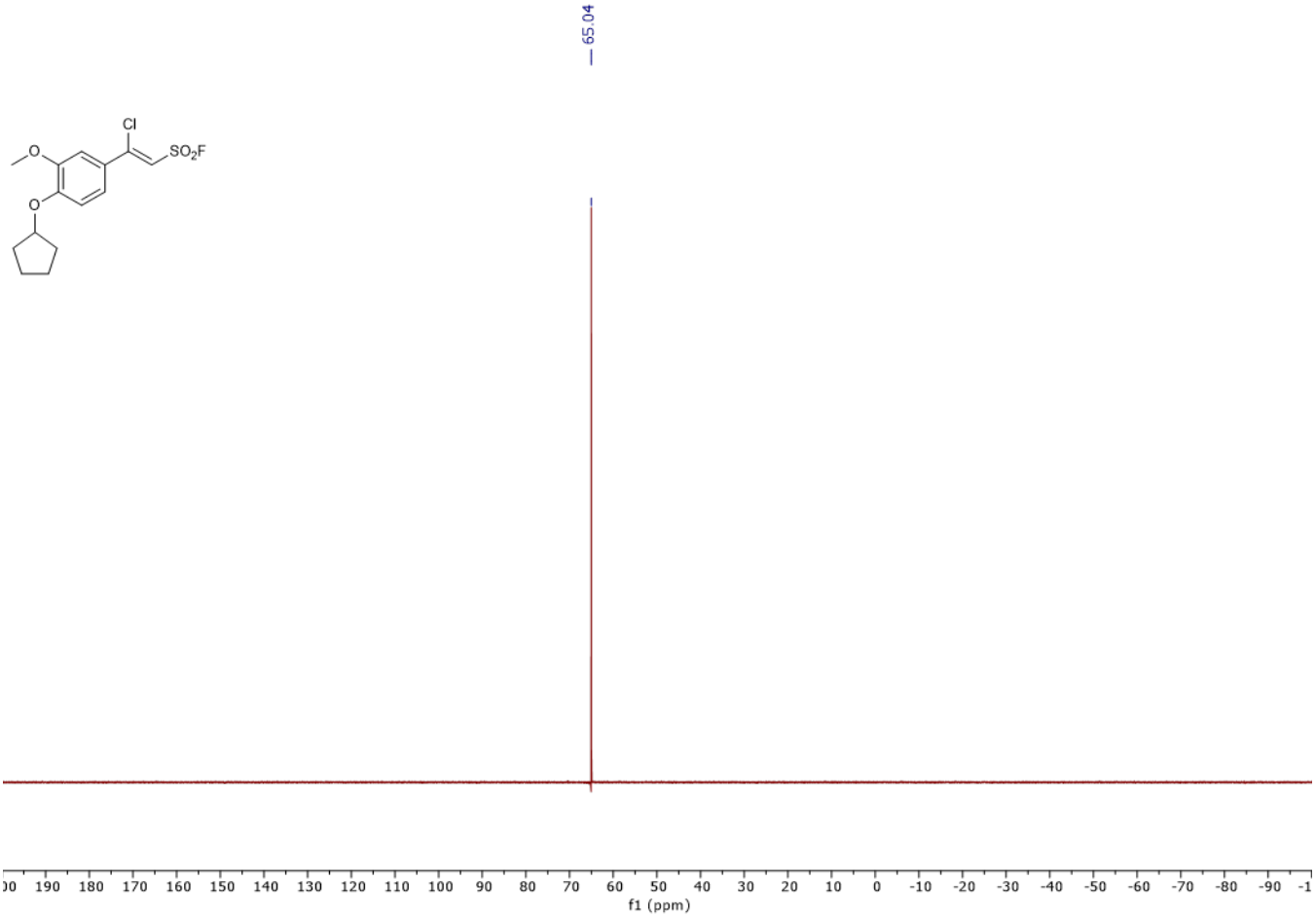

Extended Data Fig. 22. ^{19}F NMR Spectrum for pghi-4 (377 MHz, $CDCl_3$)

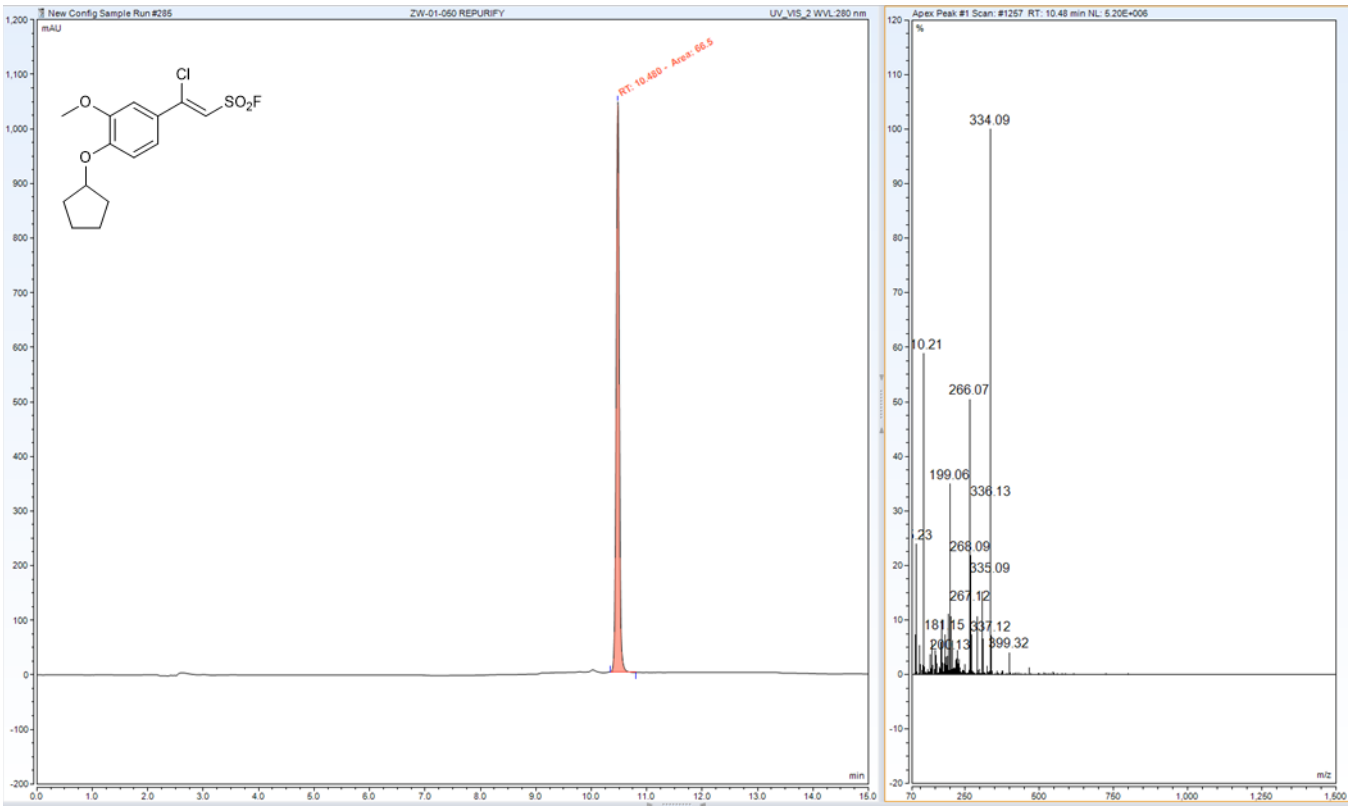

Extended Data Fig. 23. Liquid chromatography-mass spectrometry (LCMS) analysis of pghi-4.

1296 **Extended Data Table 1. Minimum inhibitory concentration (MIC) values of VREfm**
1297 **susceptibility to vancomycin.**

1298

ERV165 strain	MIC in BHI (µg/mL)	MIC in MHB (µg/mL)
WT	256	256
Δ*sagA*	128	128
Δ*sagA*::*sagA*	256	256

1299

1300 **Extended Data Table 2. Missense mutations detected by whole-genome sequencing (WGS)**
1301 **in ERV165-Δ*sagA***

№	Gene	Mutation	Annotation
1	*sagA*	Clean KO	NlpC/p60 PG hydrolase
2	*coaD*	2 missense mutation, pre-maturely terminated	Pantetheine-phosphate adenylyltransferase
3	EEHMGE_02485	Many mutations	DUF2129 domain-containing protein) YlbG family protein
4	EEHMGE_02475	Many mutations	CAP-associated-N domain-containing protein
5	EEHMGE_14260	N233D	PTS mannose transporter subunit EIIAB
6	ISL3-like element IS1251 family transposase	Insertion at ~2.3 kb region. No obvious gene disruption observed.	
7	EEHMGE_11825	R159H	DNA-binding protein
8	EEHMGE_08940	N104D	glycosyl hydrolase
9	EEHMGE_08165	T424N	glycine/betaine ABC transporter permease
10	EEHMGE_02500	I277 D278 to DQL	SepM family pheromone-processing serine protease
11	EEHMGE_01745	S68L	MapZ (MapZ (Midcell Anchored Protein Z) locates at the division site before FtsZ and guides septum positioning). The mutation occurred outside annotated functional domains and in a region lacking conserved sequence features.

1302

1303 **Extended Data Table 3. Silent mutations detected by WGS in ERV165-Δ*sagA***

№	Gene	Mutation	Annotation
1	*neuC*	I51I, L21L	UDP-N-acetylglucosamine 2-epimerase
2	EEHMGE_14675	K25K	Terminase large subunit
3	*xseA*	Q312Q	Exodeoxyribonuclease VII large subunit
4	EEHMGE_11955	I74I	MarR family transcriptional regulator
5	EEHMGE_11645	I71I	Universal stress protein
6	Gly_trna	ttg to tcg	Glycyl-tRNA synthetase
7	EEHMGE_09405	K167K	Insulinase family protein
8	EEHMGE_08170	L116L	Glycine betaine/L-proline ABC transporter ATP-binding protein
9	EEHMGE_07965	Q284Q	Alpha-N-arabinofuranosidase
10	EEHMGE_04975	A162A	LTA synthase family protein
11	EEHMGE_04420	V29V	Thioredoxin
12	EEHMGE_03730	I213I	NAD(P)-dependent dehydrogenase

1304

1305 **Extended Data Table 4. Missense/non-sense mutations detected by WGS in ERV165-**
1306 **Δ*sagA*::*sagA***

№	Gene	Mutation	Annotation
1	*sagA*	Clean KO	NlpC/p60 PG hydrolase
2	BJDOAF_01965	T424N	glycine/betaine ABC transporter permease
3	BJDOAF_02650	316-Non-sense	ISL3 family transposase; premature termination.
4	Neutral locus	SagA insertion downstream to ruvX and DUF1292 domain-containing protein	Trans complementation of *sagA*
5	BJDOAF_05155	W256R	ISL3 family transposase
6	BJDOAF_08385	L68S	MapZ (Midcell Anchored Protein Z) locates at the division site before FtsZ and guides septum positioning. The mutation occurred outside annotated functional domains and in a region lacking conserved sequence features.
7	BJDOAF_09950	N233D	PTS mannose transporter subunit EIIAB
8	Arg_trna	Adenine to Guanine	tRNA-Arg(tct)
9	Integenic region of mnmA and arcD	tnp-IS1251 insertion downstream to tRNA 2-thiouridine(34) synthase MnmA	tnp-IS1251 encodes ISL3 family IS1251 transposase; mnmA encodes tRNA 2-thiouridine(34) synthase MnmA; arcD encodes arginine-ornithine antiporter
10	BJDOAF_12380	R159H	DNA-binding protein
11	Gly_trna	Adenine to Guanine	tRNA-Gly(gcc)
12	BJDOAF_14340	W256R	ISL3 family transposase
13	tnp-ISL3	C256R	ISL3 family transposase
14	BJDOAF_00185	Many non-sense mutations	Tn3 family transposase; premature termination.
15	BJDOAF_00190	Around 20 missense mutations	hypothetical protein; This gene is present in between Tn3 family transposase and IS1216 family transposase
16	BJDOAF_00870	A274V	IS1182 family transposase

1307

1308 **Extended Data Table 5. Silent mutations detected by whole-genome sequencing (WGS) in**
1309 **ERV165-Δ*sagA*::*sagA***

№	Gene	Mutation	Annotation
1	BJDOAF_01640	V160V	Cytochrome P450
2	BJDOAF_01960	L116L	Glycine betaine/L-proline ABC transporter ATP-binding protein
3	BJDOAF_05660	I98I	2-phospho-L-lactate transferase CofD
4	BJDOAF_12250	I74I	MarR family transcriptional regulator
5	BJDOAF_13200	Q101Q	Metallophosphoesterase

1310

1311 **Extended Data Table 6. Minimum inhibitory concentration (MIC) values of VREfm**
1312 **susceptibility to vancomycin in the presence of pghi-4 in BHI analyzed by checkerboard**
1313 **assay (Fig. 4b).**

pghi-4 (μM)	MIC (μg/mL)	ΔMIC (fold)
0	320	1
6.25	320	1
12.5	320	1
25	160	2
50	80	4
100	40	8

1314

1315 **Extended Data Table 7. VREfm strain information.**

VREfm strain	Sequence Type	Van Type
ERV165	412	*vanA*
TX0082	17	*vanA*
700221	17	*vanA*
DVT 1238	412	*vanA*
DVT 1574	80	*vanA*
DVT 1576	117	*vanA*
DVT 3347	18	*vanA*
DVT 3350	203	*vanA*
DVT 3351	664	*vanA*

1316

1317 **Extended Data Table 8. Minimum inhibitory concentration (MIC) values of vancomycin**
1318 **susceptibility of VREfm clinical isolates relative to ERV165.**

VREfm strain	Δ MIC (folds)
ERV165	1
TX0082	4
700221	4
DVT 1238	4
DVT 1574	4
DVT 1576	4
DVT 3347	>4
DVT 3350	0.5
DVT 3351	2

1319

1320 **Extended Data Table 9. Bacterial strains used in this study.**

Organism	Description	Source
Enterococcus faecium ERV165	WT	Lab stock
Enterococcus faecium ERV165-Δ*sagA*	Δ*sagA* (clean knock-out)	This work
Enterococcus faecium ERV165-Δ*sagA*::*sagA*	Δ*sagA*::*sagA* (*sagA* chromosomal complementation in Δ*sagA* background)	This work
Enterococcus faecium ERV165-Δ*pgh2*	Δ*pgh2* (clean knock-out)	This work
Enterococcus faecium ERV165-Δ*pgh3*	Δ*pgh3* (clean knock-out)	This work
Enterococcus faecium ERV165-Δ*pgh4*	Δ*pgh4* (clean knock-out)	This work
Enterococcus faecium TX0082	WT	Lab stock
Enterococcus faecium 700221	WT	Lab stock
Enterococcus faecium DVT 1238	Clinical isolate	Van Tyne lab
Enterococcus faecium DVT 1574	Clinical isolate	Van Tyne lab
Enterococcus faecium DVT 1576	Clinical isolate	Van Tyne lab
Enterococcus faecium DVT 3347	Clinical isolate	Van Tyne lab
Enterococcus faecium DVT 3350	Clinical isolate	Van Tyne lab
Enterococcus faecium DVT 3351	Clinical isolate	Van Tyne lab
Escherichia coli BL21-CodonPlus (DE3)-RIL[1]	*Efm*_Com15_SagA-NlpC/p60_ΔSS-His_6	Lab stock
Escherichia coli BL21-CodonPlus (DE3)-RIL[1]	*Efm*_Com15_SagA-NlpC/p60_ΔSS_C443A-His_6	Lab stock

1321 [1] *Escherichia coli* BL21-CodonPlus (DE3)-RIL cells contain extra copies of the argU, ileY, and
1322 leuW tRNA genes in a plasmid encoding Cam resistance

1323 **Extended Data Table 10. Plasmids constructed**

1324 The details of the plasmid construction are described below.

№	Plasmid	Description	Source	Notes
1.	pJC005.gent[1]	CRISPR-Cas12a genome editing plasmid	Chua et al. [27]	Gent^R
2.	pUCsRNAP[2]	pUC; small RNA promoter and 23-bp spacer sequence flanked by two 19-bp repeats	Chua et al. [27]	Amp^R
3.	pPK126	pLZ12-empty vector	This work	Spec^R
4.	pPK111	pLZ12-*sagA*^{WT}	This work	Spec^R
5.	pPK125	pLZ12-*sagA*^{C425A}	This work	Spec^R
6.	pPK99	pJC005.gent-Δ*sagA*	This work	Gent^R. This plasmid is used for constructing Δ*sagA* using the CRISPR-Cas12a counter-selection recombineering method described in Chua et al. (*27*)
7.	pPK158	pJC005.gent-*sagA*	This work	Gent^R. This plasmid carries ERV165 *sagA* for chromosomal integration at a neutral locus in sPK377 using the CRISPR-Cas12a counter-selection recombineering method described in Chua et al. (*27*)
8.	pPK156	pJC005.gent- Δ*pgh2*	This work	Gent^R. This plasmid is used for constructing Δ*pgh2* using the CRISPR-Cas12a counter-selection recombineering method described in Chua et al. (*27*)
9.	pPK107	pJC005.gent- Δ*pgh3*	This work	Gent^R. This plasmid is used for constructing Δ*pgh3* using the CRISPR-Cas12a counter-selection recombineering method described in Chua et al. (*27*)
10.	pPK154	pJC005.gent- Δ*pgh4*	This work	Gent^R. This plasmid is used for constructing Δ*pgh4* using the CRISPR-Cas12a

				counter-selection recombineering method described in Chua et al. [27]

1325

1326 [1]Gift from James Collins (Addgene plasmid # 182739; http://n2t.net/addgene:182739; RRID:
1327 Addgene_182739).

1328 [2]Gift from James Collins (Addgene plasmid # 182746; http://n2t.net/addgene:182746; RRID:
1329 Addgene_182746)

1330 **Extended Data Table 11. Masses of peptidoglycan fragments were detected with MSD API-**
1331 **ES.**

Peak[a]	RT (min)	Calculated molecular weight	Observed mass	Proposed structure[b]
1	5.01	825.4	413.6 $[M+2H]^{2+}$	GM-tri
2	6.77	697.3	349.6 $[M+2H]^{2+}$	GMDP
3	9.63	896.44	449.2 $[M+2H]^{2+}$	GM-tetra
4	12.58	939.45	470.8 $[M+2H]^{2+}$	GM-tri (Asn)[c]
5	15.04	940.43	471.2 $[M+2H]^{2+}$	GM-tri (Asp)[c]
6	18.02	1010.5	506.2 $[M+2H]^{2+}$	GM-tetra (Asn)
7	19.33	1081.5	541.6 $[M+2H]^{2+}$	GM-penta (Asx)
8	31.54	1818.9	909.8 $[M+2H]^{2+}$	2GM-tri (Asx) - tetra
9	35.47	1932.9	966.6 $[M+2H]^{2+}$	2GM-tri (Asn) - tetra (Asn)[c]
10	37.22	1933.9	967.4 $[M+2H]^{2+}$	2GM-tri (Asx) - tetra (Asx)[c]
11	39.93	2004.0	1002.4 $[M+2H]^{2+}$	2GM-tetra (Asn) - tetra (Asn)[c]
12	41.57	2005.9	1004.2 $[M+2H]^{2+}$	2GM-tetra (Asp) - tetra (Asp)[c]
13	47.72	2927.4	975.8 $[M+3H]^{3+}$	3GM-tetra (Asx) - tetra (Asx) - tri (Asx)[c]
14	49.02	2928.4	977.0 $[M+3H]^{3+}$	3GM-tetra (Asx) - tetra (Asx) - tri (Asx)[c]
15	50.94	2999.4	1001.4 $[M+3H]^{3+}$	3GM-tetra (Asx) - tetra (Asx) - tetra (Asx)[c]

1332

1333 [a.] Peak numbers refer to Extended Data Fig. 4a and 15a.

1334 [b.] GM, disaccharide (GlcNAc-MurNAc); 2GM, disaccharide-disaccharide (GlcNAc-MurNAc-
1335 GlcNAc-MurNAc); 3GM, disaccharide-disaccharide-disaccharide (GlcNAc-MurNAc-GlcNAc-
1336 MurNAc-GlcNAc-MurNAc); GM-Tri, disaccharide tripeptide (L-Ala-D-iGln-L-Lys); GM-Tetra,
1337 disaccharide tetrapeptide (L-Ala-D-iGln-L-Lys-D-Ala); GM-Penta, disaccharide pentapeptide (L-
1338 Ala-D-iGln-L-Lys-D-Ala -D-Ala).

1339 [c.] The assignment of the amide and the hydroxyl functions to either peptide stem is arbitrary.

1340 RT = retention time